2002

Hydrodynamics and freshwater diversion within Barataria Basin

Dongho Park
Louisiana State University and Agricultural and Mechanical College

HYDRODYNAMICS AND FRESHWATER DIVERSION WITHIN BARATARIA BASIN

A Dissertation

Submitted to the Graduate Faculty of the
Louisiana State University and
Agricultural and Mechanical College
in partial fulfillment of the
requirements for the degree of
Doctor of Philosophy

in

The Department of Oceanography and Coastal Sciences

by
Dongho Park
B.S., National Fisheries University of Pusan, 1986
M.S., Louisiana State University, 1998
August 2002

ACKNOWLEDGEMENTS

First, I wish to express my sincerest gratitude to my co-advisor professors, Dr. William J. Wiseman, Jr. and Dr. Masamichi Inoue, for their guidance, encouragement, inspiration, and keen sense of organization throughout my graduate studies. I would like to thank the other members of my committee, Dr. Dubravko Justic, Dr. Lawrence J. Rouse, Jr., and Dr. C. Federick Bryan for their encouragement and insightful comments.

I would like to extend my deepest thanks to Dr. S. A. Hsu, Mr. Eric Swenson, Dr. Christopher M. Swarzenski, and Dr. Susan Welsh for their help. I have been supported, during this effort, by a contract from the Minerals Management Service (1435-0001-30660, task order numbers 19953 and 19965).

Finally, I want to thank my beloved wife, Minjeong, my mother, my parents-in-law, and my sister-in-law and her husband for their sacrifice, understanding, and encouragement. I dedicate this dissertation to them.

TABLE OF CONTENTS

ABSTRACT

In order to understand the physical processes in the Barataria estuary, a previously developed two-dimensional, depth-integrated hydrodynamic model is applied to simulate estuarine processes. The equations for conservation of mass and momentum predict specific physical processes when forced by tidal and salinity variations at the open boundaries, wind forcing patterns, precipitation and evaporation over the model domain, and freshwater runoff as point sources.

This study is focused on examining the impact of freshwater dispersion from the freshwater sources. Thus, a hydrologic model was developed to estimate runoff. Furthermore grid size was reduced, a new advective code added, and baroclinic effects included. The model was run with and without freshwater diversions from the Mississippi River.

When compared to observations the correlation coefficients (r^2) of model water levels are larger than 0.9 at all but one station. For the hydrologic calibration, a big flood event was tested. Agreement between observed and model results with runoff is surprisingly good. The observed agreement provides a justification for adopting 100 % coupling between the hydrologic model and hydrodynamic model, at least for this flood event.

In terms of water level within the basin, the freshwater diversions seem to affect most of the Barataria Basin system water level within 3 days. Using a Hovmüller diagram, tidal phase speed was estimated within the basin as 16 hours to travel from the mouth of Barataria Bay to the top of the basin, Lac des Allemands.

In terms of salinity within the basin, the impact of freshwater diversion reaches Barataria Bay within 5 and 10 days from Naomi and West Pointe à la Hache, respectively, and the Gulf of Mexico 15 to 20 days after freshwater release.

1. INTRODUCTION

An estuary is a partially enclosed body of water formed where freshwater from rivers and streams flows into the ocean, mixing with the seawater. Estuaries come in all shapes and sizes, each unique to their location and climate. Mixing is a crucial component of estuarine habitats. It establishes a gradient between freshwater and saltwater. In some places, the gradient is steep, and salinities increase quickly from fresh to marine habitats, while in others the influence of large rivers ensures that true mesohaline habitats are found only offshore. The location and strength of the freshwater-saltwater gradient vary seasonally, but the mixing results in high biological productivity and a diversity of species. Estuarine environments are among the most productive on earth, creating more organic matter each year than comparably-sized areas of forest, grassland, or agricultural land.

Estuaries support unique communities of plants and animals, specially adapted for life at the margin of the sea. Many different habitat types are found in and around estuaries, including shallow open waters, freshwater and salt marshes, sandy beaches, mud and sand flats, rocky shores, oyster reefs, mangrove forests, river deltas, tidal pools, sea grass and kelp beds, and wooded swamps. Besides serving as important habitat for wildlife, the wetlands that fringe many estuaries also perform other valuable services. Water draining from the uplands carries sediments, nutrients, and pollutants. As the water flows through fresh and salt marshes, much of the sediments and pollutants are filtered out. This filtration process creates cleaner and clearer water, which benefits both people and marine life.

Estuarine gravitational circulation, driven by longitudinal pressure gradients that result from the distribution of temperature and salinity, is modified by flows occurring as a result of other processes such as winds and tides (Fisher et al., 1979). Estuarine-coastal exchange

processes cause the formation of buoyant effluent plumes, which influence shelf chemistry and biology as well as physics (Wiseman, 1986).

Louisiana estuaries are typically shallow with subaerial barrier beach formation at their mouths. They are the result of subsidence and reworking of abandoned deltaic sedimentary deposits. The area enclosed by the barrier beaches is generally elongated parallel to the coastline. Because the inlets connecting the bar-built estuary with the ocean are usually relatively small compared to the dimensions of the sound behind the barrier, tidal action is often considerably reduced in such estuaries (Pritchard, 1967).

Barataria Basin is located immediately west of the Mississippi River delta and is bounded on the north and east by the Mississippi River, on the west by Bayou Lafourche, and on the south by the Gulf of Mexico (Figure 1). The total area of the basin covers approximately $6{,}300\,km^2$ (1,565,000 acres). The region contains major corridors of developed areas along the Mississippi River and Bayou Lafourche. The basin is an irregularly shaped area bounded on each side by a levee formed by the present and a former channel of the Mississippi River. A chain of barrier islands separates the basin from the Gulf of Mexico. In the northern half of the basin, several large lakes occupy the sump position. The southern half of the basin consists of tidally influenced marshes interconnected by a convoluted suite of ponds, lakes, and channels that ultimately empty into a large bay system behind the barrier islands.

During the last several hundred years, in coastal Louisiana, land building processes have been greatly reduced, while the erosion rate continues and probably has accelerated due to the activities of man (Van Sickle et al., 1976). The primary pattern of land loss in the Louisiana coastal zone results from the submergence of coastal marshes and subsequent

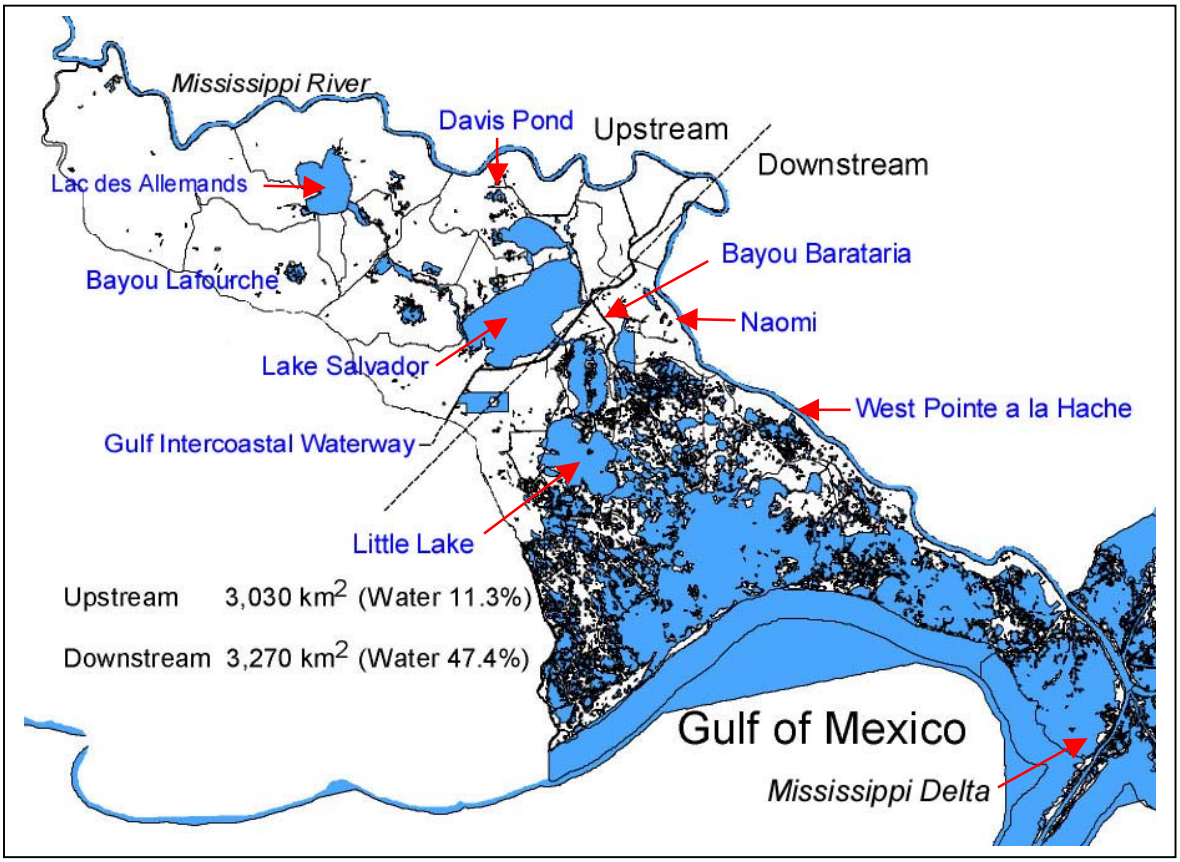

Figure 1. Barataria Basin.

conversion to open water (Turner, 1990). Within the Barataria Basin, wetland loss rates averaged nearly 23.1 km^2 (5,700 acres) per year between 1974 and 1990 (Louisiana Coastal Wetlands Conservation and Restoration Task, 1993). This high rate appears due to a combination of natural processes such as subsidence, sea-level rise, canal dredging, and the river funneling sediments across the continental shelf making them unavailable for coastal marshes (Bowman et al. 1995). Of the numerous factors contributing to this loss, perhaps the leveeing of the Mississippi River for flood control has had the most far-reaching impact. Historically, the Mississippi River was the major source of freshwater and sediment for the entire deltaic Louisiana coastal marsh system. Artificial flood control levees were

constructed along the Mississippi River and in 1904 Bayou Lafourche was artificially dammed. Ever since construction of the flood control levee along the Mississippi River, rainfall had been the main source of freshwater to the Barataria Basin. Only a small amount of riverine input, designed to mimic a natural crevasse, was introduced into the basin's wetlands through the recently completed siphons at Naomi and West Pointe à la Hache. These have been working at a maximum pumping rate of 60 $m^3 s^{-1}$ of freshwater at each site. Another diversion site, Davis Pond, was recently opened with a maximum design-pumping rate of 300 $m^3 s^{-1}$ of freshwater.

The lack of freshwater from the Mississippi River and the loss of the accompanying sediments and nutrients form the most critical problem of the Barataria Basin. Alteration of the natural flow regimes can have significant effects upon the water quality and distribution of living resources in the receiving estuaries. Freshwater is an increasingly limited resource in many areas of the country. Human management of this resource has altered the timing and volume of inflow to some estuaries. Changes in the natural freshwater inflow to estuaries can have significant impacts on the health and distribution of plants and wildlife. Too much or too little freshwater can adversely affect fish spawning, shellfish survival, bird nesting, seed propagation, and other seasonal activities of fish and wildlife. In addition to changing salinity levels, inflow provides nutrients and sediments that are important for overall productivity of the estuary.

Within the Barataria Basin, the freshwater-saltwater gradient can be seen reflected in the change of marsh types from north to south. Fresh marshes are found near Lac des Allemands and Lake Salvador. Intermediate marshes are located immediately south of Lake Salvador. Brackish marshes stretch from near Little Lake to the middle of Bayou Barataria.

Freshwater is contributed to Barataria estuary largely by four sources: rainfall on the water surface, runoff from numerous streams, man-made diversions, and through the Gulf Intercoastal Waterway. Proper management of the system, particularly the diversion structures, requires an understanding of the water movements and mixing processes within the estuary, and how these affect salinity distributions, in response to variations in external forcing and freshwater inputs. Once this understanding is in hand, a secondary benefit will accrue: information concerning the dispersion of sediments, larvae, and pollutants through the system. As a contribution to this understanding, the present dissertation describes a model of the Barataria estuary and interprets the model output.

Estuarine flow can be described by equations, expressing the conservation of heat, salt, mass, momentum, and an equation of state for saltwater. In general terms, these equations form a coupled set of non-linear partial differential equations. There are various methods available for the solution of these equations; recently, numerical modeling has received much attention as a result of the increased computational power and improved numerical methods presently available. A fundamental application of these equations is the prediction of physical processes due to specified inputs, including tidal and salinity variations at the open boundaries, wind forcing patterns, precipitation and evaporation over the model domain, and freshwater runoff as point sources.

In order to understand the physical processes in the Barataria estuary, a previously developed two-dimensional, depth-integrated hydrodynamic model is applied to simulate estuarine processes. This study is focused on examining the impact of freshwater dispersion by controlling the freshwater sources.

2. BACKGROUND

In terms of salinity, Barataria Basin can be divided into two areas, upstream (freshwater) and downstream (salty water). The salinity variability within these regions is strongly dependent upon the hydrodynamics responsible for the advection and dispersion of salt. The tide from the Gulf of Mexico enters the basin through five main passes, which act as the source of salt water for the estuary: Caminada Pass, Barataria Pass, Pass Abel, Quatre Bayou Pass, and Grand Bayou Pass. In the past, based on a 1976 nautical chart, Grand Bayou Pass, which is located 15 *km* east of Quatre Bayou Pass, was not connected to the Barataria Basin system. According to recent satellite images and aerial photos, Grand Bayou Pass is now openly connected to the basin (Figure 2). Another unnamed narrow pass was found to the east of Grand Bayou Pass.

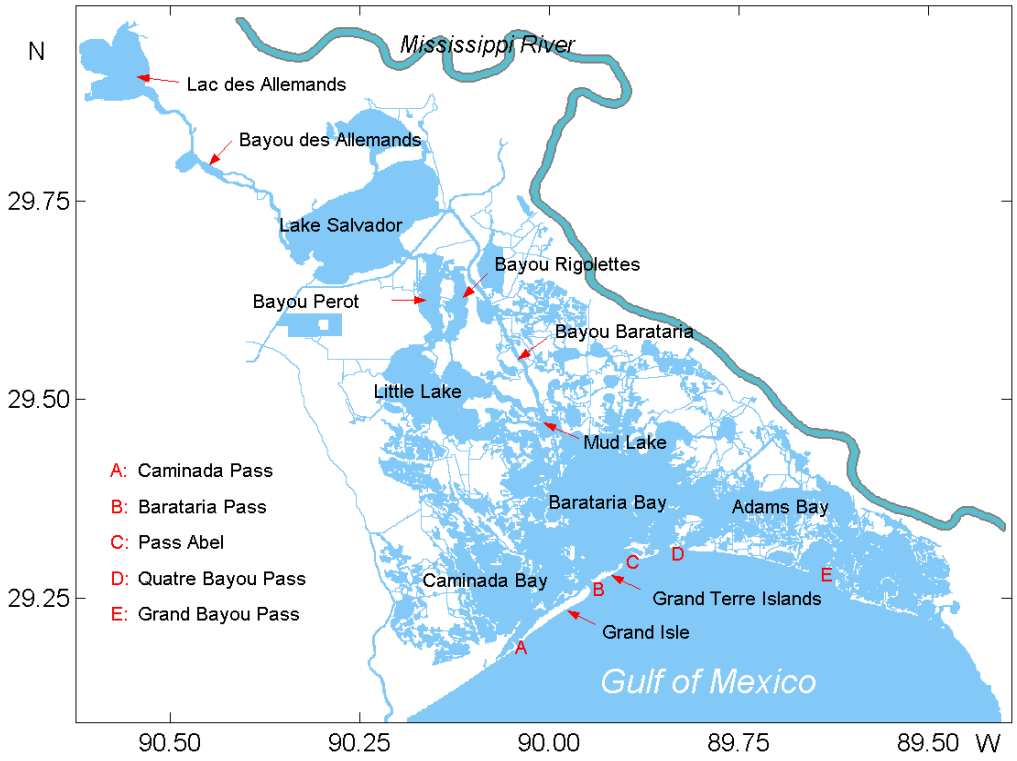

Figure 2. Barataria Basin system including bays, lakes, bayous, and passes.

The total fresh water run-off is largely due to rainfall and agricultural runoff over the Barataria Basin (Marmer, 1954; Kjerfve, 1973; Light et al.; Butler (1975); and Van Sickle et al., 1976). These fresh waters mix with the salty waters, entering the system from the ocean, as they advect and disperse through the estuary, ultimately being flushed to the Gulf of Mexico. There exist a number of historical estimates of flushing time for Barataria Basin. Marmer (1948) estimated 30 % of the waters in Barataria Bay would be replenished each tidal cycle. Kjerfve (1971) estimated a 50 % renewal time for Airplane Lake (in Barataria Basin) over 12 tidal cycles using a method developed by Pritchard (1952b). Wiseman and Swenson (1989) estimated tidal prisms using a formulation by Wood (1979), implying a 90 % renewal time of 40 tidal cycles. Byrne et al. (1976) reported 50 % renewal times with and without wind stress as 12 and 96 cycles, respectively. Recently, Park (1998) estimated the flushing time for several subbasins using particle-tracking techniques assuming that there were no freshwater sources to the basin.

Water exchange within the basin is highly variable. The dominant water exchange route between the upper and lower basin is through Little Lake, Bayou Perot and Lake Salvador. Secondary exchange is through Mud Lake and Bayou Barataria. A chain of barrier islands and barrier beaches separates the basin from the Gulf of Mexico. Barataria Bay proper is the largest of the constituent bodies and possesses the most commodious inlet for the tide from the Gulf of Mexico. Of the other constituent bodies, Caminada Bay has direct contact with the tide of the Gulf of Mexico and also with Barataria Bay proper, while Little Lake receives its tide from and empties drainage waters into Barataria Bay (Marmer, 1947).

Water volume and levels in the Barataria Basin are strongly influenced by astronomical tides, winds, steric effects and precipitation. Further, man-made diversion structures from two sites provide a controlled flow of freshwater from the Mississippi River into the Barataria Basin. Probably another important factor along the Louisiana coast, in terms of the long-term trends in sea level changes, is the effect of subsidence because of the consolidation and compaction of recent deltaic sediments (Byrne et al., 1976). The Davis Pond Freshwater Diversion was constructed to preserve 3145.5 km^2 (777,000 acres) of marsh and bays (Boshart, 1998).

In the northwestern Gulf of Mexico, the sea level, adjusted for barometric pressure variations, exhibits strong semiannual and annual signals. The amplitude of this seasonal signal approaches that of the tidal signal (Wiseman, 1986). Part of this very low frequency variation is due to steric effects, part is due to local Ekman effects over the shelf, and the remainder is suspected of being caused by seasonal variations in the curl of the large-scale wind stress field (Blaha and Sturges, 1981). The range of monthly mean sea level variations at the four main passes, Caminada Pass, Barataria Pass, Pass Abel, and Quatre Bayou Pass, is reported as being 27.8, 34.8, 36.4, and 38.9 *cm*, respectively (Marmer, 1947). The flows responsible for these changes in water level and associated volume of the estuary contribute significantly to the flushing of freshwater from the estuary and the import of salt water.

Tides in this region are small and diurnal (Marmer, 1954). The associated tidal currents also contribute significantly to the exchange of salt between Barataria Basin and the adjacent Gulf of Mexico, as did the lower frequency, atmospherically-driven flows mentioned in the preceding paragraph. Because of their predictability, these tidal flows

are particularly important during the summer months when wind forcing is characteristically weak.

The tidal currents off the Barataria Bay-Caminada Bay complex are characterized by clockwise rotation (Wiseman et al., 1975). Kjerfve (1973) found that during the equatorial tide, the phase rotated counter-clockwise in Caminada Bay. Marmer (1948) suggests characteristic currents for Barataria Pass are 69.5 $cm\,s^{-1}$ (1.35 *knots*) for average flood strength and 68.4 $cm\,s^{-1}$ (1.33 *knots*) for average ebb strength, while Byrne et al. (1976) reported, at maximum ebb, 59.7 $cm\,s^{-1}$ (1.16 *knots*) and, at maximum flood, 45.8 $cm\,s^{-1}$ (0.89 *knots*). The durations of flood and ebb show the latter to be longer, 13.7 hours against 11.1 hours for Barataria Bay (Marmer, 1948). The asymmetry of duration of flood and ebb was attributed to the rain water drainage through the basin (Marmer, 1948; von Arx, 1950). Quatre Bayou Pass was the only pass that exhibited flood domination in duration (Marmer, 1948). Harper (1974) reported two sets of data for Caminada Pass, one for the outer pass and one for the inner pass. The outer pass was characterized by equal maximum flood and ebb currents, while the inner pass was characterized by maximum flood currents of 61.7 $cm\,s^{-1}$ (1.2 *knots*) and maximum ebb currents of 87.5 $cm\,s^{-1}$ (1.7 *knots*). Marmer (1948), however, reported that the velocities of flood and ebb are practically the same as in Barataria Pass. Because of the restricted cross-sectional area, current velocities can be high at the passes, but, in the wider regions in the interior of the Bay, they rapidly diminish (Dyer, 1973). In a narrow channel, the configuration of the channel constrains the movement of the water in one direction on the flood and in the opposite direction on the ebb. Hence in the narrow channels of Barataria Basin, the variations in the direction of the current brought about by wind and weather

may be considered of little importance. In the wider passes and open areas of the bays, the nontidal current, which may be affected by wind forcing, interacts with the tidal current (Marmer, 1954).

One physical factor of great importance to the accurate prediction of currents in these shallow systems is the bottom friction, which is determined by characteristics of the bottom deposits. The bays of southern Louisiana are typically hard bottomed around the periphery with the bottom increasing in softness toward the center (Mackin and Hopkins, 1961). The sediment type distribution in Barataria Bay is described as being predominantly clayey silt. The Gulf side of the bay has higher sand content than that of the north and central regions, which have a siltier character. Clay content in the bottom sediments of Barataria Bay is low (Barrett, 1971).

Another type of bottom found in Barataria Basin is the shell reef. Barataria Bay is an important area for oyster production. Oyster spat require hard surfaces for attachment. Galtsoff (1964) stated that the most valuable type of bottom for oyster culture is firm and stable, composed of rocks and hard sticky mud. Planted shell or clutch placed in areas of relatively high current velocity tend to collect more spat than those placed in low velocity areas (Keck et al. (1973). Oyster larvae concentrations are high where the current is fairly strong and salinity shows no stratification (Perkins, 1952). But the single most important environmental factor affecting oyster populations is salinity (Butler, 1949). Lowered salinities have been directly correlated with increased oyster mortalities. It has been long known that marine bivalves have little power of osmo-regulation when placed in dilute seawater. Even though oysters are euryhaline organisms, with a salinity range of 5 to 40 *ppt*, the optimum salinity range for natural oyster growth and survival in

Louisiana waters is much lower, 5 to 15 *ppt* (Galtsoff, 1964). Therefore most oyster (shell) reefs are limited to the mid-regions of estuaries, away from the low salinity waters of the upper estuaries and the high salinity waters of the lower estuaries. In Barataria Basin the oyster reefs are concentrated in Little Lake, Bayou St. Denis, Grand Bayou, and northern Barataria Bay.

As mentioned above, estuarine water levels can be modified and maintained by a number of different factors other than the astronomical tide, the most obvious being atmospheric pressure gradient and wind stress. Although the major water level fluctuations in Barataria Basin are governed by the diurnal tide at high frequencies, the wind controls the time-averaged estuarine water level on time-scales of a few days. It has long been known that sea level, alongshore wind, and current generally appear to be mutually coherent at time scales where local wind forcing is dominant. A number of authors have studied the influence of wind stress on coastal sea level response (Pickard and Rogers, 1959; Hansen and Rattray, 1965; Kjerfve, 1973; Weisberg and Sturges, 1976; Smith, 1978; Elliott and Wang, 1978; Wang, 1979; Chuang et al., 1982; Chuang and Wiseman, 1983; Hearn, 1987; and Signell et al., 1990). In shallow water, such as in Louisiana coastal areas, the effects of wind stress usually overpowers the effects of the accompanying atmospheric pressure system (Byrne et al., 1976). For example, a strong winter northerly wind (~ 15 $m\,s^{-1}$) imposes a stress of 4 $dynes\ cm^{-2}$ and is associated with observed sea level changes of order 1 *m*. An associated atmospheric pressure change might be from 1013 to 1033 *mb,* which implies an inverse barometer sea level response of 20 *cm*. Strong winds from the south "pile up" water along the coast, forcing water into the estuaries and raising water level about 0.3~0.5 *m* above normal. Conversely, winds

from the north force water out of the estuaries depressing the water levels 0.3~0.5 *m* below normal (Swenson and Turner, 1998). The magnitude of these wind-driven water level variations is commensurate with the astronomical tides (Kjerfve, 1973). This processes appears to be most significant at periods of one to four days. On the Louisiana-Texas shelf, sea level and alongshore wind generally appear to be coherent at slightly longer time scales where local wind forcing is dominant, between 4 and 7 days (Chuang and Wiseman, 1983). Chuang et al. (1982) noted that sea levels on the Alabama shelf are driven by the alongshore wind at time scales longer than a week, but the two signals are generally not correlated at shorter periods. Kjerfve (1973) found that the time-averaged estuarine water level is quite sensitive to changes in wind direction.

The summer weather encountered along coastal Louisiana is usually dominated by the Bermuda High Pressure system, which puts the Louisiana coast under the influence of synoptic winds with southerly and easterly components. The winter, on the other hand, is characterized by a greater percentage of winds out of the east and north. Gutierrez de Velasco and Winant (1996) recently found that the seasonal change of atmospheric parameters could be described in terms of two seasons: fall and winter when frontal incursions dominate the variability, and spring and summer when wave activity can build to tropical storm or even hurricane intensity. A notable lack of westerly wind components is apparent throughout the year. Both September and October represent times of peak tropical storm and hurricane activity, although such storms may occur from June through November.

Salinity studies in coastal areas are common because of the variability and distribution of salinity and its effect on biota and flow regimes (Byrne et al., 1976).

Barrett (1971) and Gagliano et al. (1973) described an inverse relation between Mississippi River flow and coastal salinities in Louisiana. Salinity in Louisiana coastal waters is seasonally variable, fluctuating primarily with seasonal changes in tide, rainfall, river discharge, and evaporation rate (Barrett, 1971). The salinity signal is highly coherent with Mississippi River discharge on time scales of the order of a year (Wiseman and Swenson, 1989). Gagliano et al. (1970) show that average salinities in Barataria Bay vary about 4.5 *ppt*, with 2 *ppt* attributed to surface runoff and 2.5 *ppt* due to Mississippi River discharge entering through the tidal passes. Philomena (1983) reported that mean salinities were fresh in the upper basin and increased toward the coast. Salt wedges and salinity stratification were found to be absent in most of coastal Louisiana's estuaries. Increasing salinity has been widely mentioned as a factor contributing to the loss of coastal wetlands in Louisiana. One natural phenomenon suggested to be responsible is saltwater intrusion. Wetland deterioration, channelization and increased tidal exchange are thought to be primary factors that could result in increased estuarine salinity (Wiseman and Swenson, 1989). Byrne et al. (1976) investigated long-term salinity trends using 14 to 19 years of data at three stations within Barataria Basin. They found that the trends vary in space, but generally, the highest values occurred during September to November, and the spring low had a three-month (February to May) lag between Grand Terre and Bayou Barataria. Recently, Wiseman et al. (1990) studied salinity trends in Louisiana estuaries and concluded that a negative trend in mean salinity was presently occurring at the mouth of Barataria Bay.

A number of hydrodynamic modeling studies of Barataria Bay and/or neighboring regions have been made invoking numerous assumptions and model techniques. Even

though the study was unpublished due to the request of the Freeport Sulphur Company, one of the pioneers of hydraulic model studies for Barataria Bay was von Arx (1950). His results have remained largely unknown; only his procedures for model testing have been known, unofficially. Kjerfve (1973) studied circulation and dynamics in Caminada Bay, using a set of linearized differential equations to investigate time-dependent behavior of the water surface; he found that the simulated slope vector reproduced measured conditions extremely well, as a function of time. The main feature of his model was the input of two perpendicular long waves assumed to represent tidal waves entering the estuary through two different passes. Hacker (1973) developed two-dimensional, time-dependent transport equations to predict velocity profiles, tidal fluctuations, and temperature and salinity profiles. He also introduced an energy transport model to describe temperature distributions and energy transport. He found that the hydrodynamic model and energy transport model accurately predicted the dynamics of tidal fluctuations and velocity profiles and the time-varying temperature distribution, respectively, in the Barataria Bay. Banas (1978) computed salt and momentum balances in Barataria Bay. He assumed that salt is a conservative property and molecular diffusion is negligible. Lateral and longitudinal velocities and salt were tidally averaged, while vertical velocity was assumed zero as a surface boundary condition. He found that the baroclinic pressure gradient and vertical eddy stress gradient were the dominant two forces in the lateral force balance, while the barotropic pressure gradient and Coriolis force prevailed in the longitudinal balance. He also studied circulation patterns using a depth-averaged two-dimensional hydrodynamic model and showed that, while the

general directional trends are similar, the modeled current velocities were approximately half those observed.

3. EVAPORATION AND FRESHWATER SOURCES

3.1 Evaporation

Evaporation is the process by which water is transferred from land and water masses to the atmosphere. Because there is a continuous exchange of water molecules between an evaporating surface and its overlying atmosphere, it is common in hydrologic practice to define evaporation as the net rate of vapor transfer (Viessman et al., 1989). It is a function of solar radiation, differences in vapor pressure between the water surface and overlying air, temperature, wind, atmospheric pressure and the quality of the evaporating water. Since about 70% of the annual precipitation on the land surface of the earth is returned to the atmosphere by evaporation and transpiration, it is clear that evaporation and transpiration are important elements of the hydrological cycle (Raudkivi, 1979).

The controls on evaporation rate may vary with conditions. 1) A supply of water must be present for evaporation to occur, either in the form of falling rain, intercepted rain, or some type of surface-water body. Once the source of supply disappears, then free evaporation ceases. 2) Solar radiation is the dominant source of heat affecting evaporation. In the evaporation process solar radiation warms the water so that it can more readily vaporize and warms the air so that it can hold more water vapor. Solar radiation varies enormously from place to place, and at any one place on both a daily and seasonal basis. 3) Evaporation is dependent on the saturation deficit within an air mass. This is the amount of moisture that can be taken up by the air mass before it becomes saturated. The saturation deficit tends to be higher in inland areas than in coastal regions where air is constantly exposed to the ocean. 4) Wind is an important factor in controlling the rate of evaporation in that it disturbs the water surface, thus increasing the

rate of molecular diffusion, and carries saturated air away from the free water surface. 5) Weather patterns also affect evaporation according to whether these tend to be wet or dry.

Methods used to estimate the amount of evaporation include: 1) measurement by evaporation pan, 2) empirical formulae, 3) water budget methods, 4) mass transfer methods, and 5) energy budget methods (Raudkivi, 1979). Near the Barataria Basin study area, pan measurements are available. Evaporation pan measurement is relatively simple and the results are in reasonably constant ratio to evaporation estimates from large open water surfaces using other techniques. The measurements are relatively consistent from region to region, as well. The rate of pan evaporation depends on the input of energy, chiefly solar radiation. In addition to the solar radiation at the water surface of a pan, there is also a considerable transfer of heat through the wall, which affects the water's temperature and hence its rate of evaporation. Insulating the wall and base reduces evaporation by as much as 29 %. Heat flux through the wall consists partly of radiation, and partly advection by the wind. As regards the extra irradiance, there are four factors: a) exposure of the wall to direct sunshine, b) diffuse radiation from the sky onto the wall, c) solar radiation reflected onto the wall from the ground around, and d) longwave radiation from the surroundings. All this additional heating more than offsets the reduction of evaporation due to the albedo of a pan being about 14%, instead of 7% for water (Linacre, 1994). Pans located above ground exhibit heat exchange problems related to side walls and bottom, but these difficulties may be overcome by the use of insulation (Viessman et al, 1989).

Figure 3(a) shows measured evaporation at Houma station. The measured evaporation using a class A Pan at Houma, however, is only available as a daily

measurement while all other data in the model simulation are hourly data. Therefore, the empirical formulae method was used for this study, which has been well developed for the Gulf coastal regions. The regional average evaporation is dependent primarily upon the energy available and vapor pressure gradients above the evaporating surface.

Latent heat flux occurs as a result of the transfer of water vapor from the ocean to the atmosphere. This flux, H_l, is estimated as (Roll, 1965)

$$H_l = L_T E = L_t C_E \rho (q_{sea} - q_{air}) U_{10}$$

where L_T is the latent heat of vaporization, E is the evaporation rate, C_E is the latent heat coefficient, ρ is the air density, q_{sea} and q_{air} are the specific humidities for the sea and air, respectively, and U_{10} is wind speed at the 10 m reference height.

At the sea surface, the specific humidity, q_{sea}, is related to the saturation vapor pressure, e_{sea}, through (Hsu, 1988)

$$q_{sea} = 0.62(e_{sea} p^{-1})$$

where, $e_{sea} = 6.1078 \times 10^{[7.5T_{sea}/(237.3+T_{sea})]}$, p is atmospheric pressure, and T_{sea} is the sea surface temperature (^{o}C). Similarly,

$$q_{air} = 0.62(e_{air} p^{-1})$$

where, $e_{air} = 6.1078 \times 10^{[7.5T_{dew}/(237.3+T_{dew})]}$, and T_{dew} is the dew-point temperature (^{o}C).

Since we are dealing with heat loss from the sea to the air, the following values are used in our computations: $C_E = 1.12 \times 10^{-3}$ (Smith et al., 1994); $\rho = 1.2 kg\ m^{-3}$, and $L_T = 2.5 \times 10^{5} J\ kg^{-1}$ (Hsu, 1988). Note that a latent heat flux of $1 W\ m^{-2}$ is equivalent to an evaporation rate of $3.56 \times 10^{-3} cm\ day^{-1}$ (Colon, 1963).

Hourly measurements of atmospheric pressure, wind speed, sea surface temperature, and dew-point temperature were available from GDIL1 station. In 1999, a dry year, the total amount of evaporation estimated using the GDIL1 data was about 124 *cm*, which exceeded the total Class A Pan measured by nearly 10 *cm*. Figure 3(b) shows the estimated evaporation time series using GDIL1 station data. Evaporation was generally higher than the mean for the year 1999, with small variation, in summer. It was generally lower than the mean, but highly variable with several-day time scales, during the other seasons. Even though the estimated annual mean, 0.34 $cm\ day^{-1}$, is slightly higher than the measured mean, 0.32 $cm\ day^{-1}$, there are some seasonal differences. It is notable that the measurement value is slightly higher on average during summer and exhibits lower fluctuations during the other seasons than the estimated evaporation rate due to several reasons. It has been found that cold fronts are the meteorological forcing agents affecting many air-sea interaction mechanisms, including evaporation and heat loss to the atmosphere from the Gulf of Mexico (e.g., Henry, 1979; Huh et al., 1984; Hsu, 1997).

Butler (1975) demonstrated that the low discharge into Lac des Allemands in July and August is the result of two different phenomena. Evapotranspiration normally exceeds rainfall during the summer, so swamp drainage, the major hydrologic input to the lake and bayous, is reduced. Furthermore, during the summer, Ekman convergence due to the prevailing southeasterly winds retards the flow of water from Bayou des Allemands. The flow is further retarded during the day because of the sea breeze effect. At night the flow direction is typically reversed in a gulfward direction due to the land breeze effect. These tendencies are, of course, modulated by tides.

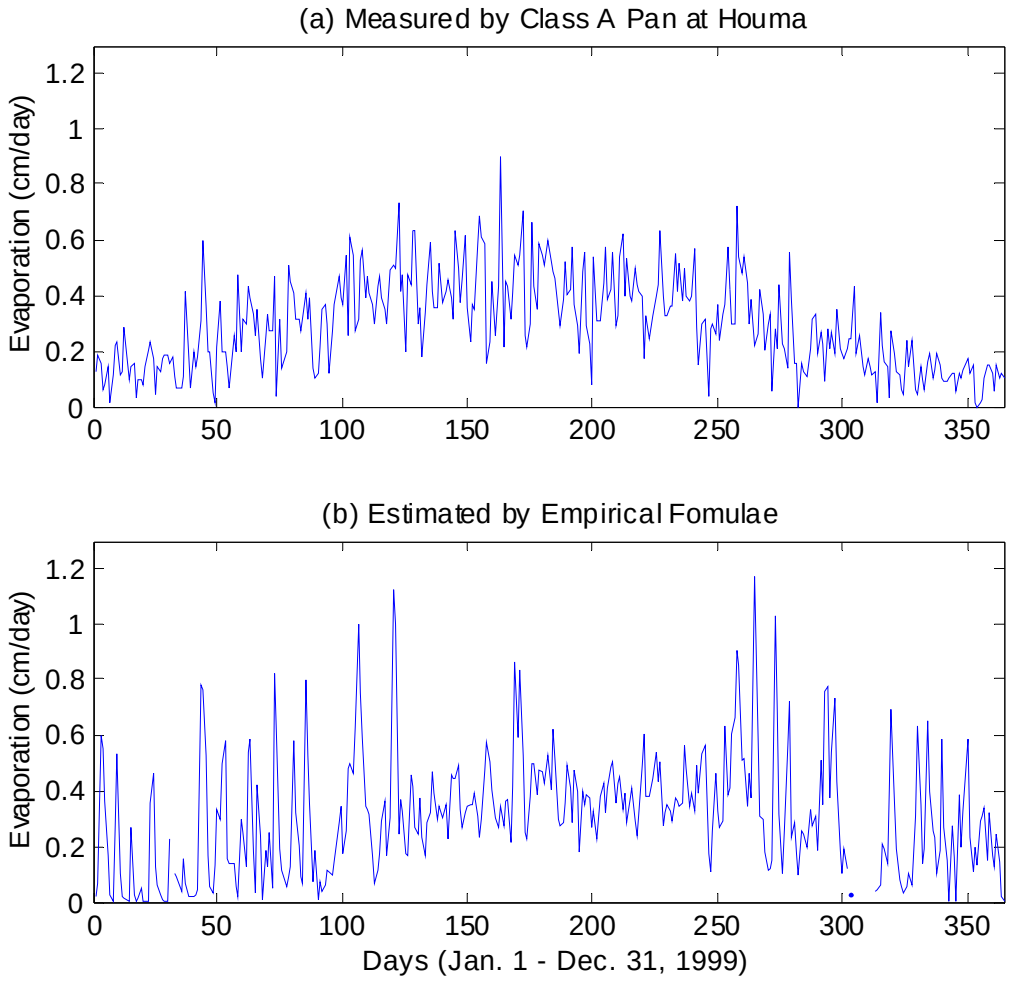

Figure 3 (a) and (b). Measured evaporation at Houma (a) and estimated evaporation rate time series in 1999 from GDIL1 station (b).

As noted above, many factors affect evaporation rate such as wind speed, air pressure, water temperature, and dew point temperature. Coherence squared was used to estimate the relationships between evaporation and other parameters. Estimates were averaged over 30 frequencies, giving 60 degrees of freedom, with 95% significance level of 0.098 (Figure 4). As was expected from the empirical formula used estimated evaporation, the coherence between evaporation and wind speed is significant at all frequencies. It is notable that the coherence is relatively high, near one cycle per day for all factors.

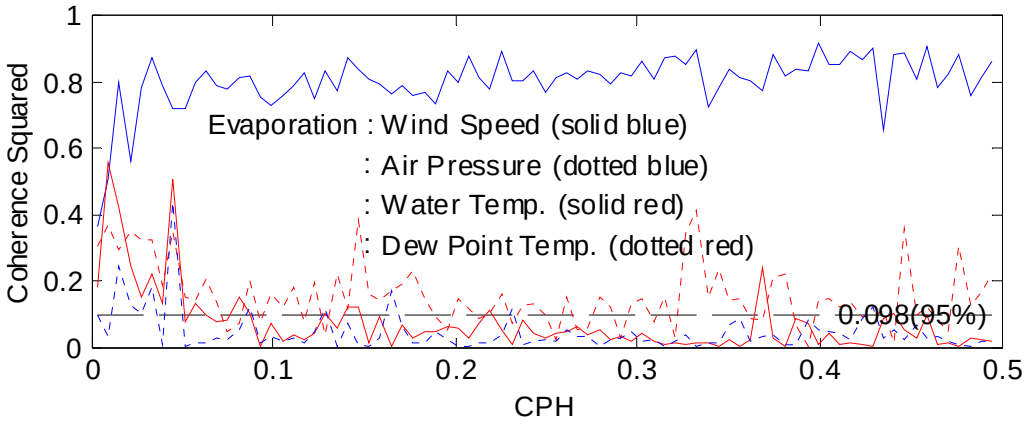

Figure 4. Coherence squared between evaporation rate and wind, atmospheric pressure, water temperature, and dew point temperature.

3.2 Freshwater Sources and Their Applications

Runoff enters the Barataria Bay estuarine system through a complex series of coastal swamps and wetlands, mostly from local precipitation. On a long-term (1961-1990) annual basis, precipitation over coastal Louisiana exceeds evaporation. Annual mean precipitation for the 30 years was reported as 160 *cm* (Baumann, 1987). In 1999, however, total precipitation was recorded as 114 *cm* due to the prolonged impact of the 1997-1998 El-Nino Southern Oscillation event. The salinity distribution in the estuary is a strong function of freshwater from various sources. Estuarine salinity decreases during periods of high runoff as the freshwater-saltwater interface moves down the estuary toward the sea, and it reverses when runoff decreases.

There are several previous studies of runoff from land in Barataria Basin. Light et al. (1973) developed a hydrologic model to analyze freshwater flow in the Barataria area using the watershed management unit method. This model used precipitation, evapotranspiration, and physiographic data to calculate annual discharge from Bayous

Chevreuil, Boeuf, and des Allemands. The investigators also developed a mean annual precipitation map based on a long-term record (1945-1970), and found mean annual rainfall excess values of more than 50.8 *cm* (20 inches) in the upper-basin watershed. Similarly, Gagliano et al. (1973) modeled runoff from land and freshwater inputs to water bodies using the cell method and assuming water losses from the water surface, both open and vegetation-covered. They computed the mean geographical distribution of freshwater flow over the basin. Wax et al. (1978) produced a water budget based on climatic conditions to estimate periods of freshwater surplus and deficit for the Barataria Basin system.

Butler (1975) studied the characteristics of freshwater discharge and the drainage area near Lac des Allemands. He indicated that the freshwater inflow into Lac des Allemands was 42~54 $m^3 sec^{-1}$ under average flows and ~80 $m^3 sec^{-1}$ under peak flow conditions. Wiseman and Swenson (1989) pro-rated this number to give a total runoff into the basin ~150 $m^3 sec^{-1}$. Muller (1975) estimated that the freshwater input to the Barataria Basin was $12 \times 10^6 m^3$ per tidal cycle or 266 $m^3 sec^{-1}$. Howard (1982) estimated that the total precipitation over Barataria Basin was $21 \times 10^6 m^3$ per tidal cycle. Sklar (1983) produced an annual water budget for the upper portions of the Barataria Basin system based upon data from 1914 through 1978 and estimated that 40 % of the precipitation was available for runoff. His results showed that most of the surplus of freshwater occurred in winter, with deficits of freshwater most likely to occur during the summer. He also noted that deficits should not be expected to occur regularly, because precipitation is usually greater than evaporation. Recently, Swenson and Turner (1998) calculated a water budget using the 28-year average (1960~1988) of precipitation and

found similar results to these of Sklar. For this study, freshwater input by rainfall was estimated simply by multiplying total amount of rainfall by the total drainage area. The long-term average rainfall is known to be $160\,cm$, and the total drainage area is about $4{,}400\,km^2$. Therefore, the freshwater input into the basin is $4{,}400\,km^2 \times 1.6m\ year^{-1} = 1.15\times10^6\,m^3$ per tidal cycle or $223\,m^3 sec^{-1}$, of which 25 percent flows to Lac des Allemands, which is comparable to some of the previous results.

Data on hydrologic variables are fundamental to analysis, forecasting, and modeling simulation of hydrology. Freshwater over Barataria Basin is contributed largely by four sources:

1) rainfall on the open water surface,
2) runoff of rainfall to the surrounding drainage basins,
3) man-made freshwater diversions; Naomi Freshwater Diversion and West Pointe à la Hache Freshwater Diversion from the Mississippi River, and
4) the Gulf Intercoastal Waterway as a conduit of freshwater from the Atchafalaya River, a major distributary of the Mississippi River (Table 1, Figure 5).

Table 1. Freshwater Sources in Barataria Basin system

Freshwater Sources	Location	Amount ($m^3 sec^{-1}$)
Rainfall	Rainfall on Water Surfaces	Variable with Rainfall
Runoff by Rainfall from Various Streams	64 Known Streams	Variable with Rainfall and Drainage Area
	522 Unknown Streams	
Diversion from Mississippi River	Naomi	60 at Maximum
	West Point a La Hache	60 at Maximum
Gulf Intercoastal Waterway	From West of Basin	50 on Average

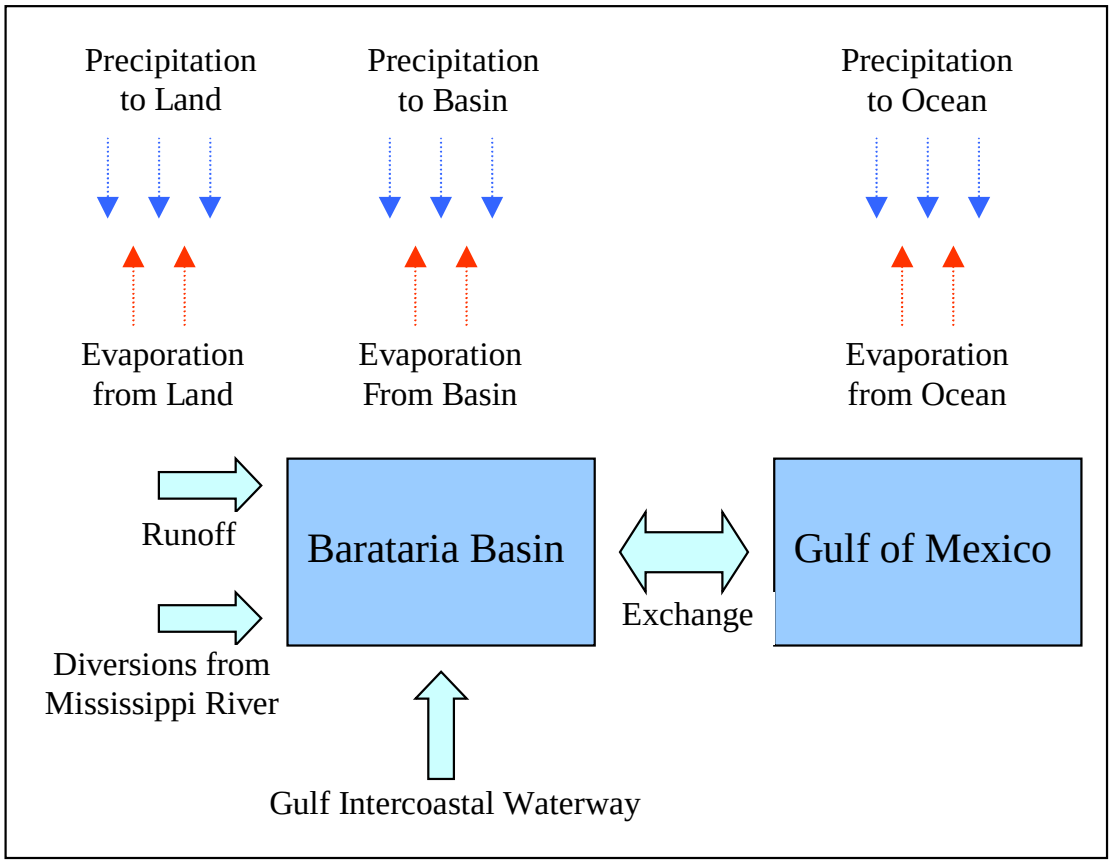

Figure 5. Major hydrologic variables in Barataria Basin.

Diversion structures provide a controlled flow of freshwater and nutrients from the Mississippi River into a target area in Barataria Basin. The essential goals of freshwater diversions were to manage the productivity of wildlife and fishery resources by controlling salinity and to maintain marsh elevation by introducing additional freshwater and sediments to the marsh (Roberts et al., 1992). Two freshwater diversions, Naomi and West Pointe à la Hache, currently exist along the Mississippi River. The Naomi project area contains approximately 13,000 acres (5,261 ha) of intermediate and brackish marsh. The West Pointe à la Hache project area contains approximately 9,300 acres (3,764 ha) of open-water and 7,600 acres (3,076 ha) of brackish marsh. Another diversion site, Davis

Pond, was recently opened with a maximum design-pumping rate of $300\,m^3\,s^{-1}$ of freshwater to preserve about 33,000 acres (13,354 ha) of marsh and benefiting 777,000 acres (31,444 ha) of marshes and bays (Boshart, 1998).

Water flow in the Barataria Basin is often controlled by man-made navigation and drainage canals. Perhaps the best example is the Gulf Intercoastal Waterway. The Gulf Intercoastal Waterway is a coastal waterway route extending from Apalachee Bay, Florida to the Mexican border. As part of the Intercoastal Waterway system, the Gulf Intercoastal Waterway provides a practical navigation route along the coast of the Gulf of Mexico. Within Louisiana, the Gulf Intercoastal Waterway extends along the coast of the Gulf of Mexico from Lake Borgne to the Sabine River, a distance of 432 *km*. The Gulf Intercoastal Waterway is a conduit of freshwater and sediments to coastal Louisiana. The amount of freshwater and sediments introduced to coastal wetlands depends on the difference in head between the Lower Atchafalaya River and surrounding waters. The Lower Atchafalaya River varies in stage from year to year, depending upon what happens in the basin of the Mississippi River and Red River (Swarzenski et al., 1999). They found that the relationship with Larose water level and discharge in the Gulf Intercoastal Waterway, although positive, was less than linear. Water level 1.2 *m* above mean sea level at Larose is critical in terms of transport direction. For this study, long-term average flow, 50 $m^3 s^{-1}$, in the Gulf Intercoastal Waterway from west of the Barataria Basin was assumed as a constant volume flux.

Since the amount of freshwater from diversions and the Gulf Intercoastal Waterway is controllable or almost constant, rainfall is the primary concern with respect to freshwater supply. The rate of precipitation is defined as the total accumulated volume

per unit of time. Precipitation, as a function of time, is highly variable (Figure 6). Likewise, the distribution of precipitation in space is not uniform. Thus, in addition to an interpolation of rainfall volumes in time to produce the storm profile, it may also be necessary to interpolate in space, since rain gauge measurements represent only single point measurements. Figure 6 shows examples of the daily precipitation record at New Orleans Moisant Airport (MSY) and the Grand Isle C-MAN (GDIL1) station. Although the distance between the two sites is only about 80 *km*, the correlation coefficient is low ($r^2 = 0.34$) and appears to vary seasonally.

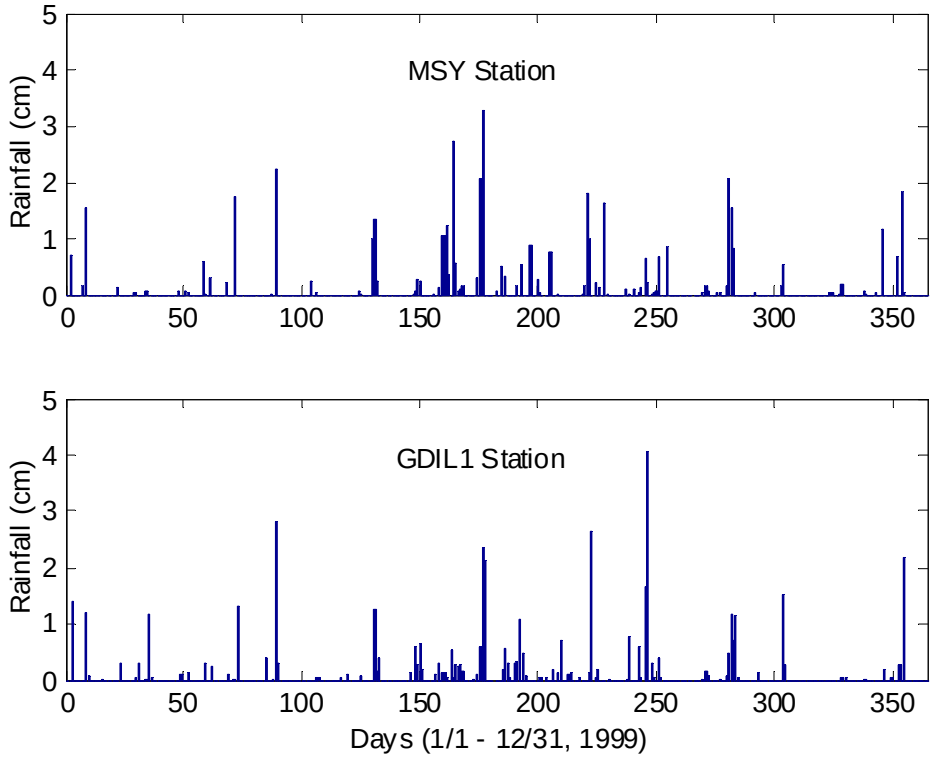

Figure 6. Daily precipitation at MSY (upper) and GDIL1 ($r^2 = 0.34$).

Runoff modeling depends on the records from single point rain gauges, some of which provide estimates of rainfall intensities in time steps of one hour or better, while others provide daily estimates. In large catchments, models using a daily time step may

be adequate for applications. In small catchments, a daily time step may be longer than the storm response time of the catchment and finer time resolution may be required (Beven, 2000). There were five sites where precipitation records were available near Barataria Basin. For this study, however, the precipitation record from MSY was used for the following reason. The dominant upstream regions which account for 61% of total land are best represented by MSY station. In addition, MSY was the only station where rainfall was measured at hourly intervals. Therefore, a uniform spatial distribution of precipitation over the entire domain was assumed based on the measurement at MSY station.

The water that contributes to streamflow may reach the stream channel by any of several paths from the point where it first reaches the ground as precipitation. The rainfall-produced runoff enters the system through a complex series of coastal swamps and wetlands, providing a mechanism for the slow release of fresh water over large wetland areas. The primary physical characteristics of the drainage basin are its area, shape, elevation, slope, orientation, soil type, drainage channel system, water storage capability and vegetal coverage (Raudkivi, 1979). Some water flows over the soil surface as surface runoff and reaches the stream soon after its occurrence as rainfall. Other water infiltrates through the soil surface and flows beneath the surface to the stream. The groundwater contribution to streamflow cannot fluctuate rapidly because of its very low flow velocity.

Because the relation between precipitation and runoff is influenced by various storm and basin characteristics, usually many approximate formulas are used to relate rainfall and runoff. Since most of the land area for the Barataria Basin is less than 1.5 meters

above mean sea level (Gagliano, 1973) and covered with wetland that is saturated by water, no groundwater flow is assumed. Only surface flow is considered significant and is incorporated into the model. In many environments, evapotranspiration is as significant a contribution to the water balance as stream discharge. Thus, for extended periods of runoff simulation, it will be necessary to estimate actual evapotranspiration losses from a catchment area. However, due to the relatively small drainage areas considered here, resulting in relatively quick runoff and short periods of simulation, transpiration was ignored for this study. As a result, the following simple model was adapted to relate rainfall to runoff for any drainage basin,

$$\text{Runoff } (m^3 hour^{-1}) = (\text{Rainfall} - \text{Evaporation})(m\ hour^{-1}) \times \text{Area } (m^2).$$

Definition of runoff catchment areas is one of the real challenges in modeling estuarine hydrology in South Louisiana. The availability of discharge data is important for the model calibration process. Streamflow rates may be determined from stream stage data calibrated using measurements of velocity and cross-sectional area. Butler (1975) estimated discharge rate, using this method, for two main streams, Bayou Chevreuil and Bayou Boeuf, draining into Lac des Allemands. Discharge data are, however, generally available at only a small number of sites in any region. Runoff modeling for sites where there are no available discharge data is a difficult task. Barataria Basin has numerous known or recognizable, as well as unknown, streams that vary considerably in size and length. It is impossible to install gauges to measure all their discharges. Even though most small streams are not immediately discernible on a map, one can assume that there should be runoff from all subaerial land.

In order to estimate the discharge rate from unknown and ungauged streams, the basin was divided into twenty-two watershed management units using a pre-existing watershed chart (A Digital Map of the State). The area of each watershed management unit was estimated (Figure 7). Each area segment contains land and water surface. Since the hydrodynamic model that was previously developed for shallow water accounts for freshwater input due to direct rainfall on the water surface separately, runoff estimates should only account for precipitation over land. Therefore, the area of water surface was subtracted from each watershed unit area. Based on a minimum two square kilometers of land area, at least 1 stream was arbitrarily specified for unknown streams. Known streams were also associated with drainage areas (Figure 8). Most unknown drainages are smaller than nine square kilometers. The length of unknown streams was estimated by assuming that all drainages are semi-circular in shape (length= $\sqrt{2 \times area / pi}$).

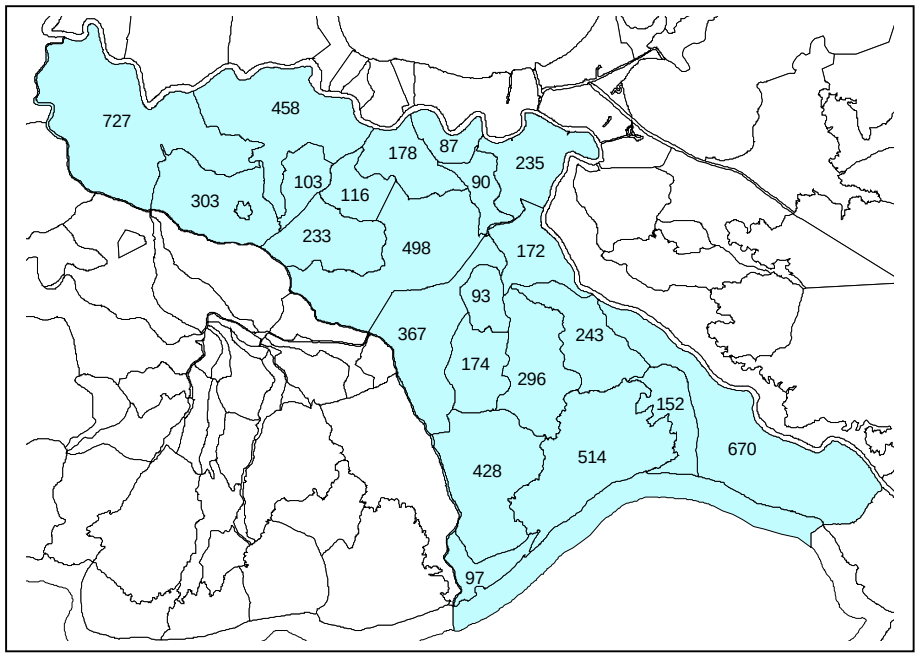

Figure 7. Twenty-two watershed management units of Barataria Basin. The numbers on the map are the area of each subbasin in km^2.

The persistence time is defined as the time required for surface runoff to flow from the most remote point in a subbasin or subwatershed to the outlet (Walesh, 1989). All drainages were categorized based on their size and estimated persistence time (Table 2). The longest drainage system, Bayou Chevreuil (26 *km*), was known to have a 3-day (72 hours) persistence time. Other streams' persistence times were estimated by a linear extrapolation relative to the longest stream's persistence time.

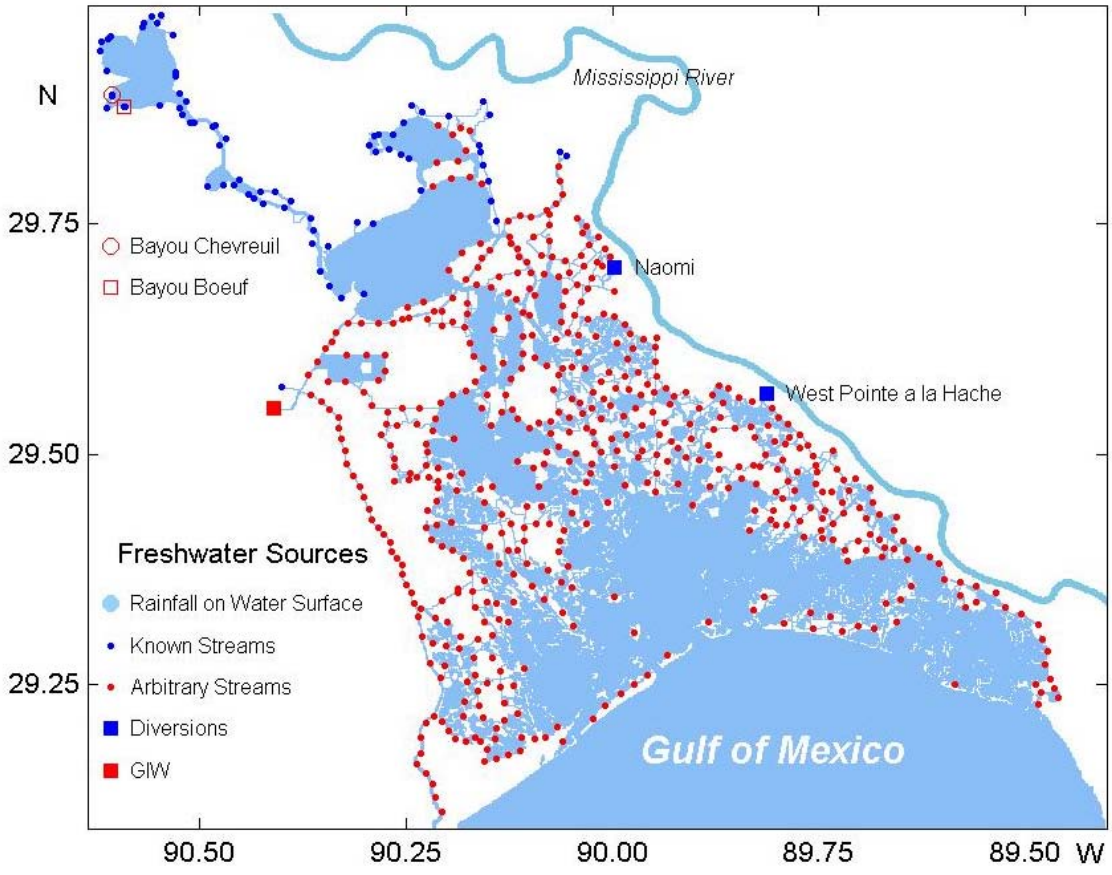

Figure 8. Freshwater sources for the Barataria Basin.

Table 2. Drainage types and their estimated drainage length and persistence time

Drainage Types	1*	2*	3*	4	5	6	7	8**
Drainage Size (km^2)	2	3-4	5-8	9-16	17-32	33-64	228	672
Drainage Length (km)	1.1	1.5	2.1	2.8	4.0	5.6	11.5	26.0
Persistence Time (Hour)	3.1	4.2	5.8	7.8	11.0	15.5	32.0	72.0
Number of Streams	373	124	25	32	26	4	1	1
Sub Total Area (km^2)	746	496	164	424	616	202	228	672

* unknown length of drainages
** known persistence time of drainage

Streamflow, at a given location on a watercourse, is represented by a hydrograph. The hydrograph produced in a stream is the result of various hydrologic processes that occur during and after any precipitation event. This continuous graph displays the properties of streamflow with respect to time, normally obtained by means of a continuous recorder that shows stage versus time, and then transformed into a discharge hydrograph by applying a rating curve. The shape of a hydrograph depends on precipitation pattern and characteristics and basin properties (Viessman et al., 1989). A stream's behavior is greatly affected by the characteristics of its watershed. For instance, the steadiness of the stream's flow at a given point is controlled by the area of the watershed upstream of the point. Typically, during a rainfall event, the hydrograph of an undisturbed stream rises fairly rapidly, and after reaching a peak value, falls off rather gradually. Streams differ from one another in many features besides area, though.

A complete analysis of the relation between rainfall and runoff, determining the characteristic shape of hydrographs for a basin, involves a knowledge of the basin's physical, vegetative, and climatic characteristics, all of which affect the quantity of streamflow generated in a drainage basin. These parameters are not well known for the

Barataria Basin. Another, simpler methodology must be employed for estimating the relationship between rainfall and runoff for the various sub-basins discharging into the Barataria Bay estuary.

The unit hydrograph, expected in response to a unit input of rainfall per unit area of marsh, may be considered to consist of three general parts: 1) the rising limb or concentration curve, 2) the crest segments, and 3) the recession curve or falling limb. Generally, the falling limb lasts longer than the rising limb, skewing the curve to the right. In order to estimate the total volume runoff entering the estuarine system, such a hydrograph should be multiplied by the amount of precipitation and the area of the sub-basin.

The impulse response of a Butterworth filter of order 2 has a shape that is very similar to that of the desired hydrograph described in the proceeding paragraph. The filter takes the form

$$Y(t)=[b(1)x(t)+b(2)x(t-1)]/[a(1)Y(t-1)+a(2)Y(t-2)]$$

Where x(t) is rainfall per unit time per unit area and Y(t) is the resultant discharge from the sub-basin. The a's and b's are the filter coefficients. By selecting a cutoff frequency equal to 1.4 divided by the persistence time of the sub-basin, the effective runoff is limited to the persistence time. In order to eliminate unrealistic negative runoff values, the negative lobes of the filtered rainfall signal were hard-limited to zero. The small errors introduced by this procedure (a few percent) should not be significant when compared to the errors introduced by the necessity of assuming that the spatial distribution of rainfall is adequately represented by the gauge at Moisant airport.

The unit hydrographs used in this study were determined using MATLAB © (Figure 9). For the present study, estimating total runoff volume is more important than the details of the hydrographs. The slight differences in persistence time between sub-basins do not result in a significant change in the system response except for the relatively long streams, Bayou Chevreuil and Bayou Boeuf (type 7 and 8, respectively), which contribute almost 25 percent of freshwater to the Barataria Basin system.

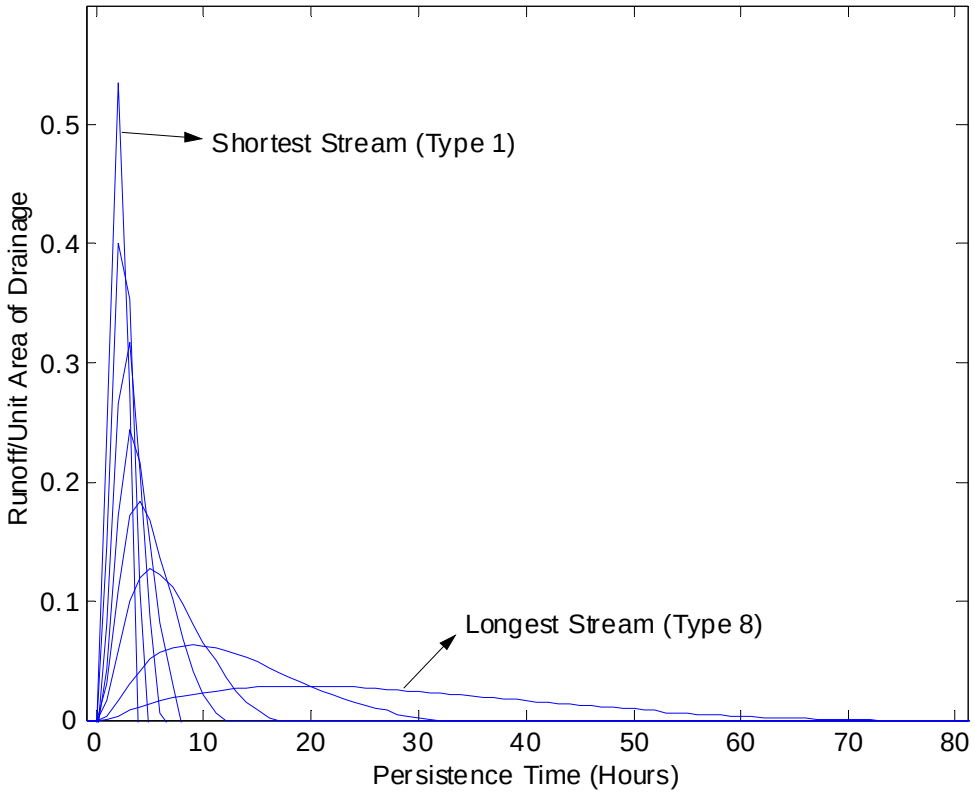

Figure 9. The results of each type's runoff features by one-side filtering for the length of persistent time. The hydrographs area under the curve represent the sum of 1 *cm* precipitation.

3.3 Glossary

watershed – land area from which water drains toward a common watercourse in a natural basin

hydrograph – a graph of stage or discharge versus time

catchment – catching or collecting of water, especially rainwater. The area drained by a river or body of water

rising limb – the rising portion of a hydrograph

crest segment- the curve in the vicinity of the peak

recession curve- falling portion of a hydrograph

4. NUMERICAL MODEL FORMULATION

4.1 Background

In estuarine studies, it has been customary to work with the equations of motion and continuity to predict circulation and mixing patterns. A depth-integrated two-dimensional model of estuarine circulation is adapted to Barataria Basin with the aim of being able to simulate flushing, mixing, dispersion, and circulation. It was assumed that use of two-dimensional depth-integrated equations for conservation of mass and momentum was adequate, considering the typically well-mixed water column and due to wind and tidal stirring of the system (Inoue et al., 1998). In this chapter, an enhancement of the hydrodynamic model to include baroclinic pressure gradient is described. The model used here is based on the model initially developed for other neighboring estuaries including Terrebonne-Timbalier Basin (Inoue and Wiseman, 2000), Fourleague Bay (Wiseman and Inoue, 1994), as well as Barataria Basin (Park, 1998).

One of the novel features of the present enhancement of the model is the incorporation of a very accurate advection scheme. Traditionally, a simple centered-difference scheme has been used for advective transport in hydrodynamic models. This scheme induces so-called numerical dispersion, which causes nonphysical spatial oscillation in the tracer field (Hasumi and Suginohara, 1999). These oscillations could be damped out by using a large diffusion coefficient. However, as the model grid size is reduced to resolve finer and finer spatial scales, the use of large diffusion coefficients is no longer justified. Some hydrodynamic models adopt the upstream or the weighted upstream scheme for advective transport (e. g., Maier-Reimer et al., 1993). These schemes do not induce nonphysical oscillation. Instead, their accuracy is lower than that of the centered differencing scheme

and the effect of the error is to enhance diffusion. Several schemes have been developed that have little numerical dispersion and a higher order of accuracy compared with the centered differencing scheme. One of the most accurate schemes to date is the flux corrected transport (FCT) scheme of Boris and Book (1973). However, the FCT scheme could double computational costs compared to the centered-differencing or the upstream schemes (Gerdes et al., 1991). There are some less expensive alternative schemes: the Uniformly Third-Order Polynomial Interpolation Algorithm (UTOPIA; Leonard et al., 1993), the Quadratic Upstream Interpolation for Convective Kinematics (QUICK; Leonard, 1979) and the Multidimensional Positive Definite Advection Transport Algorithm (MPDATA; Smolarkiewicz, 1984). They have the same or higher order of accuracy when compared with the centered differencing scheme and exhibit little numerical dispersion. Recently, Inoue et al. (2001) applied an advection scheme by Hsu and Arakawa (1990) (hereafter referred to as the Hsu-Arakawa scheme), that was based on the Takacs scheme (1985). This scheme is an upstream scheme; however, this scheme completely eliminates unrealistic negative values, and its computational cost is reasonable. The description of the numerical model formulation being presented here comes from Inoue et al. (2001).

4.2 Numerical Model Formulation

The model equations for conservation of mass and momentum, written in Cartesian coordinates in terms of depth-integrated transport, including the baroclinic pressure gradient (e. g., Leendertse, 1967; Elliott and Reid, 1976) are:

$$\frac{\partial U}{\partial t} + \frac{\partial}{\partial x}\frac{U^2}{H} + \frac{\partial}{\partial y}\frac{UV}{H} - fV = -gH\frac{\partial \zeta}{\partial x} - \frac{1}{2}gH^2\frac{\partial \rho}{\partial x} - g\frac{\frac{U}{H}\left\{\left(\frac{U}{H}\right)^2 + \left(\frac{V}{H}\right)^2\right\}^{\frac{1}{2}}}{C^2} + \frac{\tau_x}{\rho} + A\nabla^2 U$$

$$\frac{\partial V}{\partial t} + \frac{\partial}{\partial x}\frac{UV}{H} + \frac{\partial}{\partial y}\frac{V^2}{H} + fU = -gH\frac{\partial \zeta}{\partial y} - \frac{1}{2}gH^2\frac{\partial \rho}{\partial y} - g\frac{\frac{V}{H}\left\{\left(\frac{U}{H}\right)^2 + \left(\frac{V}{H}\right)^2\right\}^{\frac{1}{2}}}{C^2} + \frac{\tau_y}{\rho} + A\nabla^2 V$$

$$\frac{\partial \zeta}{\partial t} + \frac{\partial U}{\partial x} + \frac{\partial V}{\partial y} = 0$$

$$\frac{\partial HS}{\partial t} + \frac{\partial HS}{\partial x} + \frac{\partial HS}{\partial y} = D_S\left(\frac{\partial H\frac{\partial S}{\partial x}}{\partial x} + \frac{\partial H\frac{\partial S}{\partial y}}{\partial y}\right)$$

$$\frac{\partial HT}{\partial t} + \frac{\partial HT}{\partial x} + \frac{\partial HT}{\partial y} = D_T\left(\frac{\partial H\frac{\partial T}{\partial x}}{\partial x} + \frac{\partial H\frac{\partial T}{\partial y}}{\partial y}\right)$$

where $U = \int_h^\zeta u dz$

$V = \int_h^\zeta v dz$

$H = h + \zeta$

$S = \frac{1}{H}\int_h^\xi s dz$

$\mathrm{T} = \frac{1}{\mathrm{H}}\int_{\mathrm{h}}^{\xi}\theta \mathrm{dz}$

where *t* denotes time, *x*, *y*, and *z* are Cartesian coordinates, *u* and *v* denote velocity components in the direction of *x* and *y*, respectively, ζ is the elevation of the free surface above mean sea level, *h* is the undisturbed depth of the water, *f* is the Coriolis parameter (assumed to be a constant), *g* is the acceleration due to gravity, τ_x and τ_y are the *x* and *y* components of wind stress, respectively, ρ is the density of water, *A* is the horizontal eddy

viscosity, and s and θ are salinity and temperature, respectively. D_S and D_T are horizontal eddy diffusivities for *S* and *T*, respectively, and *C* is the Chezy coefficient, which is depth dependent. The bottom roughness is introduced through Manning's n coefficient, such that the Chezy coefficient is evaluated as

$$C = \tfrac{1}{n} H^{\frac{1}{6}}$$

The model equations are subjected to boundary conditions to complete the model formulation. At land boundaries, no normal flow and no-slip boundary conditions are used.

The following equation of state, by UNESCO (1981), relating temperature and salinity to density (g/cm^3) of seawater is adopted.

$$\begin{aligned}\rho &= 999.842594 + 6.793952\times10^{-2}T - 9.095290\times10^{-3}T^2 + 1.001685\times10^{-4}T^3 \\ &- 1.120083\times10^{-6}T^4 + 6.536332\times10^{-9}T^5 \\ &+ S(0.824493 - 4.0899\times10^{-3}T + 7.6438\times10^{-5}T^2 - 8.2467\times10^{-7}T^3 + 5.3875\times10^{-9}T^4) \\ &+ S^{3/2}(-5.72466\times10^{-3} + 1.0227\times10^{-4}T - 1.6546\times10^{-6}T^2) + 4.8314\times10^{-4}S^2\end{aligned}$$

where *S* = salinity (parts per thousand)

T = temperature (centigrade)

The model equations are discretized into a finite-difference formulation on the staggered mesh grid C of Arakawa (Mesinger and Arakawa, 1976; Figure 2). The numerical scheme adopted here is the Grammeltvedt C scheme (Grammeltvedt, 1969), which conserves mass and total energy. A Leapfrog scheme is used for time integration with an Euler scheme inserted at regular time steps to eliminate the computational mode due to the central time differencing. The frictional terms are lagged in time for numerical stability. The resulting finite difference forms of the momentum and continuity equations are:

$$\frac{U_{i,j}^{n+1}-U_{i,j}^{n-1}}{2\Delta t}=-\frac{1}{\Delta s}\left[\begin{array}{l}\frac{1}{2}(U_{i+1,j}^{n}+U_{i,j}^{n})\times\frac{1}{2}\left\{\frac{U_{i+1,j}^{n}}{\frac{1}{2}(H_{i+2,j}^{n}+H_{i+1,j}^{n})}+\frac{U_{i,j}^{n}}{\frac{1}{2}(H_{i+1,j}^{n}+H_{i,j}^{n})}\right\}\\ -\frac{1}{2}(U_{i,j}^{n}+U_{i-1,j}^{n})\times\frac{1}{2}\left\{\frac{U_{i,j}^{n}}{\frac{1}{2}(H_{i+1,j}^{n}+H_{i,j}^{n})}+\frac{U_{i-1,j}^{n}}{\frac{1}{2}(H_{i,j}^{n}+H_{i-1,j}^{n})}\right\}\end{array}\right]$$

$$-\frac{1}{\Delta s}\left[\begin{array}{l}\frac{1}{2}(V_{i+1,j}^{n}+V_{i,j}^{n})\times\frac{1}{2}\left\{\frac{U_{i,j+1}^{n}}{\frac{1}{2}(H_{i+1,j+1}^{n}+H_{i,j+1}^{n})}+\frac{U_{i,j}^{n}}{\frac{1}{2}(H_{i+1,j}^{n}+H_{i,j}^{n})}\right\}\\ -\frac{1}{2}(V_{i+1,j-1}^{n}+V_{i,j-1}^{n})\times\frac{1}{2}\left\{\frac{U_{i,j}^{n}}{\frac{1}{2}(H_{i+1,j}^{n}+H_{i,j}^{n})}+\frac{U_{i,j-1}^{n}}{\frac{1}{2}(H_{i+1,j-1}^{n}+H_{i,j-1}^{n})}\right\}\end{array}\right]$$

$$+f\times\frac{1}{4}(V_{i+1,j}^{n}+V_{i+1,j-1}^{n}+V_{i,j}^{n}+V_{i,j-1}^{n})$$

$$-\frac{g}{2}(H_{i+1,j}^{n}+H_{i,j}^{n})\times\frac{1}{\Delta s}(H_{i+1,j}^{n}-H_{i,j}^{n})-\frac{g}{2}\left\{\frac{1}{2}(H_{i,j}^{n}+H_{i+1,j}^{n})\right\}^{2}\frac{\rho_{i+1,j}^{n}-\rho_{i,j}^{n}}{\Delta s}$$

$$-\frac{g}{C^{2}}\times\left\{\frac{U_{i,j}^{n-1}}{\frac{1}{2}(H_{i,j}^{n-1}+H_{i+1,j}^{n-1})}\right\}$$

$$\times\left[\begin{array}{l}\left\{\frac{U_{i,j}^{n-1}}{\frac{1}{2}(H_{i,j}^{n-1}+H_{i+1,j}^{n-1})}\right\}^{2}\\ +\left[\frac{1}{4}\left\{\frac{V_{i,j}^{n-1}}{\frac{1}{2}(H_{i,j}^{n-1}+H_{i,j-1}^{n-1})}+\frac{V_{i+1,j}^{n-1}}{\frac{1}{2}(H_{i+1,j}^{n-1}+H_{i+1,j+1}^{n-1})}+\frac{V_{i,j-1}^{n-1}}{\frac{1}{2}(H_{i,j-1}^{n-1}+H_{i,j}^{n-1})}+\frac{V_{i+1,j-1}^{n-1}}{\frac{1}{2}(H_{i+1,j-1}^{n-1}+H_{i+1,j}^{n-1})}\right\}\right]^{2}\end{array}\right]^{1/2}$$

$$+\frac{\tau^{x}}{\rho}$$

$$+\frac{A}{(\Delta s)^{2}}(U_{i+1,j}^{n-1}+U_{i-1,j}^{n-1}+U_{i,j+1}^{n-1}+U_{i,j-1}^{n-1}-4U_{i,j}^{n-1})$$

$$\frac{V_{i,j}^{n+1}-V_{i,j}^{n-1}}{2\Delta t}=-\frac{1}{\Delta s}\left[\begin{array}{l}\frac{1}{2}(U_{i,j+1}^{n}+U_{i,j}^{n})\times\frac{1}{2}\left\{\frac{V_{i+1,j}^{n}}{\frac{1}{2}(H_{i+1,j+1}^{n}+H_{i+1,j}^{n})}+\frac{V_{i,j}^{n}}{\frac{1}{2}(H_{i,j+1}^{n}+H_{i,j}^{n})}\right\}\\ -\frac{1}{2}(U_{i-1,j+1}^{n}+U_{i-1,j}^{n})\times\frac{1}{2}\left\{\frac{V_{i,j}^{n}}{\frac{1}{2}(H_{i,j+1}^{n}+H_{i,j}^{n})}+\frac{U_{i-1,j}^{n}}{\frac{1}{2}(H_{i-1,j+1}^{n}+H_{i-1,j}^{n})}\right\}\end{array}\right]$$

$$-\frac{1}{\Delta s}\left[\begin{array}{l}\frac{1}{2}(V_{i,j+1}^{n}+V_{i,j}^{n})\times\frac{1}{2}\left\{\frac{V_{i,j+1}^{n}}{\frac{1}{2}(H_{i,j+2}^{n}+H_{i,j+1}^{n})}+\frac{V_{i,j}^{n}}{\frac{1}{2}(H_{i,j+1}^{n}+H_{i,j}^{n})}\right\}\\ -\frac{1}{2}(V_{i,j}^{n}+V_{i,j-1}^{n})\times\frac{1}{2}\left\{\frac{V_{i,j}^{n}}{\frac{1}{2}(H_{i,j+1}^{n}+H_{i,j}^{n})}+\frac{V_{i,j-1}^{n}}{\frac{1}{2}(H_{i,j}^{n}+H_{i,j-1}^{n})}\right\}\end{array}\right]$$

$$+f\times\frac{1}{4}(U_{i,j+1}^{n}+U_{i,j}^{n}+U_{i-1,j+1}^{n}+U_{i-1,j}^{n})$$

$$-\frac{g}{2}(H_{i,j+1}^{n}+H_{i,j}^{n})\times\frac{1}{\Delta s}(H_{i,j+1}^{n}-H_{i,j}^{n})-\frac{g}{2}\left\{\frac{1}{2}(H_{i,j}^{n}+H_{i,j+1}^{n})\right\}^{2}\frac{\rho_{i,j+1}^{n}-\rho_{i,j}^{n}}{\Delta s}$$

$$-\frac{g}{C^{2}}\times\left\{\frac{V_{i,j}^{n-1}}{\frac{1}{2}(H_{i,j}^{n-1}+H_{i,j+1}^{n-1})}\right\}$$

$$\times\left[\begin{array}{l}\left\{\frac{V_{i,j}^{n-1}}{\frac{1}{2}(H_{i,j}^{n-1}+H_{i,j+1}^{n-1})}\right\}^{2}\\ +\left[\frac{1}{4}\left\{\frac{U_{i-1,j}^{n-1}}{\frac{1}{2}(H_{i-1,j}^{n-1}+H_{i-1,j+1}^{n-1})}+\frac{U_{i,j}^{n-1}}{\frac{1}{2}(H_{i,j}^{n-1}+H_{i+1,j}^{n-1})}+\frac{U_{i-1,j+1}^{n-1}}{\frac{1}{2}(H_{i-1,j+1}^{n-1}+H_{i,j+1}^{n-1})}+\frac{U_{i,j+1}^{n-1}}{\frac{1}{2}(H_{i,j+1}^{n-1}+H_{i+1,j+1}^{n-1})}\right\}\right]^{2}\end{array}\right]^{1/2}$$

$$+\frac{\tau^{y}}{\rho}$$

$$+\frac{A}{(\Delta s)^{2}}(V_{i+1,j}^{n-1}+V_{i-1,j}^{n-1}+V_{i,j+1}^{n-1}+V_{i,j-1}^{n-1}-4V_{i,j}^{n-1})$$

$$\frac{H_{i,j}^{n+1} - H_{i,j}^{n-1}}{2\Delta t} = -\frac{1}{\Delta s}(U_{i,j}^{n} - U_{i-1,j}^{n}) - \frac{1}{\Delta s}(V_{i,j}^{n} - V_{i,j-1}^{n})$$

where grid points are denoted as *i*th row and *j*th column, and the time step is denoted as *n*th time step; Δt is the size of the time step; Δs is grid spacing in both the x and y directions.

4.3 Advection Schemes Used

For advective transport of salt and temperature, the Hsu-Arakawa scheme, which was based on the Takacs scheme (1985), is adopted. In the following, first, a brief description of the Takacs scheme is presented, which is followed by a detailed description of the Hsu-Arakawa scheme.

4.3.1 Takacs Scheme

For simplicity, the formulation of the scheme will be based on the two-dimensional advection equation given by

$$\frac{\partial q}{\partial t} + u\frac{\partial q}{\partial x} + v\frac{\partial q}{\partial y} = 0 \qquad (1)$$

Here, *q* represents any arbitrary quantity being advected, while *u* and *v* are velocity component of the flow in the *x*- and *y*-direction, respectively.

Following Takacs' (1985) a two-dimensional scheme is derived by applying two passes of a one-dimensional operator. The one-dimensional operator was constructed by imposing three constraints on the time-continuous version of the scheme,

$$q_j^{n+1} = q_j^n - \frac{\mu}{2}(q_{j+1}^n - q_{j-1}^n) + \frac{\mu^2}{2}(q_{j+1}^n - 2q_j^n + q_{j-1}^n) - a\mu(\mu-1)(q_{j+1}^n - 3q_j^n + 3q_{j-1}^n - q_{j-2}^n) \quad (2)$$

First, the requirement of conservation of mass was imposed yielding a flux formulation of the scheme,

$$\frac{\partial}{\partial t}\sum_j q_j = 0 \qquad (3)$$

Second, it was required that when the flow field is constant, the time-continuous flux form reduces to the time-continuous advective form given by

$$\frac{\partial q_j}{\partial t} = \frac{-u}{2\Delta x}(q_{j+1} - q_{j-1}) + \frac{au}{\Delta x}(q_{j+1} - 3q_j + 3q_{j-1} - q_{j-2}) \qquad (4)$$

Finally, a stability criterion for the time-continuous case when the flow field is non-divergent was imposed, given by

$$\frac{\partial}{\partial t}\sum_j \frac{1}{2} q_j^2 \le 0 \qquad (5)$$

Using these requirements, it can be shown that the flux form of (4) using a staggered grid is given by

$$\frac{\partial q_j}{\partial t} = -\frac{1}{2\Delta x}\left[u_j(q_{j+1} + q_j) - u_{j-1}(q_j + q_{j-1})\right]$$

$$+ \frac{a}{\Delta x}\left[u_j(q_{j+1} - q_j) - \sqrt{u_j}\sqrt{u_{j-1}}(q_j - q_{j-1}) - u_{j-1}(q_j - q_{j-1}) + \sqrt{u_{j-1}}\sqrt{u_{j-2}}(q_{j-1} - q_{j-2})\right]$$

For the time-discrete case ($\Delta t > 0$) and changing wind speeds, a predictor-corrector sequence can be devised that will reduce to Eq. (4) when the flow field is constant. Substitution will show that Eqs. (6) and (7) satisfy this requirement.

Predictor:

$$q_j^* = q_j^n - (\mu_j q_j^n - \mu_{j-1} q_{j-1}^n) \qquad (6)$$

Corrector:

$$q_j^{n+1} = q_j^n - \frac{1}{2}\left[\mu_j(q_{j+1}^* + q_j) - \mu_{j-1}(q_j^* + q_{j-1})\right]$$
$$+ \frac{1+\mu_j}{6}\left[\mu_j(q_{j+1}^* - q_j^n) - \sqrt{\mu_j}\sqrt{\mu_{j-1}}(q_j^* - q_{j-1}^n)\right]$$
$$- \frac{1+\mu_{j-1}}{6}\left[\mu_{j-1}(q_j^* - q_{j-1}^n) - \sqrt{\mu_{j-1}}\sqrt{\mu_{j-2}}(q_{j-1}^* - q_{j-2}^n)\right] \qquad (7)$$

where $\mu_j = u_j \frac{\Delta t}{\Delta x}$

Combining the predictor and corrector steps yields,

$$q_j^{n+1} = q_j^n - \frac{1}{2}\left[\mu_j(q_{j+1}^n - \mu_{j+1}q_{j+1}^n + \mu_j q_j^n + q_j^n) - \mu_{j-1}(q_j^n - \mu_j q_j^n + \mu_{j-1}q_{j-1}^n + q_{j-1}^n)\right]$$
$$+ \frac{1+\mu_j}{6}\left[\mu_j(q_{j+1}^n - \mu_{j+1}q_{j+1}^n + \mu_j q_j^n - q_j^n) - \sqrt{\mu_j}\sqrt{\mu_{j-1}}(q_j^n - \mu_j q_j^n + \mu_{j-1}q_{j-1}^n + q_{j-1}^n)\right]$$
$$- \frac{1+\mu_{j-1}}{6}\left[\mu_{j-1}(q_{j-1}^n - \mu_j q_j^n + \mu_{j-1}q_{j-1}^n - q_{j-1}^n) - \sqrt{\mu_{j-1}}\sqrt{\mu_{j-2}}(q_{j-1}^n - \mu_{j-1}q_{j-1}^n + \mu_{j-2}q_{j-2}^n + q_{j-2}^n)\right]$$

4.3.2 Nonpositive Flow Fields

In general, advection by a non-uniform two-dimensional flow requires additional information to ensure the inclusion of the proper grid-points for an upstream-type scheme. A generalized form of the two-dimensional scheme for non-positive flow is given by

Predictor:

$$q_j^* = q_j^n - \left[F_j - F_{j-1}\right]$$
$$F_j = \mu_j^+ q_j^n + \mu_j^- q_{j+1}^n$$

where

$$\mu_j^+ = \left(\frac{\mu + |\mu|}{2}\right)_j$$
$$\mu_j^- = \left(\frac{\mu - |\mu|}{2}\right)_j$$

Corrector:

$$q_j^{n+1} = q_j^n - \frac{1}{2}(P_j - P_{j-1}) + (a_j Q_j - a_{j-1} Q_{j-1})$$

where

$$P_j = \mu_j^+ (q_{j+1}^* + q_j^n) + \mu_j^- (q_j^* + q_{j-1}^n)$$

$$Q_j = \left[\mu_j^+ (q_{j+1}^* - q_j^n) - (|\mu_j^+|)^{1/2} (|\mu_{j-1}^+|)^{1/2} (q_j^* - q_{j-1}^n) \right]$$
$$- \left[\mu_j^- (q_{j+1}^n - q_j^*) - (|\mu_j^-|)^{1/2} (|\mu_{j+1}^-|)^{1/2} (q_{j+2}^n - q_{j+1}^*) \right]$$

$$a_j = \left(\frac{1 + |\mu|}{6} \right)_j$$

Rewriting yields,

$$q_j^* = q_j^n - (\mu_j^+ q_j^n + \mu_j^{-1} q_{j+1}^n - \mu_{j-1}^+ q_{j-1}^n - \mu_{j-1}^- q_j^n)$$

$$q_j^{n+1} = q_j^n - \frac{1}{2}\left[\mu_j^+ (q_{j+1}^* + q_j^n) + \mu_j^- (q_j^* + q_{j+1}^n) - \mu_{j-1}^+ (q_j^* + q_{j-1}^n) - \mu_{j-1}^{-1} (q_{j-1}^* + q_j^n) \right]$$

$$+ \left(\frac{1 + |\mu|}{6} \right)_j \left[\mu_j^+ (q_{j+1}^* - q_j^n) - (|\mu_j^+|)^{1/2} (|\mu_{j-1}^+|)^{1/2} (q_j^* - q_{j-1}^n) \right]$$

$$- \left(\frac{1 + |\mu|}{6} \right)_j \left[\mu_j^- (q_{j+1}^n - q_j^*) - (|\mu_j^-|)^{1/2} (|\mu_{j+1}^-|)^{1/2} (q_{j+2}^n - q_{j+1}^*) \right]$$

$$- \left(\frac{1 + |\mu|}{6} \right)_{j-1} \left[\mu_{j-1}^+ (q_j^* - q_{j-1}^n) - (|\mu_{j-1}^+|)^{1/2} (|\mu_{j-2}^+|)^{1/2} (q_{j-1}^* - q_{j-2}^n) \right]$$

$$+ \left(\frac{1 + |\mu|}{6} \right)_{j-1} \left[\mu_{j-1}^- (q_j^n - q_{j-1}^*) + (|\mu_{j-1}^-|)^{1/2} (|\mu_j^-|)^{1/2} (q_{j+1}^n - q_j^*) \right]$$

4.3.3 Hsu-Arakawa Scheme

One of the drawbacks of the Takacs scheme is that it can generate negative values. Hsu and Arakawa (1990) developed an advection based on the Takacs scheme, which is positive definite when time is continuous, while maintaining third-order accuracy when applied to a uniform current. In this scheme, the outflow flux from a grid point automatically approaches zero, while the inflow flux remains non-negative. When applied to the one-

dimensional advection equation with a uniform current, the results with this scheme are very similar to those from the Takacs scheme except that generation of negative values is practically eliminated. Horizontal discretization of the continuity equation in their model is based on this advection scheme.

The Hsu-Arakawa scheme is based on the Arakawa C-grid. The only difference comes in the corrector step:

$$\textit{Corrector}:\ q_j^{n+1} = q_j^n - \frac{\Delta t}{d}\left(F_j - F_{j-1}\right)$$

$$= q_j^n - \frac{\Delta t}{d}\left(u_j^+ \frac{q_{j+1}^* + q_{j+1}^n}{2} + u_j^- \frac{q_j^* + q_{j+1}^n}{2} + G_j - u_{j-1}^+ \frac{q_j^* + q_{j-1}^n}{2} - u_{j-1}^- \frac{q_{j-1}^* + q_j^n}{2} - G_{i-1} \right)$$

$$= q_j^n - \frac{1}{2}\left[\mu_j^+(q_{j+1}^* + q_j^n) + \mu_j^-(q_j^* + q_{j+1}^n) - \mu_{j-1}^+(q_j^* + q_{j-1}^n) - \mu_{j-1}^{-1}(q_{j-1}^* + q_j^n)\right] - \frac{\Delta t}{d}(G_j - G_{j-1})$$

$$= q_j^n - \frac{1}{2}\left[\mu_j^+(q_{j+1}^* + q_j^n) + \mu_j^-(q_j^* + q_{j+1}^n) - \mu_{j-1}^+(q_j^* + q_{j-1}^n) - \mu_{j-1}^{-1}(q_{j-1}^* + q_j^n)\right]$$

$$+ \left(\frac{1+|\mu|}{6}\right)_j \left[\mu_j^+ \left\{ 1 + \left(\frac{1-2a}{2a}\right)_j \gamma_j^+ \right\} \left(q_{j+1}^* - q_j^n\right) - \left(\mu_j^+ \mu_{j-1}^+\right)^{1/2} \left(1 - \hat{\gamma}_j^+\right)\left(q_j^* - q_{j-1}^n\right) \right.$$

$$\left. + \mu_j^- \left\{ 1 + \left(\frac{1-2a}{2a}\right)_j \gamma_j^- \right\} \left(q_j^* - q_{j+1}^n\right) - \left(|\mu_j^-||\mu_{j+1}^-|\right)^{1/2} \left(1 - \hat{\gamma}_j^-\right)\left(q_{j+1}^* - q_{j+2}^n\right) \right]$$

$$- \left(\frac{1+|\mu|}{6}\right)_{j-1} \left[\mu_{j-1}^+ \left\{ 1 + \left(\frac{1-2a}{2a}\right)_{j-1} \gamma_{j-1}^+ \right\} \left(q_j^* - q_{j-1}^n\right) - \left(\mu_{j-1}^+ \mu_{j-2}^+\right)^{1/2} \left(1 - \hat{\gamma}_{j-1}^+\right)\left(q_{j-1}^* - q_{j-2}^n\right) \right.$$

$$\left. + \mu_{j-1}^- \left\{ 1 + \left(\frac{1-2a}{2a}\right)_{j-1} \gamma_{j-1}^- \right\} \left(q_{j-1}^* - q_j^n\right) - \left(|\mu_{j-1}^-||\mu_j^-|\right)^{1/2} \left(1 - \hat{\gamma}_{j-1}^-\right)\left(q_j^* - q_{j+1}^n\right) \right]$$

where

$$\gamma_j^+ = \hat{\gamma}_j^+ = \left[\frac{\left(q_{j-1}^n - 2q_j^n + q_{j+1}^n\right)^2}{\left(q_{j-1}^n - 2q_j^n + q_{j+1}^n\right)^2 + q_j^n q_{j+1}^n} \right]^2$$

$$\gamma_j^- = \hat{\gamma}_j^- = \left[\frac{\left(q_j^n - 2q_{j+1}^n + q_{j+2}^n\right)^2}{\left(q_j^n - 2q_{j+1}^n + q_{j+2}^n\right)^2 + q_j^n q_{j+1}^n} \right]^2$$

With these choices of γ and $\hat{\gamma}$, we can see that, as $q_j^n \to 0$, $F_j \to 0$ when $u_j > 0$ and $F_{j-1} \to 0$ when $u_{j-1} < 0$. For other possibilities in choosing γ and $\hat{\gamma}$, see Hsu and Arakawa (1990). It should be noted, in actual computations, one needs to make sure to set

$\gamma_j^+ \to 0$, $\hat{\gamma}_j^+ \to 0$, $\gamma_j^- \to 0$, and $\hat{\gamma}_j^- \to 0$ as $q_j^n \to 0$.

In order to apply the Hsu-Arakawa scheme to a two-dimensional depth-integrated advection equation the following procedure is followed. The 2-D depth-integrated equation for advection is given by

$$\frac{\partial HS}{\partial t} + \frac{\partial US}{\partial x} + \frac{\partial VS}{\partial y} = 0$$

where *S* is the concentration of the advected property (e. g., suspended sediment).

$$U = \int_{-h}^{\zeta} u dz$$
$$V = \int_{-h}^{\zeta} v dz$$
$$H = h + \zeta$$
$$S = \frac{1}{H} \int_{-h}^{\zeta} s dz$$

In order to apply the Hsu-Arakawa scheme to the above equation, it is necessary to account for volume changes into or out of the individual grid cells during each time-step, i. e., the following continuity equation needs to be solved at the same time,

$$\frac{\partial H}{\partial t} + \frac{\partial UH}{\partial x} + \frac{\partial VH}{\partial y} = 0$$

The hydrodynamic model used with the Hsu-Arakawa scheme takes about twenty percent longer in cpu time than the model with the Takacs scheme in this study. For a similar study based on the same hydrodynamic model applied to Breton Sound located

immediately northeast of the Mississippi delta, simulation runs using both the Takacs scheme and the Hsu-Arakawa scheme showed that there were no major differences in model results between the two schemes (Inoue, personal communication, 2002). Therefore it was decide to use the Takacs scheme for this study.

5. DRIVING FORCES AND MODEL CALIBRATIONS

The fundamental data needs for model hindcast and calibration runs are water level, salinity, precipitation and wind time series. Historical water level and salinity data from 1999 and 2001 collected by the United States Geological Survey (USGS) and the Department of Natural Resources, Louisiana (DNR), were obtained for Barataria Basin. Figure 10 shows the sites of data collected. Water level and salinity data collected at all eight sites, S1 to S8, for 1999 and three sites, S1, S2, and S9, for 2001 were used for calibration and simulation skill assessment. Water level and salinity recorded at site S1 were used to specify southern open boundary conditions.

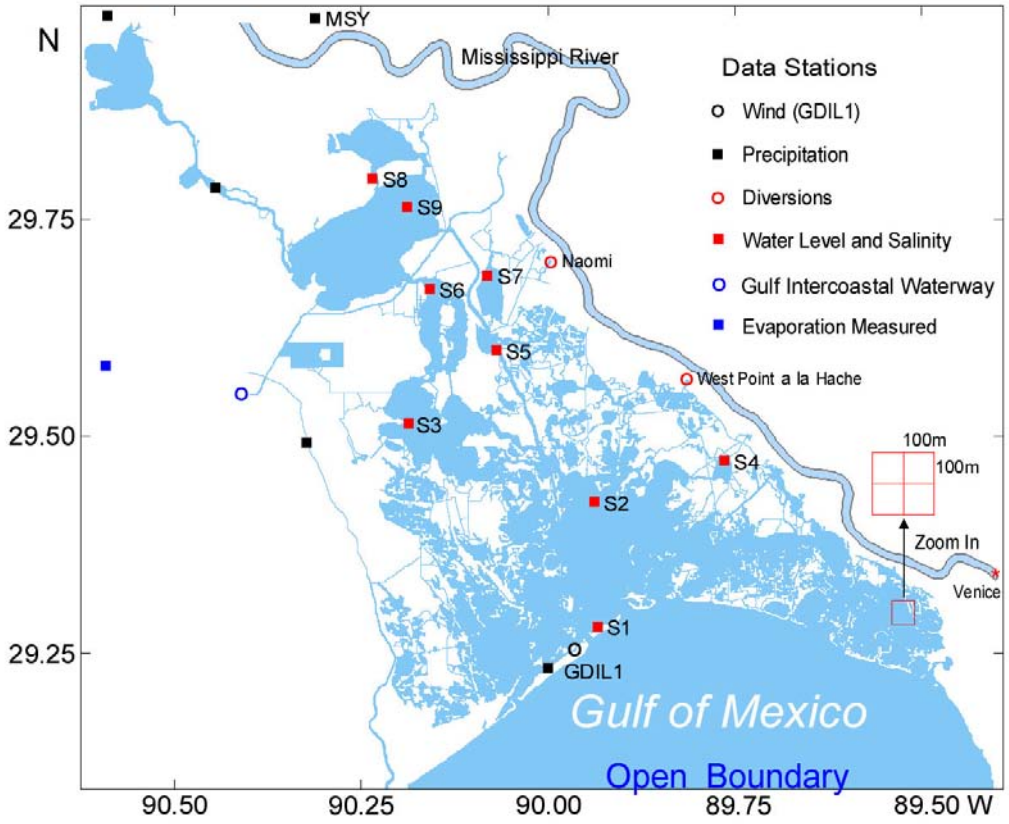

Figure 10. Data stations used model calibration and simulation skills.

The four main freshwater sources into the Barataria Basin are rainfall on the open water surface, runoff of rainfall, two man-made diversions from the Mississippi River, and the Gulf Intercoastal Waterway as a conduit of fresh water from the Atchafalaya River. There were five sites where precipitation records were available near Barataria Basin. For this study, however, the precipitation record from MSY was used. MSY was the only station where rainfall was measured at hourly intervals. In addition, the dominant upstream regions which account for 61% of total land are best represented by MSY station. A uniform spatial distribution of precipitation over the entire domain based on measurements at MSY station was assumed. In order to estimate evaporation, hourly measurements of atmospheric pressure, wind speed, sea surface temperature, and dew-point temperature were used from GDIL1 station.

The vertical distribution of the wind, or wind shear, over the water surface is an important factor to consider when specifying the wind stress (Hsu, 1994). Since the wind data measured at both sites were not from the standard reference height, 10 *m*, conversion to this reference height was necessary. The simple power-law wind profile is employed because it is quite accurate and useful (Panofsky and Dutton, 1984). The power-law wind profile states that

$$\frac{u_2}{u_1} = \left(\frac{z_2}{z_1} \right)^p ,$$

where u_2 is the wind speed at reference height z_2, u_1 and z_1 are the wind speed and height of the observation, and the exponent p is a function of both the atmospheric

stability and the underlying surface characteristics. For this study area the value of p, 0.10, was recommended (Hsu, 1988).

Most of the model bathymetry and morphology was taken from Nautical Charts (scale 1:80,000), topographic maps (scale 1:100,000) by U. S. Geological Survey, and recent satellite imagery (Figure 11). The morphology was modified using recent satellite images and aerial photos to get close to the situation of 1999, with which we will be dealing for the modeling study, since the most recent nautical charts (published in 1995) have not been changed since 1976. The coastal boundaries were approximated in the model as closely as possible. Despite the numerous small canals and creeks that may not be well resolved by 100 *m* grid, the grid size was taken uniformly as 100 *m* to reduce computational time and space requirements.

5.1 Driving Forces

The primary objective of this numerical modeling study is the realistic simulation of circulation including the influence of baroclinic gradients. The model was forced by realistic tides, salinity, water temperature, rainfall, local runoff, wind and freshwater diversion from the Mississippi River. Spatially uniform rainfall and wind forcing were included in the model (Figure 12).

At the open boundary, sea level height is specified. Open boundary conditions for salinity and temperature are set in such a way that for outflow (i. e., flowing toward the open boundary) the radiation boundary condition due to Carmerlengo and O'Brien (1980) is used, while for inflow (i.e., flowing into the model domain) a relaxation toward the specified value at the open boundary is applied.

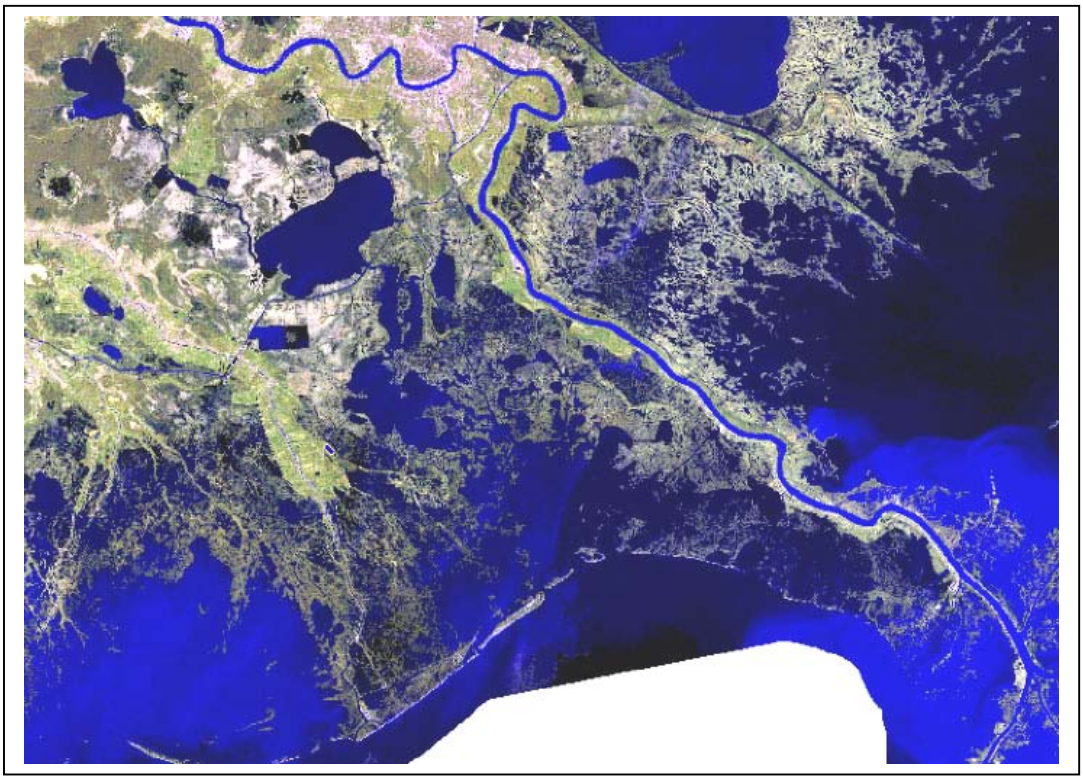

Figure 11. Satellite imagery for the Barataria System. This was taken from the Louisiana GIS CD: A Digital Map of the State.

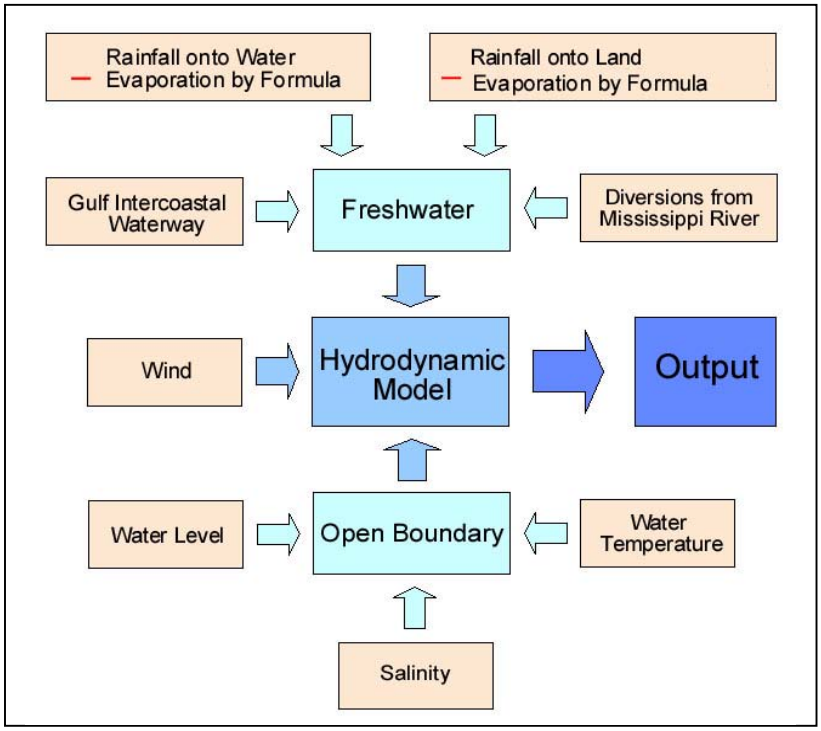

Figure 12. The driving forces for model simulation.

Due to the lack of sea level height measurements near the southern open boundary, the water elevation recorder from site S1, the nearest site to the southern open boundary, was used to estimate sea level height at the southern open boundary. Initial calibration runs were made by applying the sea level signal measured at site S1 with various values of amplification and phase shift, and the observed sea level records at site S1 were then compared to the corresponding model water level height at site S1. It was decided to use the sea level signal measured at site S1 for southern open boundary conditions with a 12 % increase in amplitude and a 1-hour phase lead, that resulted $r^2 = 0.98$ between the observed and sea level height at S1.

In addition to the water elevation, spatially uniform wind forcing was included in the model. For the project, wind data were available at both MSY (New Orleans International Airport) and GDIL1 (Grand Isle C-MAN Station) (Figure 10). After running the model with both wind data sets, the data from GDIL1 was selected for wind forcing because the computed results using the GDIL1 data showed better agreement with observed water level data, except at some upstream regions, which are located nearest to the MSY wind station (Park, 1998).

An empirical relationship derived for the Barataria Basin (Hsu, 1996, personal communication) was used to convert from wind speed to wind stress. The relationships between, the wind stress, the shear velocity, U_*, and the wind speed at 10 m height, U_{10}, for this study area are:

$$\tau = \rho_a U_*^2, \text{ and } U_* = 0.037 U_{10} - 0.03$$

where τ is the wind stress and ρ_a is the air density.

Due to the lack of salinity measurements near the southern open boundary, the salinity recorder from site S1 was used to estimate salinity values at the open boundary. The long-term horizontal salinity distribution showed that the difference between station S1 and near the southern open boundary was approximately 5 *ppt* (Swenson and Turner, 1998). Therefore, the salinity values at the southern open boundary were specified as 5 *ppt* higher than those at station S1. The salinity variability near the southern open boundary results from the mixture of open ocean water, the Mississippi River discharge, and local runoff effects. Since the salinity from the station S1 exhibited high frequency fluctuations due to sheltering of the measurement site, it was low-pass filtered with a seventy-two hour

moving average filter in order to smooth out local effects so as to mimic the characteristics near the southern open boundary (Figure 13).

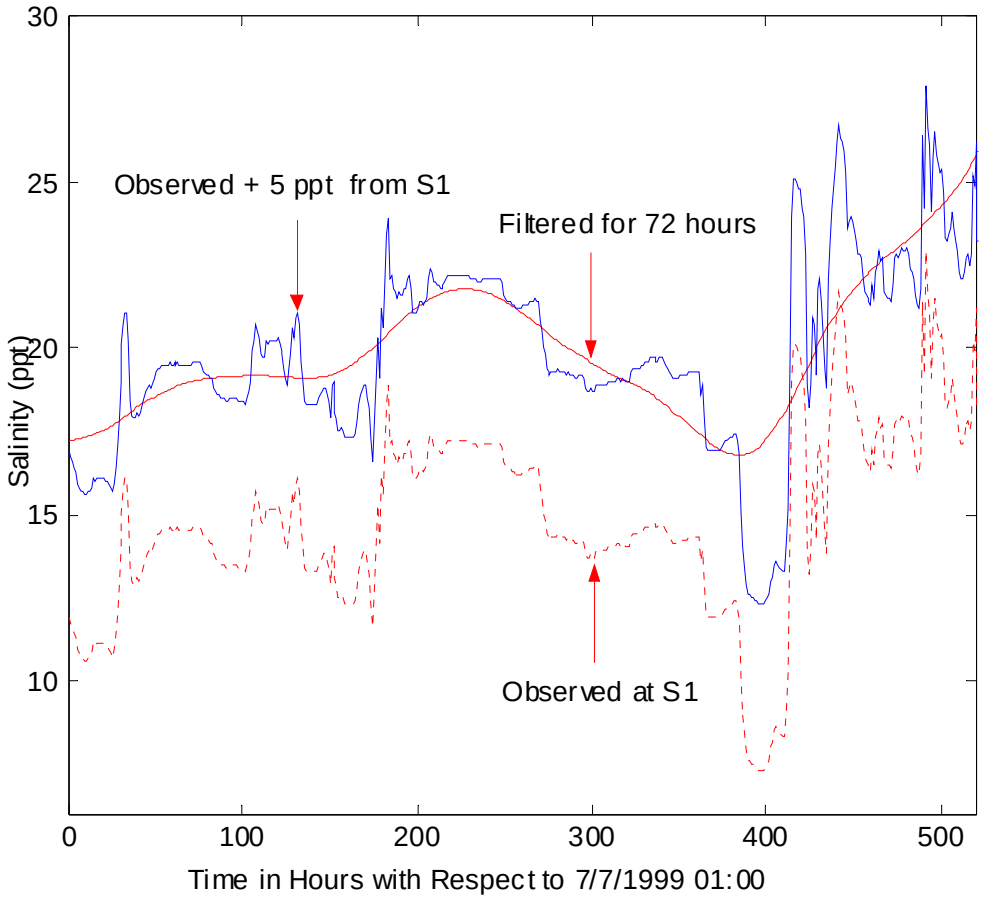

Figure 13. Salinity time series at S1 and its modifications for use as an open boundary condition.

According to the climatic mean estimates of the salinity distribution (Swenson and Turner, 1998), salinity varies spatially along the southern open boundary with presumably high values near the middle and low values near both of the edges. In order to incorporate this characteristic it was assumed that the salinity decreases with the distance from the maximum salinity value located near the center of the southern open boundary. Figure 15 shows some examples of the assumed salinity distribution along the southern open

boundary for different time steps during a model run. In order to expedite the spin-up process, salinity distribution estimates based on the climatology of Swenson and Turner (1998) were used as the initial condition for salinity (Figure 15).

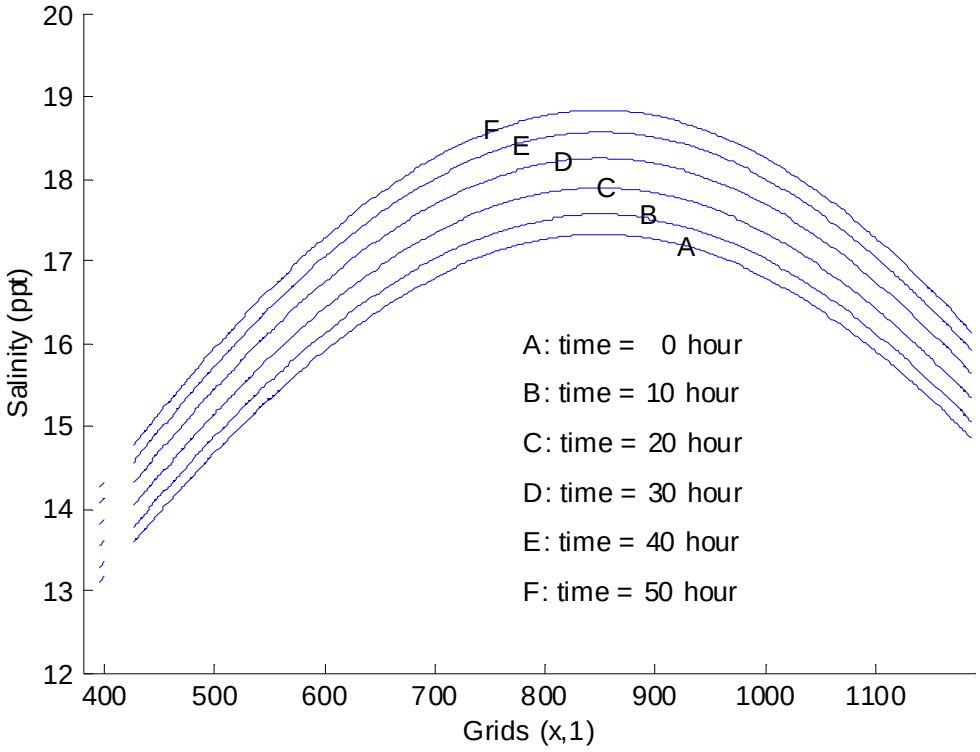

Figure 14. Examples of salinity distributions along the southern open Boundary during a period of increasing salinity.

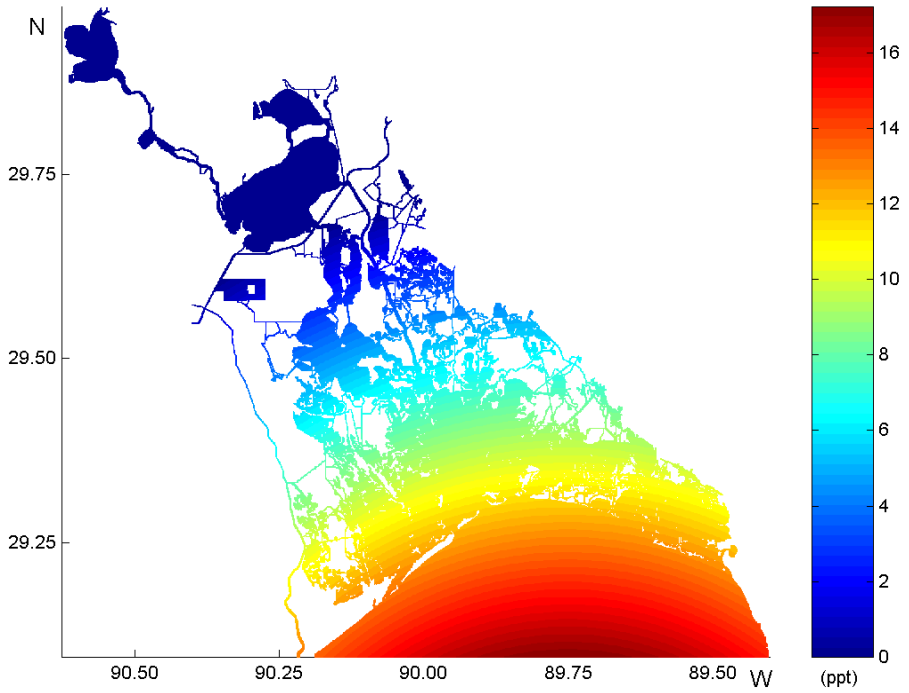

Figure 15. Initial horizontal salinity distribution for the model domain based on an average long-term distribution.

5.2 Model Parametric Calibration

During several initial model runs, the model was calibrated by adjusting the Manning's *n* coefficient until the model reproduced, as closely as possible, the observed water elevation. A series of solutions were evaluated by varying Manning's *n* (0.01, 0.02, and 0.03) and comparing observed and modeled sea level elevations. The results indicate that the modeled water surface elevations are sensitive to bottom friction. It turned out that a Manning's *n* coefficient of 0.02 appears to give the best result in terms of amplitudes and phase lags. Open channel flow literature gives a range of Manning's *n* values of 0.02 to 0.035 for channels with sand beds (Henderson, 1966). Kjerfve (1973) assumed the Manning's *n* = 0.03 in Caminada Bay for his modeling study. Recently, Park (1998) used the value 0.04 in a Barataria Basin model study. The smaller Manning's *n* used in this

model compared to the previous model (Park, 1998) is probably due to the final model grid size, 100 *m* compared to Park's, 463 *m*, and the different horizontal eddy viscosity used (5 $m^2 s^{-1}$ versus 10 $m^2 s^{-1}$).

Barataria Basin is characterized by the high energy absorption of the marsh environment (Byrne et al., 1976). As would be anticipated, a decrease in the frictional dissipation, increases the tidal range. The phase of modeled water level was slightly delayed with respect to observations, by up to two hours, moving from lower Barataria Bay to sites further upstream. The phase differences between modeled and observed water level may be attributable to the inaccuracies in bathymetry, open boundary forcing, and narrowness of canals. Nevertheless, the comparisons (Table 3) are surprisingly good for such a complex domain.

Table 3. The comparisons of phase lags for eight stations, in hours, between observed and modeled results. The bold number from each column shows the best value of the correlation coefficients (r^2).

Phase Lag Hours	Stations (Correlation Coefficient)							
	S1	S2	S3	S4	S5	S6	S7	S8
0	**0.981**	**0.941**	0.907	0.850	0.884	0.892	**0.902**	0.898
1	0.926	0.933	**0.933**	**0.911**	**0.907**	**0.898**	0.895	0.908
2	0.801	0.831	0.912	0.879	0.902	0.890	0.836	**0.911**
3	0.568	0.657	0.846	0.758	0.870	0.868	0.836	0.906
4	0.368	0.451	0.748	0.579	0.815	0.835	0.790	0.895

The model was spun up from rest using the observed wind and water level height. Hourly data records from July 7 to August 5, 1999, were obtained and linear interpolation was used to estimate values at any particular model time step in between. Spin-up time for

the tidal signal propagation in the model would normally be estimated as the travel time for the tide to propagate from the open boundary all the way up to the other end of the model domain and to propagate back to the open boundary. Based on the tidal propagation, spin-up time for the model should be approximately 1.5 days. For the model domain used here, however, a spin-up time of 5 days was found to be necessary for disturbances due to model initialization to have died down (Figure 16). Comparisons between the modeled tidal amplitude and the observed tide collected at eight sites showed that, although there are slight differences in observed and predicted phase at all sites, simulated results are in general agreement with the observations. The high frequency signal near hour 650 at S1 and S2 may be due to using linear interpolations of hourly winds.

5.3 Model Hydrologic Calibration

Freshwater runoff, together with tide, evaporation and winds, are some of the most important factors influencing physical and biological processes in coastal waters (Denes and Caffrey, 1988; Koutitonsky et al., 1990). Runoff is a function of a number of environmental variables mainly depending on climate and physical characteristics of the drainage basin. The most important effects of runoff on estuarine systems are related to changes in water column stability and horizontal mass transport.

For the hydrologic calibration, a big flood of June 2001, during tropical storm Allison, provided a rare opportunity to calibrate the model. Long-term average (30 years) precipitation for June was 15 *cm*. During June of 2001, however, the recorded precipitation was 60 *cm*, almost four-fold the long-term average. Moreover, most of it fell

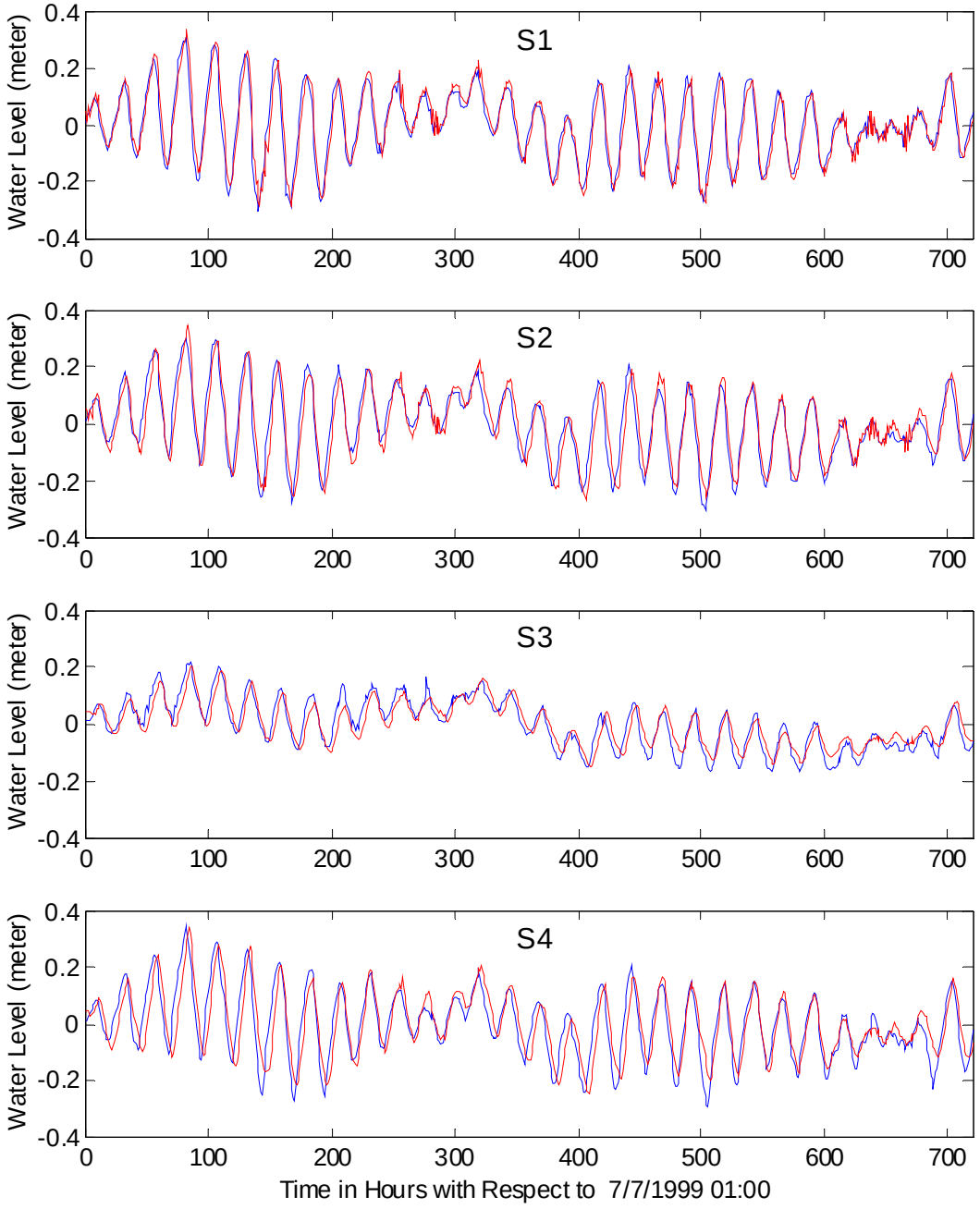

Figure 16. Comparisons of the computed (red) and observed (blue) water levels at eight stations.

(figure con'd)

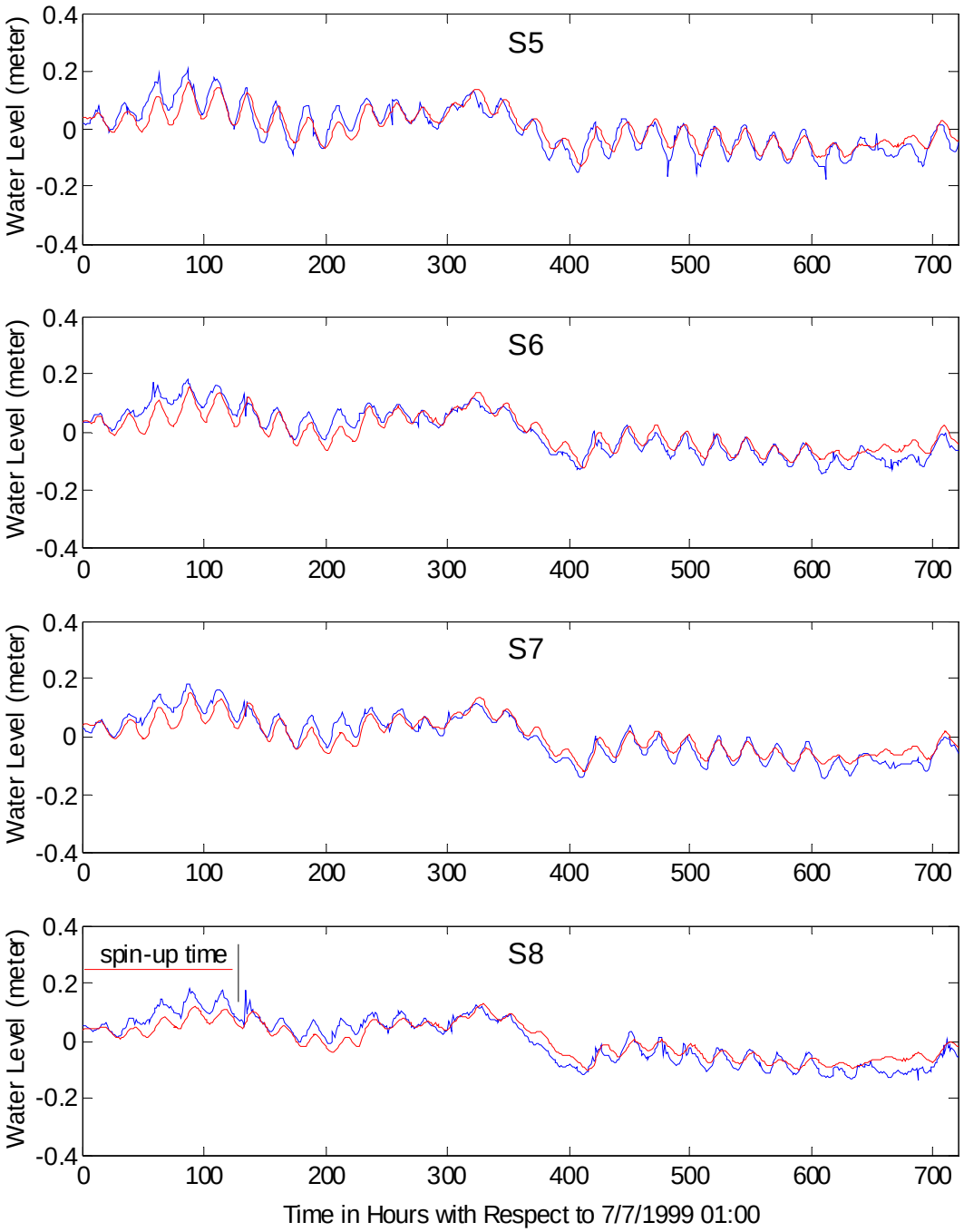
S5
S6
S7
S8
spin-up time
Water Level (meter)
0.4
0.2
0
-0.2
-0.4
0
100
200
300
400
500
600
700
Time in Hours with Respect to 7/7/1999 01:00

during tropical storm Allison (hereafter referred to as the flood of June 2001). In coupling the hydrology model to the hydrodynamic model, it was assumed that 100 % of local rainfall enters the estuary. This assumption should be reasonable considering the fact that during a heavy rainfall event such as the flood of June 2001, most of the runoff should enter the basin very quickly. Figure 17 shows two different scenarios, one corresponding to 100 % runoff and the other without any runoff, together with the observed sea level height at three stations. It is apparent that the downstream station (S1) does not exhibit any significant impact of the flood on water level height. However, the two upstream stations do display significant impact of the flood. Especially at the uppermost station, S9, runoff due to the flood overwhelms the water level signal after hour 300. The discrepancy between the observed and modeled results without runoff increases as the flood event evolves with time. Upstream, due to the relatively smaller surface area of the estuary compared to the surrounding drainage area, the impact of the rainfall event becomes more significant to water level change. Agreement between observed and model results with runoff is surprisingly good. The observed agreement provides a justification for adopting 100 % coupling between the hydrologic model and hydrodynamic model, at least for this flood event. However, it is expected that during smaller rainfall events coupling should be less than 100 %. It should be noted that the above simulation runs did include the effect of freshwater diversions from the sites. It is apparent that the impact of freshwater diversions from the two sites was negligible during this flood event.

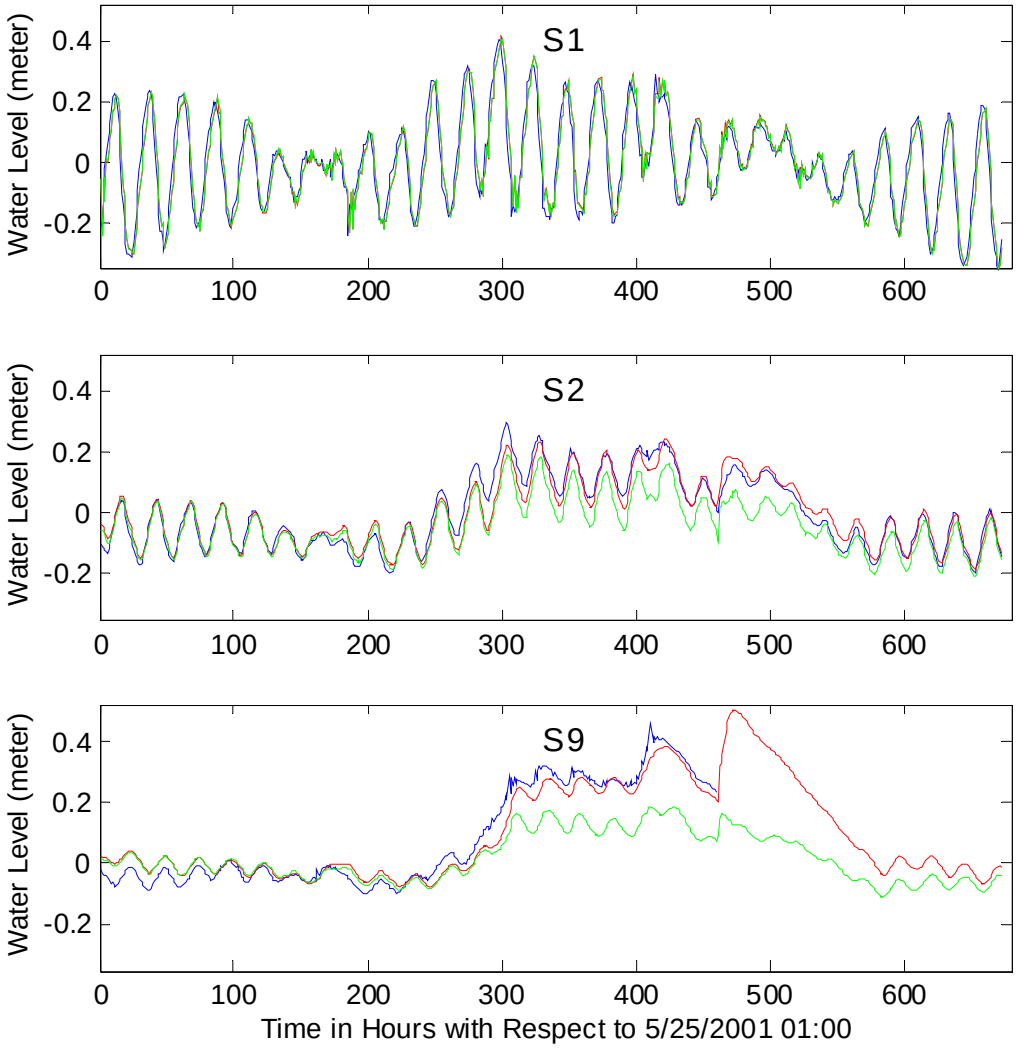

Figure 17. Water level calibrations for a heavy rainfall event (blue: observed ; red: model results with rainfall and runoff by rainfall ; green: model results without rainfall and runoff by rainfall).

6. MODEL RESULTS AND DISCUSSION

The results of this calibrated model—circulation, water level, salinity, transport, and diffusion for the Barataria Basin system using the observed sea level height and salinity as open boundary conditions, monitored wind data and precipitation, and estimated evaporation as forcing for a 30-day period from July 7 to August 5, 1999—are now discussed. The first 5-day period was considered as the spin-up period because the ocean model was started from rest on July 7, 1999. Furthermore, results are compared with those from a similar model run when freshwater from two diversions and the Gulf Intercoastal Waterway also forced the model.

Water volume and salinities in Barataria Basin are highly influenced by astronomical tides, wind, precipitation, and diversions. The dominant process in controlling water levels, particularly in the lower reaches of the Barataria Basin, is expected to be the astronomical tides. The diurnal tides are dominant in the Gulf of Mexico region but the region also is influenced by the semidiurnal and long period tides (Byrne et al., 1976).

While tidal forcing is of great importance at the southern end of the estuary, meteorological events, such as rain, wind and atmospheric pressure, are also important processes controlling water levels. Water levels tend to respond to atmospheric pressure as an inverse barometer with a theoretical response of 1.01 $cm\,mb^{-1}$ (Byrne et al, 1976). In shallow waters, the effect of wind stress will usually overpower the effect of the accompanying pressure system. Although global winds are important in determining the prevailing winds in a given area, local climatic conditions may influence the most common wind directions. Local winds are always superimposed upon the larger scale wind systems, i.e., the wind direction is influenced by the sum of global and local effects.

When larger scale winds are light, local winds may dominate the wind patterns. Meteorological forcing of estuaries along the northern Gulf of Mexico can be considered in terms of its effect on the exchange between the estuarine waters and the waters in the coastal zone, as well as local circulation occurring within the estuary proper.

Land masses are heated by the sun more quickly than the sea in the daytime. The warm air rises and creates a low pressure at ground level, which is filled by a flow of cool air from the sea. This is called a sea breeze. At nightfall there is often a period of calm when land and sea temperatures are equal. At night, the wind blows in the opposite direction. The land breeze at night generally has lower wind speeds than the sea breeze, because the temperature difference between land and sea is smaller at night. The test period represents typical, environmentally fair, summer conditions of predominantly northerly or southerly breezes of 3 to 7 $m\,s^{-1}$ with occasional shifts in wind direction (Figure 18). It is notable that the wind directions during the first half of the simulation period show primarily southerly breezes except between the 6^{th} and 8^{th} days. It should be noted that the southerly breezes are still modulated by the land-sea breeze system. During the last 12 days, however, the directions change by day and night due to the temperature differences between land and sea. The most pronounced effect of wind forcing on the Gulf of Mexico systems is the difference between a northerly and a southerly wind (Swenson and Turner, 1998).

Approximately four months of hourly records of water level and wind data from GDIL1 were used to estimate the spectral density of water level and wind components. Coherence between water level and wind components was estimated by averaging over

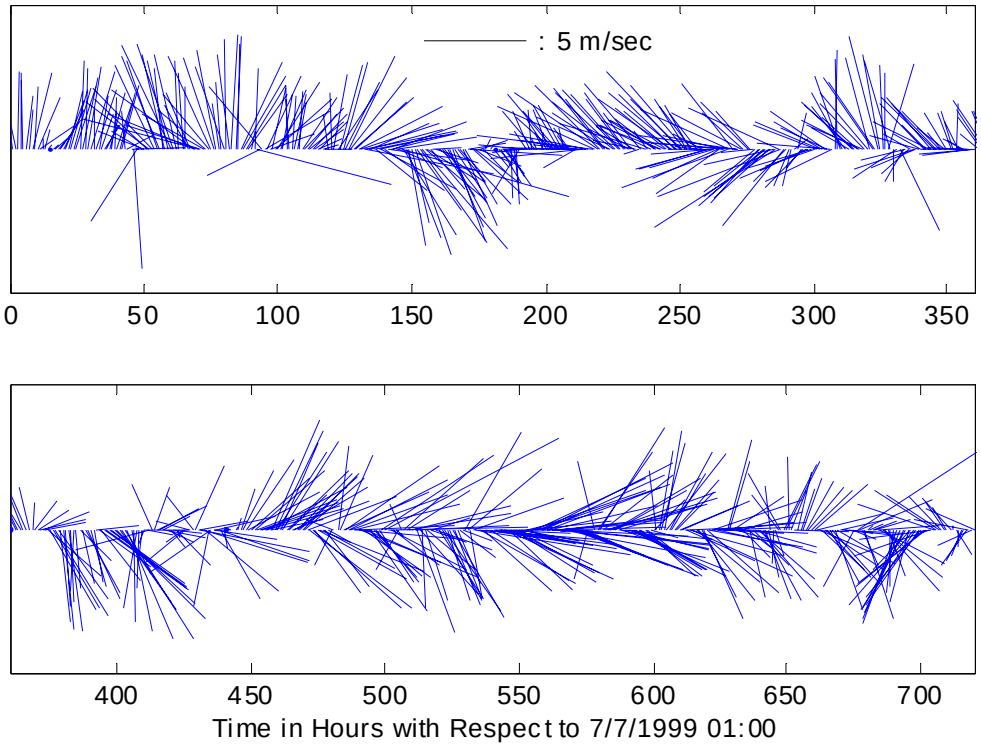

Figure 18. Wind vectors in time series of 30 days used at GDIL1.

30 frequencies, giving 60 degrees of freedom with a 95 % significance level of 0.098 (Figure 19). Coherence between water level and each wind component was found to be frequency dependent. The significant energy peak is at very low frequency, roughly less than 0.01 cph. At short sub-tidal time scales (a few days), the along-estuary wind stress drives an estuarine-shelf exchange; at longer time scales Ekman convergence/divergence driven by alongshore wind stress drives the estuarine-shelf exchange (Schroeder and Wiseman, 1986). Kjerfve (1975), based on a summer field study, suggested that Louisiana estuaries exchange water with the shelf on time scales greater than 1 day in response to Ekman convergence at the coastline driven by the alongshore wind stress.

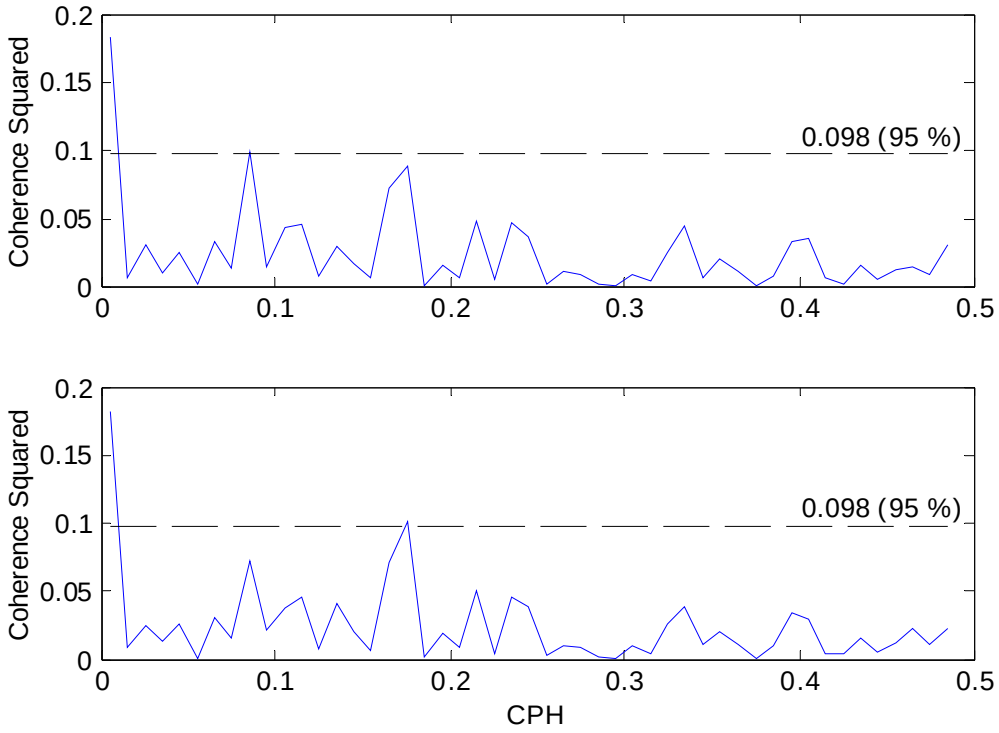

Figure 19. Coherence squared between water level at S1 and wind component at GDIL1; eastward stress (upper) and northward stress (lower).

Salinity studies in coastal areas, including estuaries, are common because of the variability of salinity distribution and its effects upon biota and flow regimes (Byrne et al., 1976). The salinities in Barataria Basin are controlled by rainfall, evaporation, diversions from the Mississippi River, and Mississippi River discharges, and seasonal changes in tide (Barrett, 1971). Until two diversion sites were constructed, the rainfall was found to be most influential in the upper basin. The Mississippi River discharge coming out of the Mississippi Delta located just east of the region is an important freshwater source in the lower basin. This is obvious in the inverse relationship between Mississippi River discharge and Barataria Basin salinity (Figure 20). In order to determine the relationship between salinities in Barataria Basin and Mississippi River discharge, the phase difference was estimated using the Mississippi River water level

data at Venice, a surrogate for discharge, and salinities at S1 (Figure 20). The regression result shows that there is almost a 13-day phase difference between the two sites.

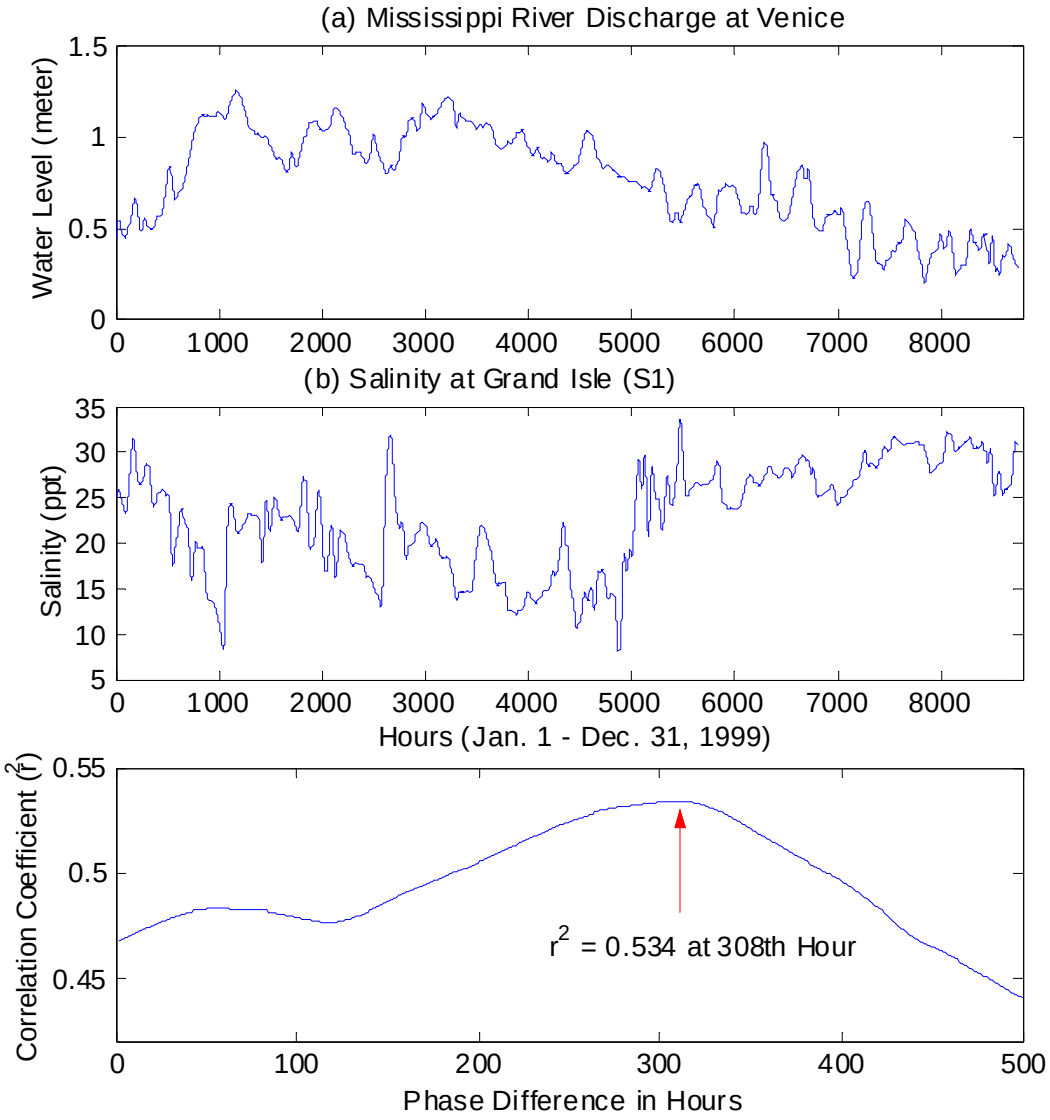

Figure 20. Mississippi River stage at Venice (a) and salinity variation in S1 (Grand Isle), and their cross-correlation function.

In the northern basin, the local rainfall and associated runoff have a more important role in controlling water levels than do tidal effects. In order to reduce the noise to signal ratio that might confound the effects of diversions, a relatively dry season was selected

for the model simulation. During this period, total precipitation was 6.8 *cm* (Figure 21), which is nearly half of the long-term average (15 *cm*). Evaporation, however, averaged 11.8 *cm* for the 30 days of the simulation (Figure 21).

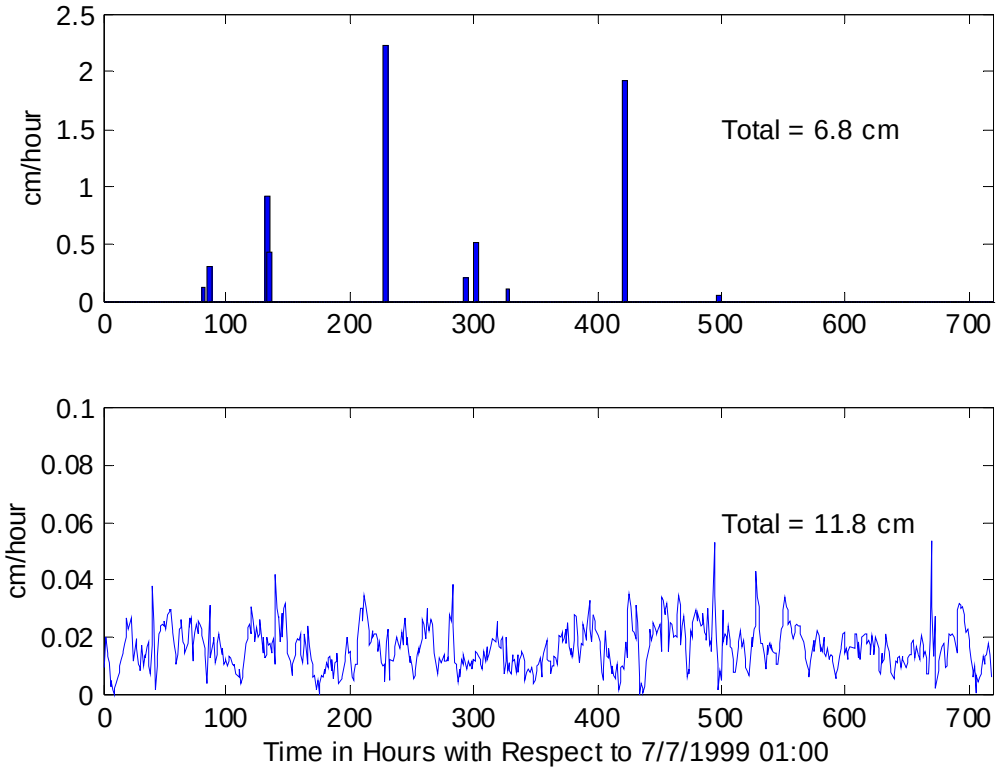

Figure 21. Measured precipitation at MSY (upper) and estimated evaporation (lower).

6.1 Results for Water Levels

The model was run with and without freshwater diversions from the Mississippi River. During this simulation period the freshwater diversion rates from the two diversion sites, Naomi and West Pointe à la Hache, varied with time while averaging $14.6\,m^3\,s^{-1}$ and $10.8\,m^3\,s^{-1}$, respectively (Figure 22). However, for this model simulation the pumping rates were fixed at either zero or their maximum rate ($60\,m^3\,s^{-1}$). When the maximum pumping rates were used in the model, they represent approximately a five-

fold increase over the true situation. Therefore, we expect the model to produce slightly different results from reality.

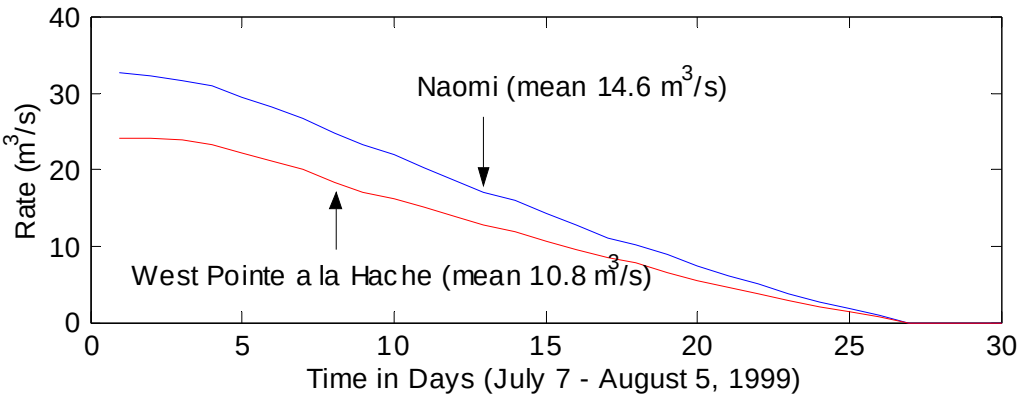

Figure 22. Freshwater diversion records from two sites during simulation period.

Figure 23 presents horizontal water level differences between the two cases, with and without freshwater diversions, at 4-hour intervals, during the first day of simulation. During the simulation with diversions, the freshwater source from the Gulf Intercoastal Waterway was set to 50 $m^3 s^{-1}$. (Because through the 30 days, the maximum water level differences at diversion sites reach 18 *cm*, to enhance the visual resolution the difference was plotted using maximum values depending on the time period of interest. Therefore, during the first day after release, the maximum was set at 0.5 *cm*.). At hour 4, the signal covered the two neighboring diversion sites and traveled over a region almost 5 *km* in diameter. By hour 8, this signal propagated almost 15 *km* including Lake Salvador. Some signal is detectable coming from the Gulf Intercoastal Waterway. At hour 12, the signal covered nearly the entire middle basin, about 20 *km* in diameter. At hour 20, the signal covered almost all of the basin, except the lower Barataria Bay and Lac des Allemands, with a value bigger than 0.2 *cm.*

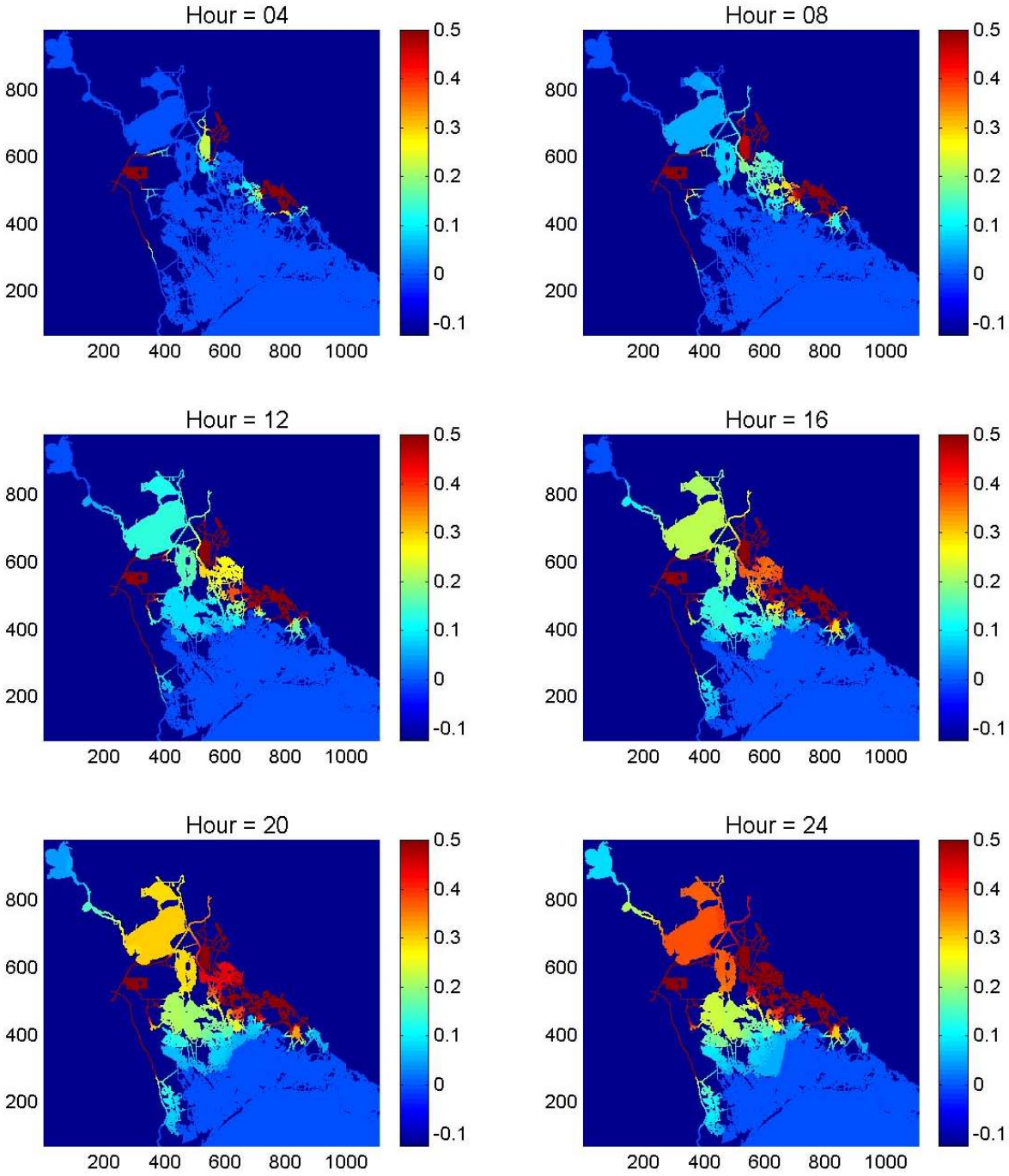

Figure 23. Water level difference (*cm*) between with and without freshwater diversion runs during the first day of simulation.

Figure 24 shows the daily water level difference snapshots during the first six days setting the maximum at 1 *cm*. On day 2, the entire basin was under the impact of the diversions except the eastern part of Barataria Bay. Some parts of Caminada Bay seemed to be affected by the Gulf Intercoastal Waterway. On day 3, the signal reached the Gulf of Mexico. On day 4, the water level difference surpassed a value of 1 *cm* in the upper Barataria Basin while the signal in Barataria Bay was rather reduced by the strong tidal dispersion. On day 5, the situation was similar to the previous day, but the downstream region exhibited increased impact due to reduced tidal energy. On day 6, the impact of the freshwater diversion remained relatively unchanged.

Figure 25 shows water level difference snapshots every 5 day during the simulation setting the maximum at 2 *cm*. On day 10, upstream, the difference seemed to have decreased compared to the previous days. On day 20, the difference was largest of all during the 30 days. The maximum water level difference between the two cases is 18 *cm*, near the Naomi diversion around day 20. In reality, because there are numerous connections between open waters and the diversions, which are not resolved by our grid, these differences between the two cases may be over estimated. On day 25, water level differences in the upper basin were similar to those of day 20. However, in Barataria Bay, the impact of freshwater decreased, causing significant gradients with neighboring waters to the north. On day 30, all impact was reduced except at the diversion sites.

In order to analyze the horizontal water level changes during a tidal cycle, a series of 3-hour interval data was extracted from the 30 days of recorded simulation results. It may be good to begin analysis near slack before flood or ebb at the mouth of the bay,

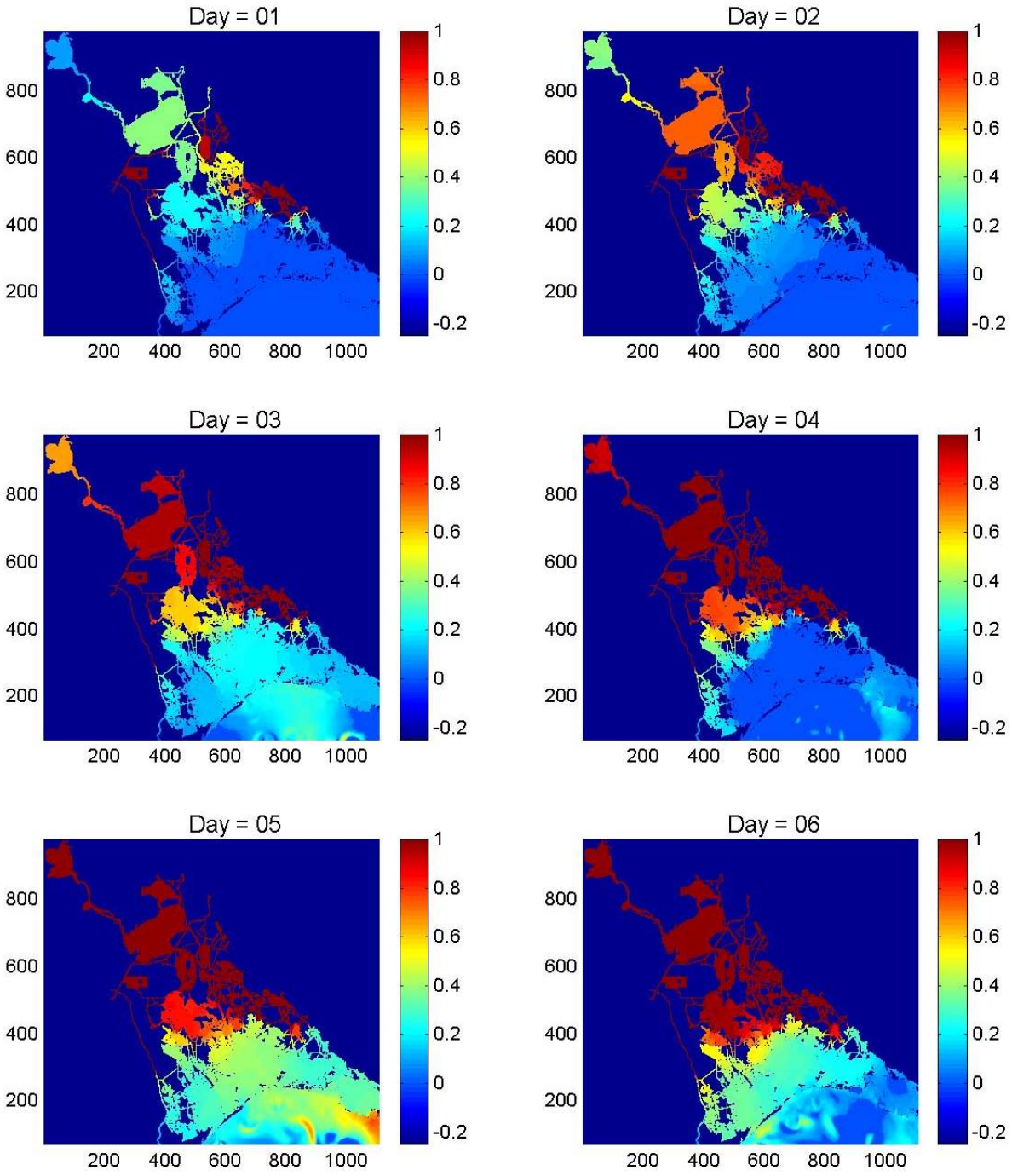

Figure 24. Water level difference between (*cm*) with and without freshwater diversion runs during 6 days of simulation.

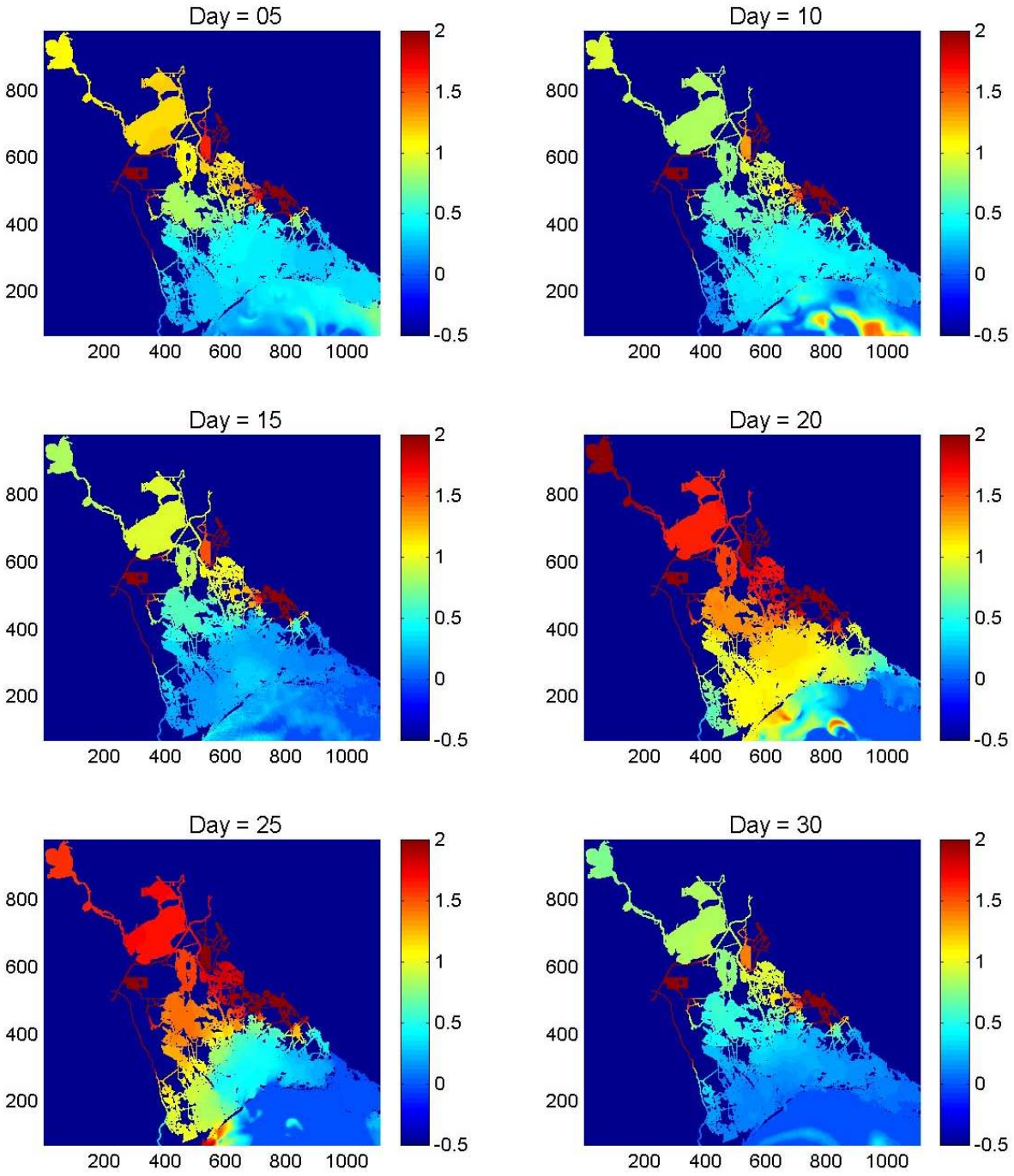

Figure 25. 5-day interval snapshots of water level difference between (*cm*) with and without freshwater diversion runs after 30 days of simulation with a maximum set at 2 *cm*.

where the highest water level changes occur during a tidal cycle in the Barataria Basin system. The water level on the 501st hour at S1 was selected as a beginning frame for the tidal cycle, slack before flood (Figure 26).

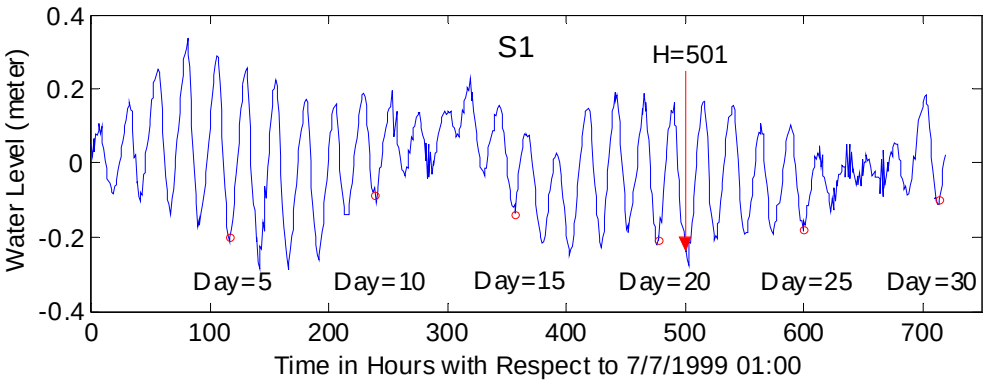

Figure 26. Water level time series at S1 and the selected start time, hour 501, of the first frame for the water level distribution discussion.

To begin understanding the tidal phenomena in Barataria Basin, it is necessary first to study the tide at the mouth of the bay. Barataria Basin is morphologically separated from the Gulf of Mexico by the several islands that block tidal energy from propagating into the bay. This is easily recognizable from the horizontal water level distribution (Figure 27). By glancing at the figures, the instantaneous water level distribution can be divided into four different regions: (1) the Gulf of Mexico, (2) Barataria Bay and Caminada Bay regions, (3) Little Lake and Barataria Waterway regions, and (4) the upper basin regions of Lac des Allemands and Lake Salvador. The separations are characterized by a chain of islands, narrow canals and bayous, and the Gulf Intercoastal Waterway. During the period pictured, the maximum water level change during the tidal cycle is roughly 40 *cm* near the mouth of the bay, except in the Gulf of Mexico. The tidal amplitudes decrease with signal propagation into the upstream regions. There are some

discontinuities at the transitions between Barataria Bay and Barataria Waterway, Little Lake, and Lake Salvador. It is difficult to distinguish water level changes at upstream sites during a tidal cycle due to the small variation compared to that in Barataria Bay and the Gulf of Mexico. Sometimes wind stress overpowers tidal energy in the shallow regions. The water level piled up at hour 501 in the northern lakes due to the consistent southwesterly wind (Figure 18).

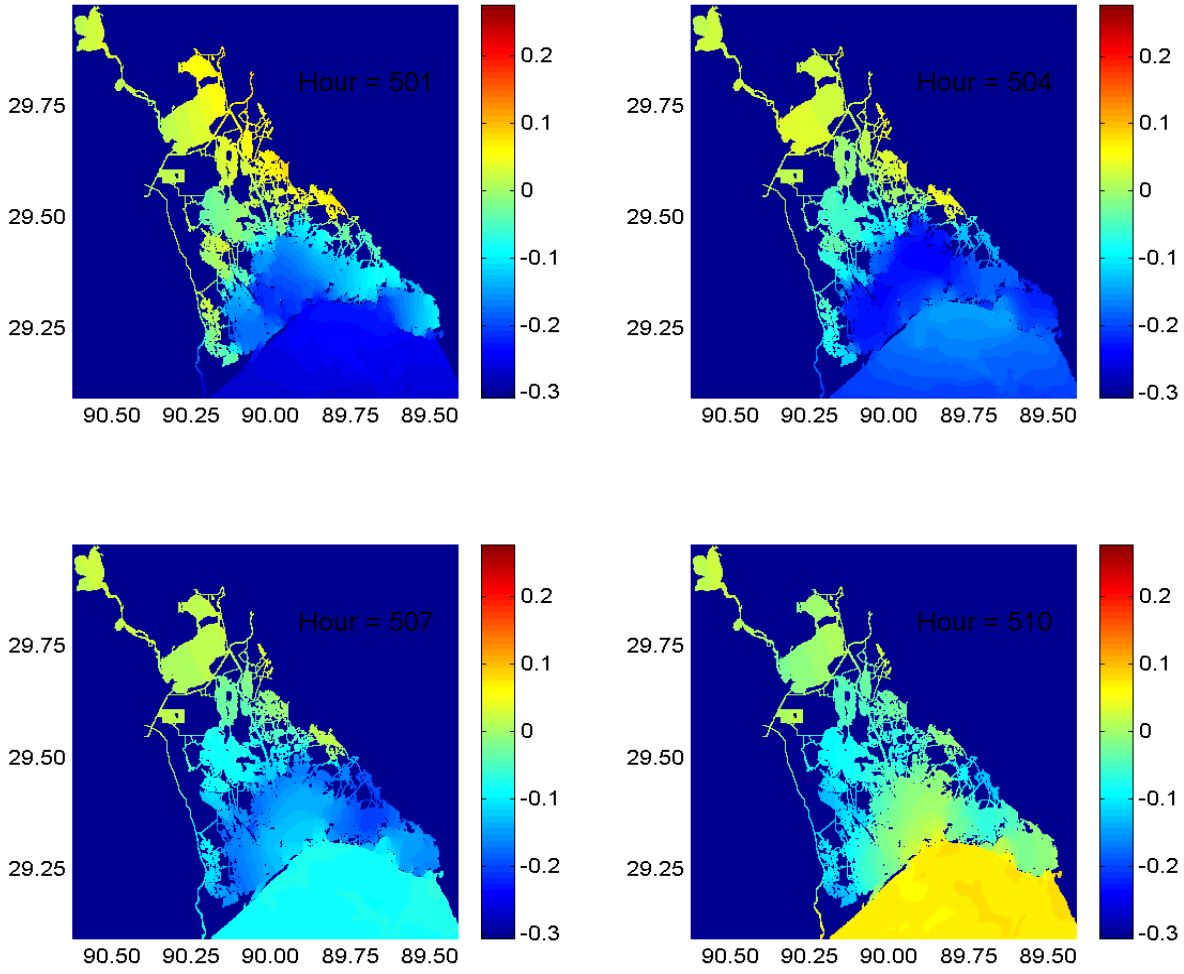

Figure 27. Instantaneous 4-hour interval horizontal water level (*m*) distribution during a tidal cycle.

(figure cont'd)

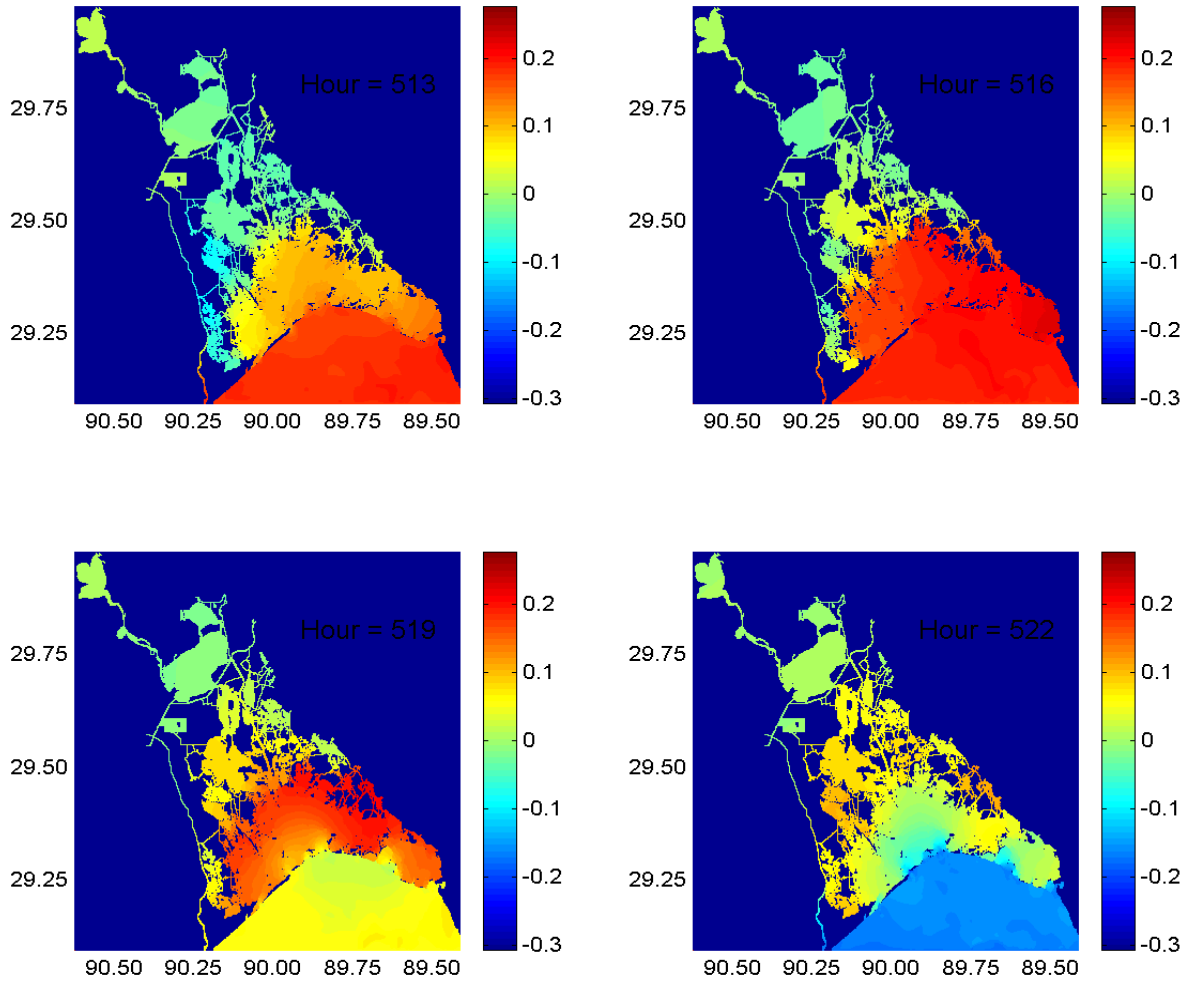

It may be convenient to examine the water level changes during a tidal cycle for selected locations. Figure 28 shows 30 locations selected from the mouth of the bay to the top of the basin (AB) and 20 locations selected from the mouth of the bay to the top of the Barataria Waterway (AC). Figure 29 shows water level changes during a tidal cycle, beginning at hour 501,for the locations indicated AB (upper) and AC (lower) in figure 28. Again, it is clearly seen that this basin is made of four different sub-regions. Within Barataria Bay, which corresponds to stations 1 through 7, the tidal amplitude is 40-45 *cm*.

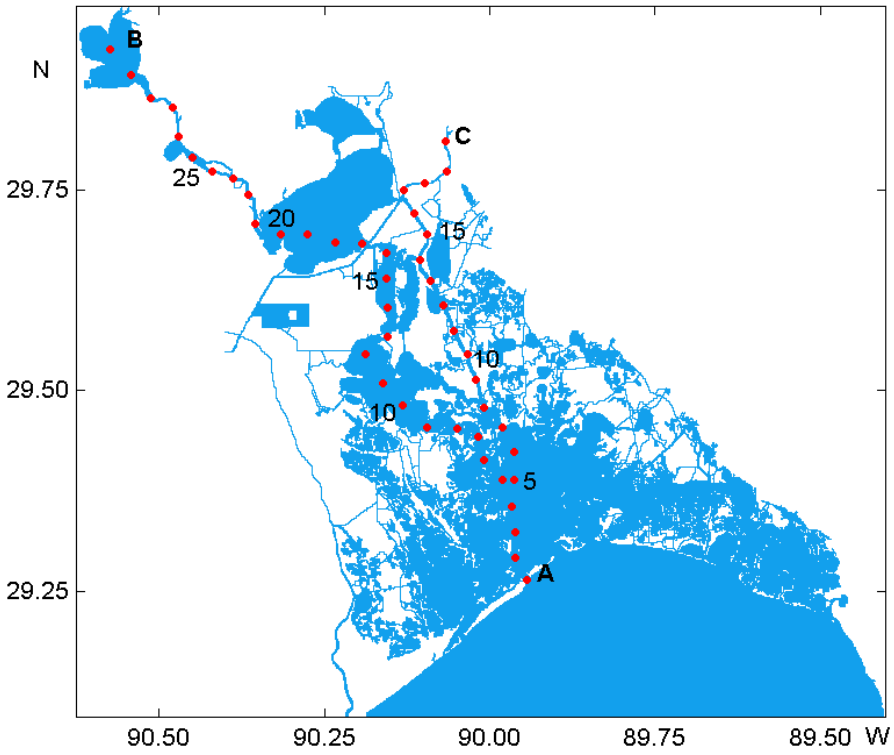

Figure 28. Selected locations from the mouth of the bay to the top of the basin (AB) and to the top of the Barataria Waterway (AC).

There is a sudden decrease in amplitude between stations 7 and 9 along transect AB, which lies in the narrow channels between Barataria Basin and Little Lake. Between stations 9 and 12 (Little Lake), the water level changes about 20 *cm* during a tidal cycle. Between stations 12 and 14, there is a sudden decrease across the narrow shoal between Little Lake and Bayou Perot. Near station 15, the water level varies roughly 10 *cm* during a tidal cycle. At station 17, there is a short sudden decrease in amplitude, as the transect enters a narrow region across the Gulf Intercoastal Waterway and proceeds into Lake Salvador. Above Lake Salvador, the water level changes during a tidal cycle are about 7 *cm*, and then they smoothly decrease into Lac des Allemands. Along the transect AC there are similar patterns to those observed in Barataria Bay (between stations 1 and

7). Between stations 7 and 8, there is a sudden decrease due to the narrowness of the Barataria Waterway. Beyond station 8, they smoothly decrease to the top of the Barataria Waterway with a small sudden decrease near station 15. It is clearly seen that the water level piled up at hour 501 and 502 in the top of the Barataria Waterway due to the consistent southwesterly wind.

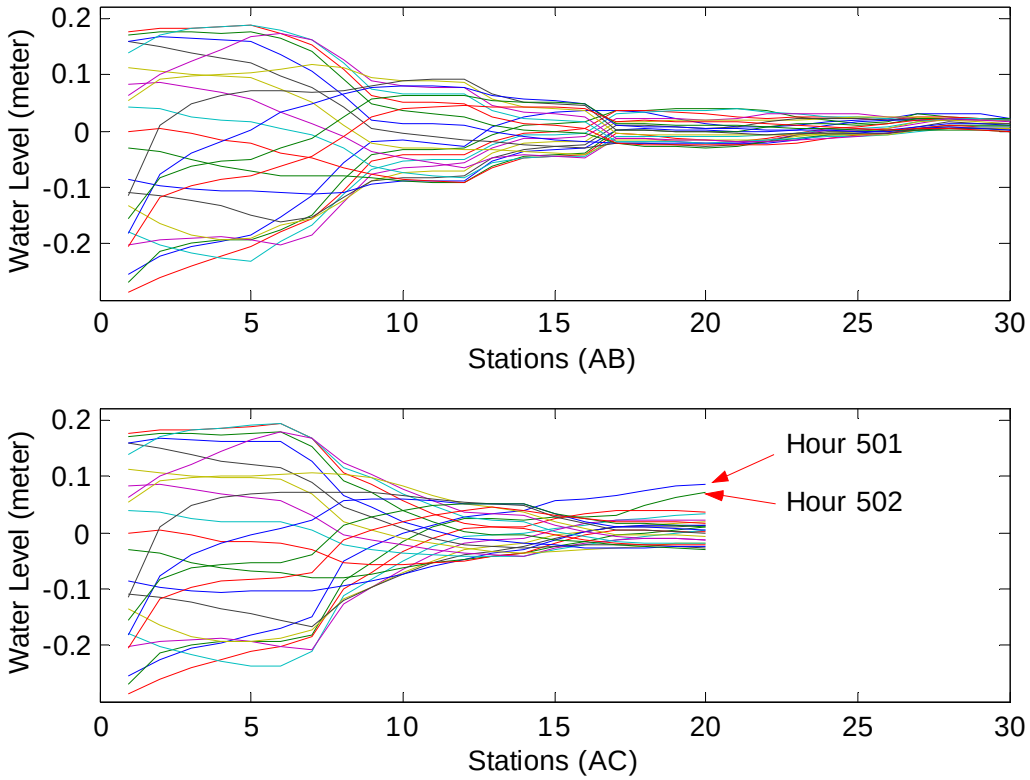

Figure 29. The water level changes during a tidal cycle beginning at hour 501 at locations indicated AB (upper) and AC (lower) in figure 9.

It is interesting to estimate tidal phase speed from the bottom to the top of the basin. We may simply apply the well-known shallow wave formula, $C = \sqrt{gH}$, as long as the water depth is known. Even though the water depth is known, though, it varies with location. Another method to estimate phase speed is by applying the Hovmüller diagram,

which is a plot of wave amplitude or phase against time and distance. In order to estimate the tidal phase speed for the basin, the thirty stations from Figure 28 were used. The tidal amplitudes are plotted against station and time (Figure 30). The blue arrow originating at station 1 near hour 81 indicates the propagation of a tidal wave crest and suggests that it takes 16 hours to traverse the system. It is easily seen that some sudden changes in phase velocity appear to occur due to the basin's morphological characteristics. For instance, there is a sudden change near station 17, possibly due to the Gulf Intercoastal Waterway.

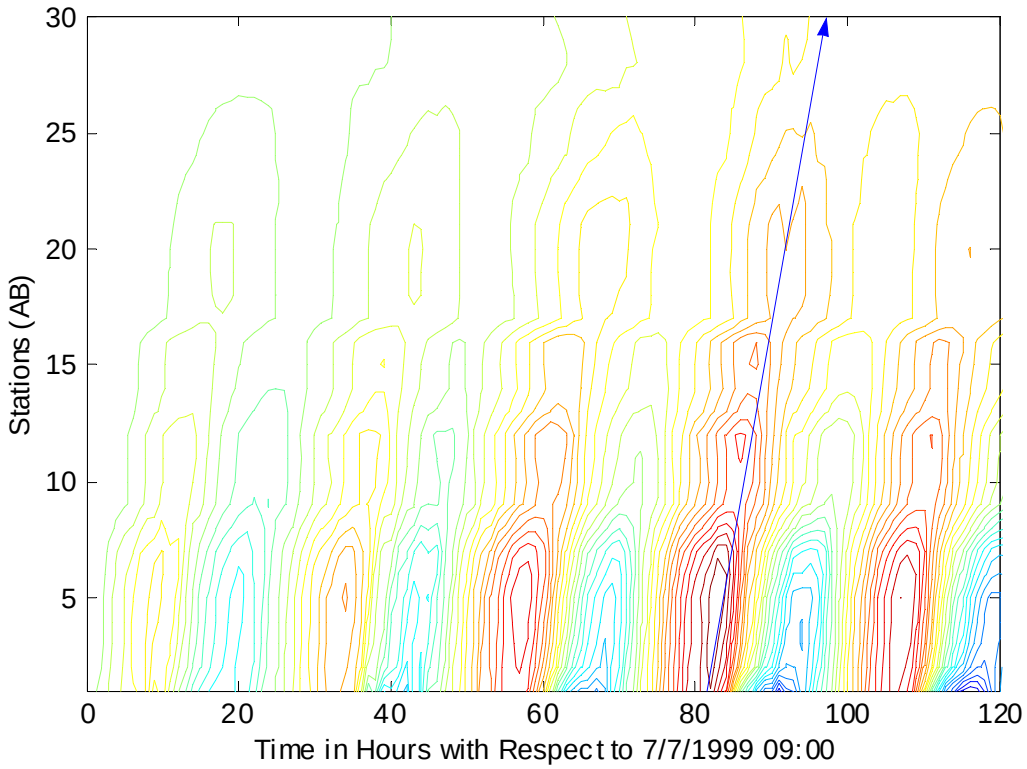

Figure 30. Hovmüller diagram: water level vs. time and station location.

6.2 Results for Salinity

The model was run with and without freshwater diversions from the Mississippi River. During the simulation period the freshwater diversion rates from the two diversion sites, Naomi and West Pointe à la Hache, varied with time. However, for this model simulation the pumping rates were fixed at $0\ m^3\ s^{-1}$, or their maximum rate, $60\,m^3\ s^{-1}$. The diffusivity was fixed at $5\ m^2\ s^{-1}$. Because of the high resolution of the model grid, the increased complexity of the advection scheme and the need to compute density at each point, CPU requirements were much greater than those of Park (1998). Furthermore, salinity adjusts through advection and diffusion, much slower than the adjustment of water level in a homogeneous model, such as investigated by Park (1998). Although the model did not reach fully spun-up conditions for salinity, the results are useful in that they describe spatial and temporal evolution of salinity field.

In order to analyze the horizontal salinity variability during the simulation period, a series of data, sampled at 5-day intervals, that does not include diversions was extracted from the 30-days of recorded results (Figure 31). All data periods selected were near the slack before flood to show maximum contrast between the two results. Therefore the selected data will not match exactly the date shown with a maximum 5 hours difference (Figure 32). On day 5, since the stage at the moment of the snapshot was near the beginning of flood for the mouth of Barataria Pass, maximum plume excursion from the mouth of the passes was observed. Inside the bay, low salinity extended to the mouth of the basin. It can be seen easily that the high salinities are coming from the open boundary. It is notable that there are big gradients in the coastal waters due to the time and space variations of salinity imposed along the open boundary.

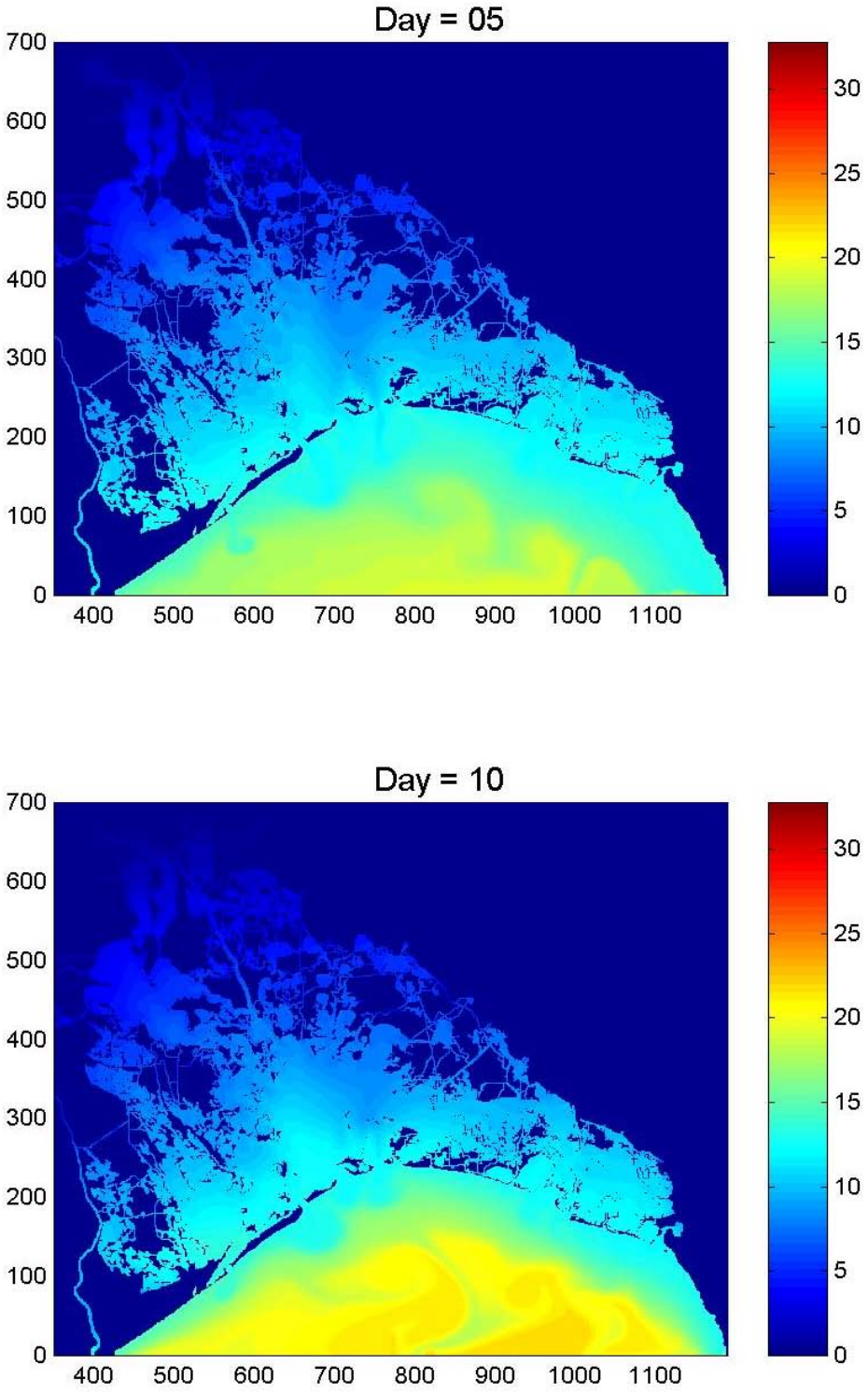

Figure 31. Horizontal salinity (*ppt*) distribution during the simulation period, a series of data sampled at 5-day interval All data period selected were near the slack before flood.

(figure cont'd)

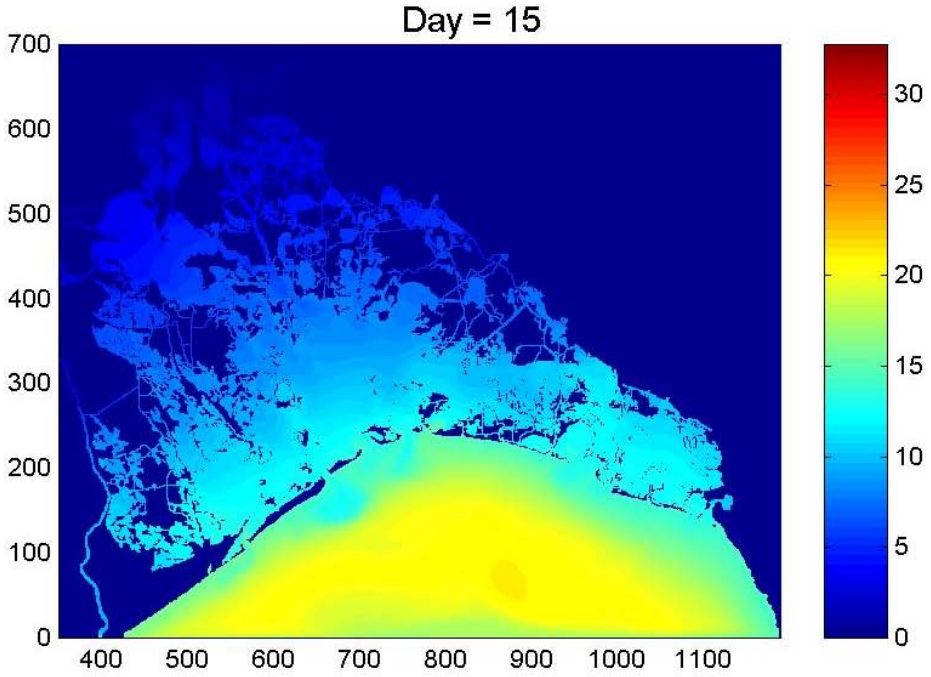

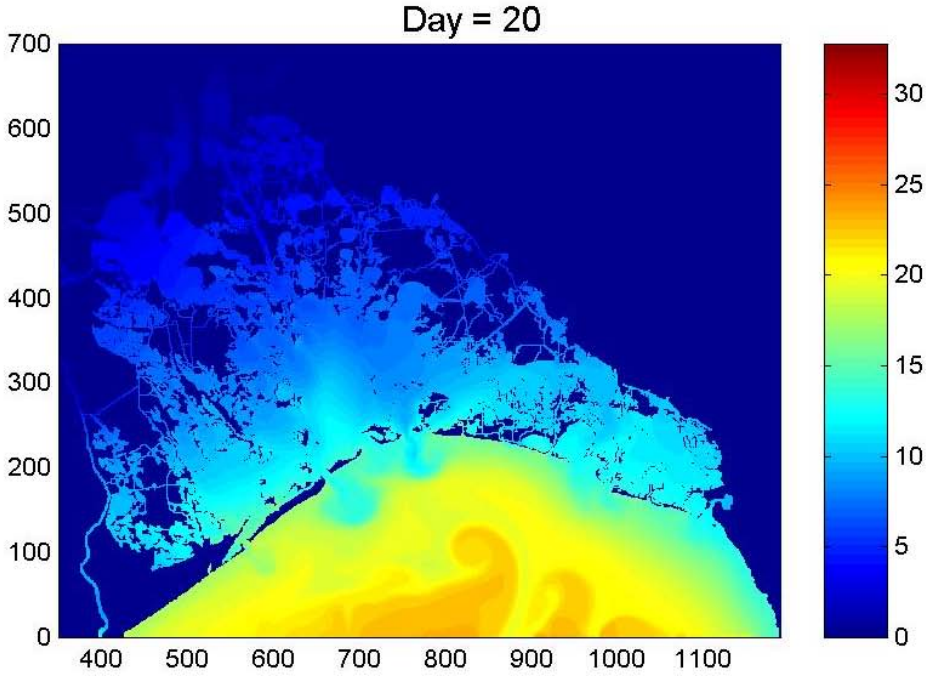

(figure cont'd)

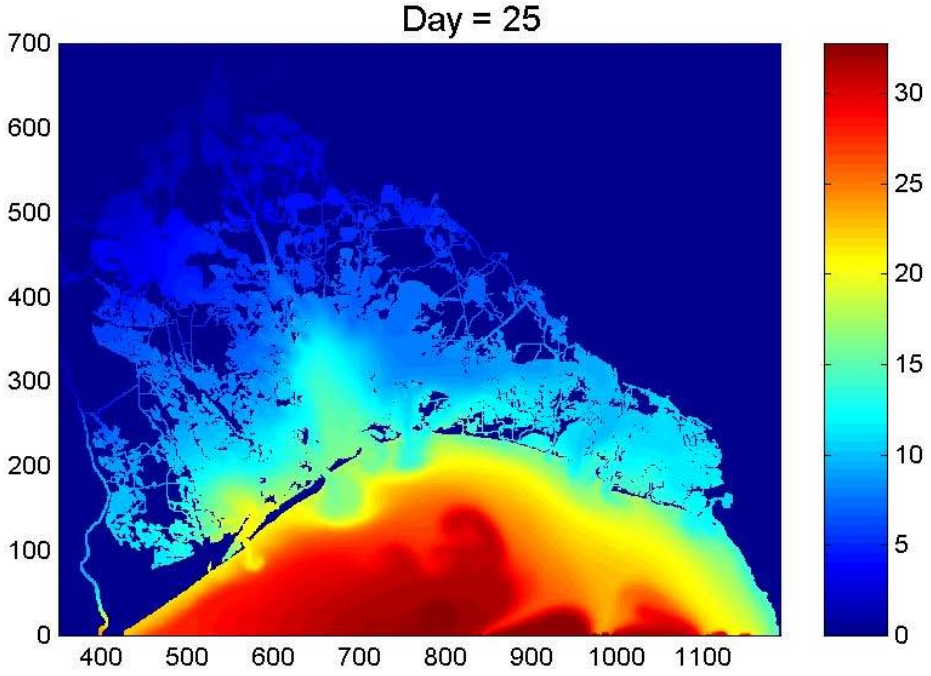
Day = 25
700
600
500
400
300
200
100
0
400
500
600
700
800
900
1000
1100
30
25
20
15
10
5
0

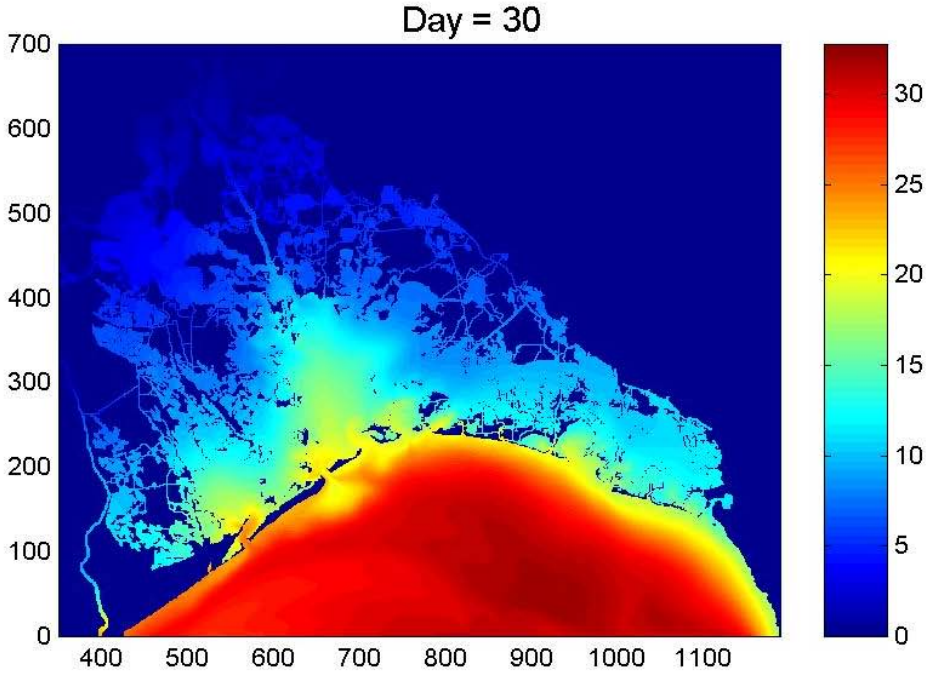
Day = 30
700
600
500
400
300
200
100
0
400
500
600
700
800
900
1000
1100
30
25
20
15
10
5
0

On day 10, the situation is similar to that of day 5 except for the higher salinity values coming from the open boundary. By day 25, very high values of salinity are coming from the open boundary and penetrating far into the basin. There are big salinity gradients in the northeast region of the Gulf of Mexico in the model domain. On day 30, after several days of high salinity values at the open boundary, the high gradients increase at the coast.

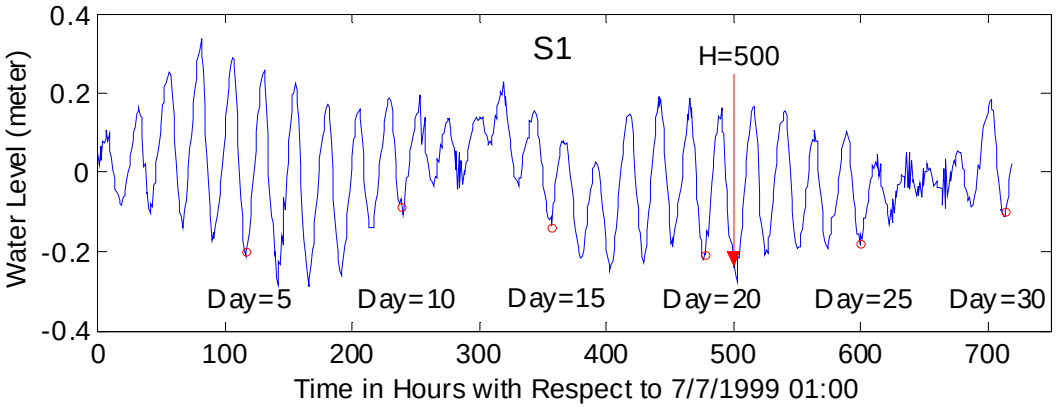

Figure 32. Water level time series at S1 and salinity snapshots' times (indicated by red circles).

In shallow, bar-built estuaries, it is often assumed that the flow field is vertically homogeneous (Wiseman, 1996). When the estuary is shallow, the velocity shear on the bottom may be large enough to mix the water column completely and make the estuary vertically homogeneous (Dyer, 1973). The concern over the use of a two-dimensional model for this modeling study is in its application to deep channels, waterways, or passes, such as the Barataria Pass. As mentioned earlier, the Barataria Basin has five passes that connect to the Gulf of Mexico (see Figure 2). Except for Barataria Pass, all of the other passes are very shallow, allowing an assumption of vertical homogeneity to be made. Barataria Pass, however, is wide (about 1 *km*) and deep (deeper than 12 *m* in the

center of the pass) permitting significant stratification to exist. This pass is the largest opening between Barataria Basin and the Gulf of Mexico. In reality, salinity intrusion along the bottom of the pass may occur. For this reason, the model is expected to have slightly less salt intrusion through the relatively deep pass than might occur in nature. For similar reasons, salt flux through Barataria Waterway may be underestimated.

Another problem we may expect from the salinity simulation is an underestimation of salt flux due to the inadequate salinity open boundary condition. First, salinity was set to vary spatially along the southern open boundary with high values near the middle and low values near both of the edges, which may cause alongshore currents that block salt intrusion into the basin. Second, due to the lack of salinity measurements near the southern open boundary, the salinity recorder from site S1 was used for salinity open boundary conditions after low-pass filtering with a seventy-two hour moving average. Although the salinity data from S1 was smoothed, it may still be far away from the real salinity value along the open boundary. Figure 33 shows the salinity comparisons between observations (blue) and simulation results with (green) and without (red) diversions. At the mouth of the bay and in Barataria Bay, S1 and S2, respectively, although the simulation results capture the general trend of the low frequency signal, they are too smooth when compared to the observed data. At station S3, the observed salinity data seems to contain instrument error. Further upstream, at S4, the results look better than those downstream in the sense that the mean value of model and data approach each other late in the simulation and the amplitudes of the tidal signals are similar.

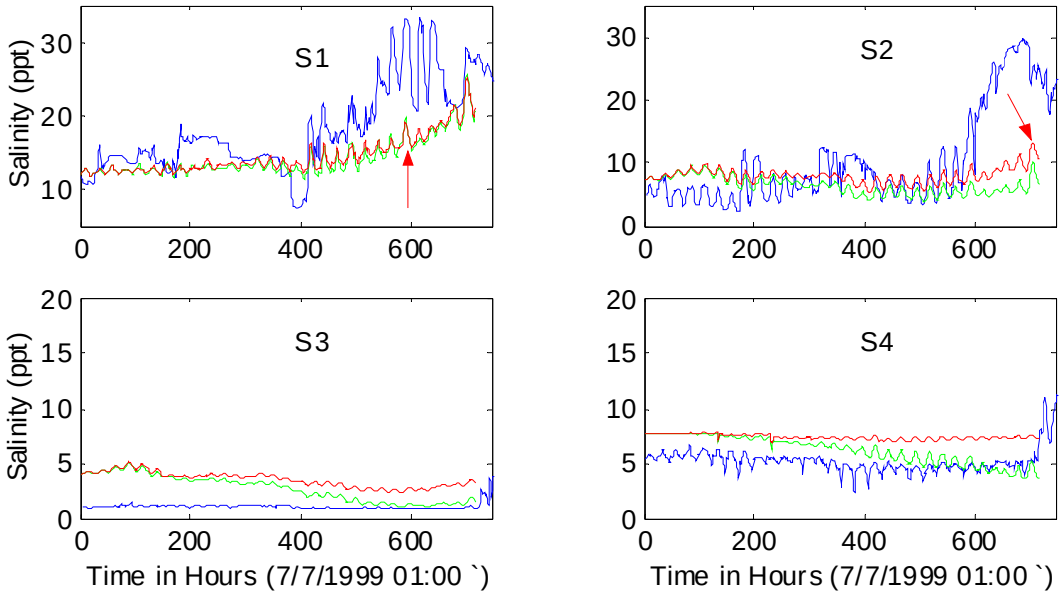

Figure 33. Salinity comparisons between observations (blue) and simulation results with (green) and without (red) diversions.

In order to describe tidal mixing of salinity and tidal plume characteristics, a series of 2-hour interval salinity snapshots over a tidal cycle were extracted and zoomed in on at the mouths of the basin (Figure 34). The first snapshot, begins at hour 500, shows slack before flood. Outflow plumes are easily seen at the three passes. During this stage, the plumes reaches maximum size. No time lags exist between tidal stage at the passes. The largest plume, 3 *km* in diameter, exits through Barataria Pass. There are large salinity gradients between the plume and neighboring waters. A mushroom-like plume 2 *km* in diameter formed at the mouth of Quatre Bayou Pass. Although the size of the plume is slightly smaller than that from Barataria Pass, the salinity gradient is greater than that at Barataria Pass due to the lower salinity inside the bay. Although the flood has already begun, the sizes of plumes do not change significantly for the next several hours, while their morphology does change. However, inflow plumes are noticeable inside the bay by

hour 506. At hour 508, the plumes from all three passes were clearly retracting into the basin under tidal forcing and forming well-defined inflow plumes inside the bay. Notice that high salinity values are detectable along the left side of Barataria Pass during the flood, probably due to the alongshore salinity gradient immediately offshore. Unlike the outflow plumes, the inflow plumes spread in several different directions due to the morphological characteristics of the bay. By hour 512, most of the outflow plumes disappeared. At hour 518, inflow plumes reached their maximum extent, a length of 11 *km*. Some of this water remained in the bay over the entire cycle. After hour 520, the inflow plume began to move back out through the passes.

To characterize the influence of the freshwater diversions from the Mississippi River, the two different results, with diversion and without diversion, were compared. One way to see the difference between the two results is to subtract the one from the other. To give a better understanding, the results with freshwater diversions were subtracted from the results without freshwater diversions (Figure 35). In the figures, red shows high differences, and blue shows low differences. The maximum difference occurs on day 30, 6.06 *ppt* at West Pointe à la Hache. It is difficult to distinguish the color differences due to the relatively broad range of salinity differences. Through the 30 days the maximum salinity difference, ranging 4.71~6.06 *ppt*, appears at West Pointe à la Hache. To enhance the color resolution, plots were limited to a maximum value depending on the starting time and duration of interest. For instance, during the first several hours or days, we may not see big salinity differences in the domain except near West Pointe à la Hache, which shows a maximum. Therefore during the first day after release, the maximum to be plotted was set at 0.5 *ppt*. Figure 36 shows 4-hour interval snapshots for the first day.

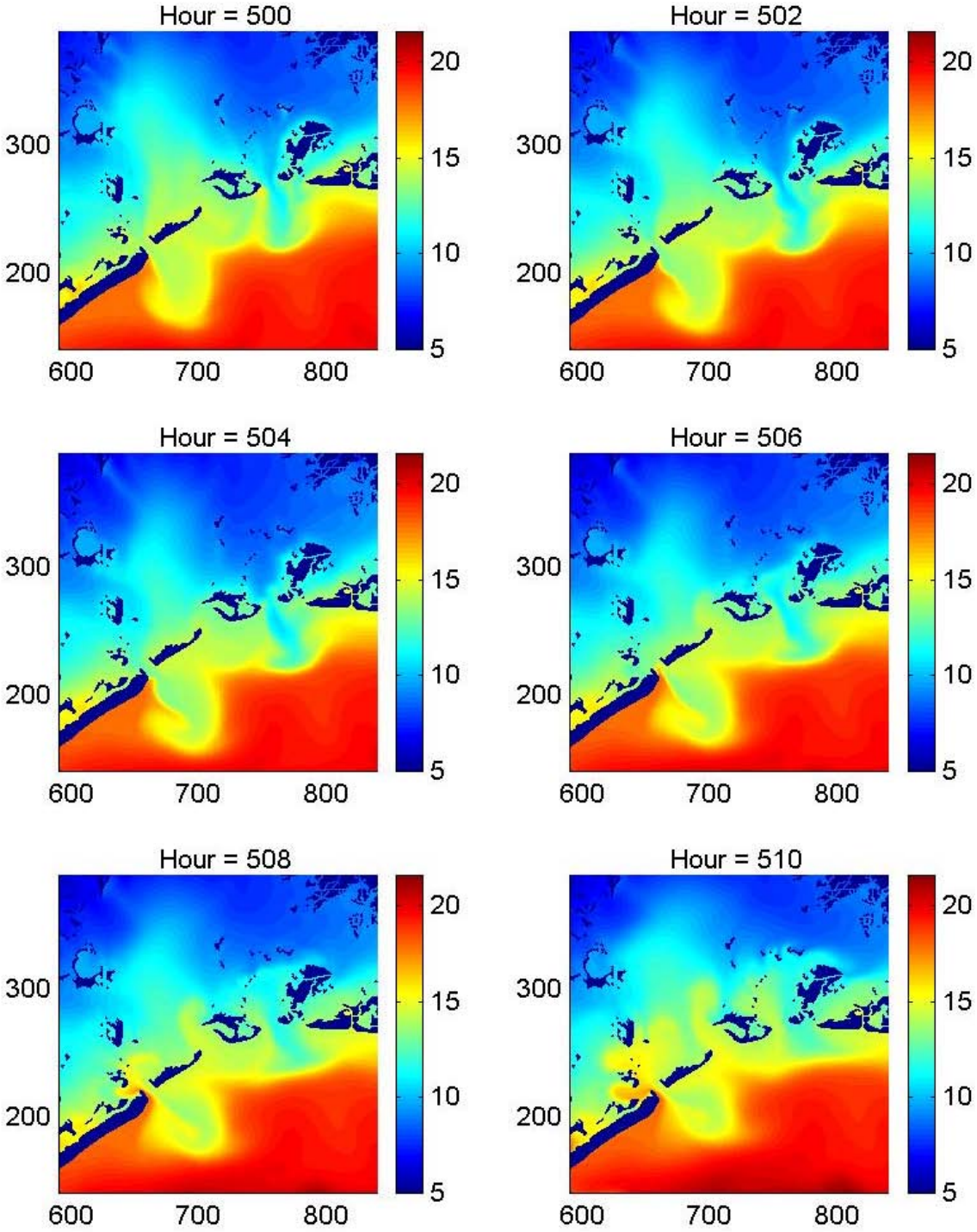

Figure 34. Inflow and outflow plumes at the mouth of the Barataria Bay .

(figure cont'd)

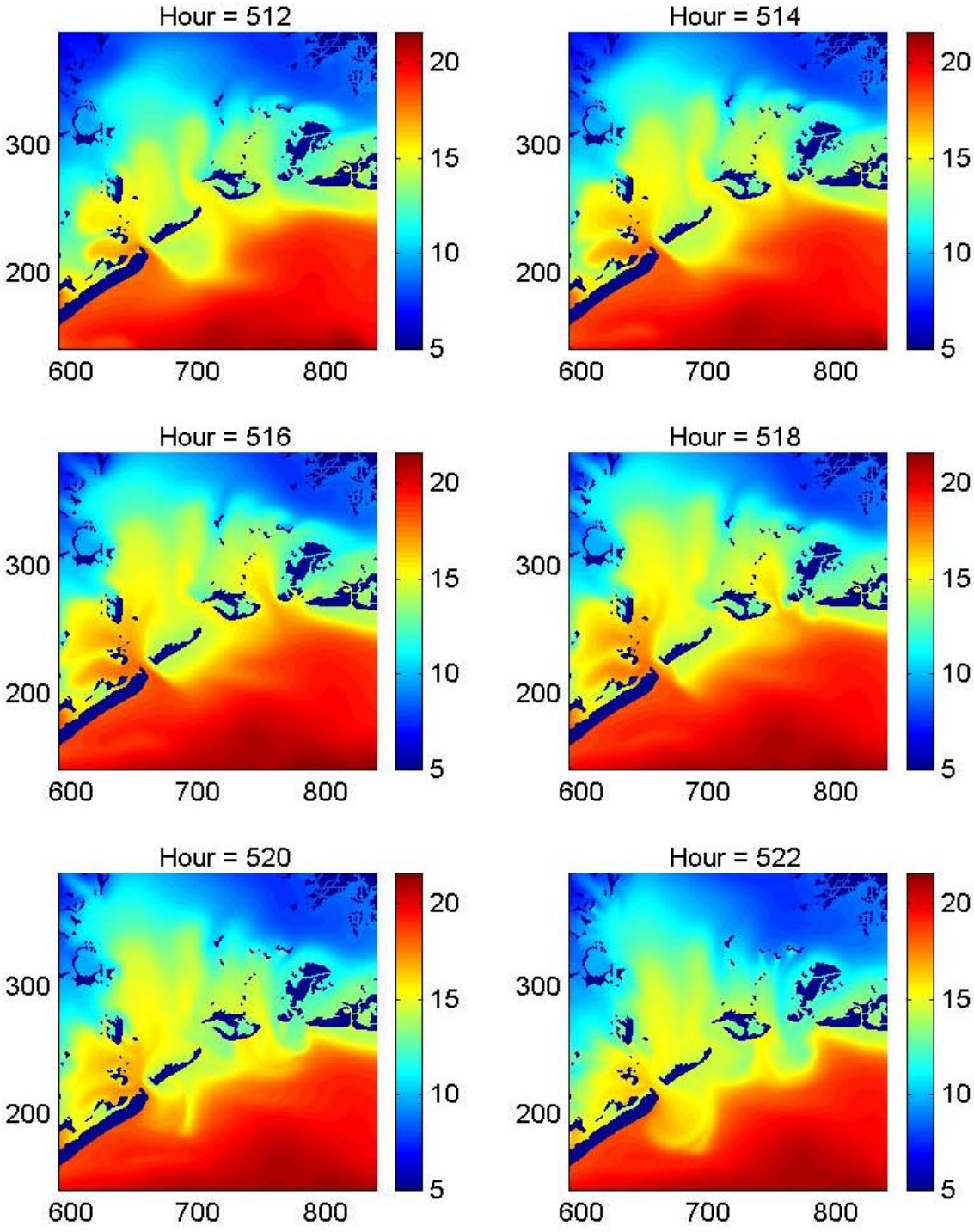
Hour = 512
Hour = 514
Hour = 516
Hour = 518
Hour = 520
Hour = 522
300
200
600
700
800
20
15
10
5

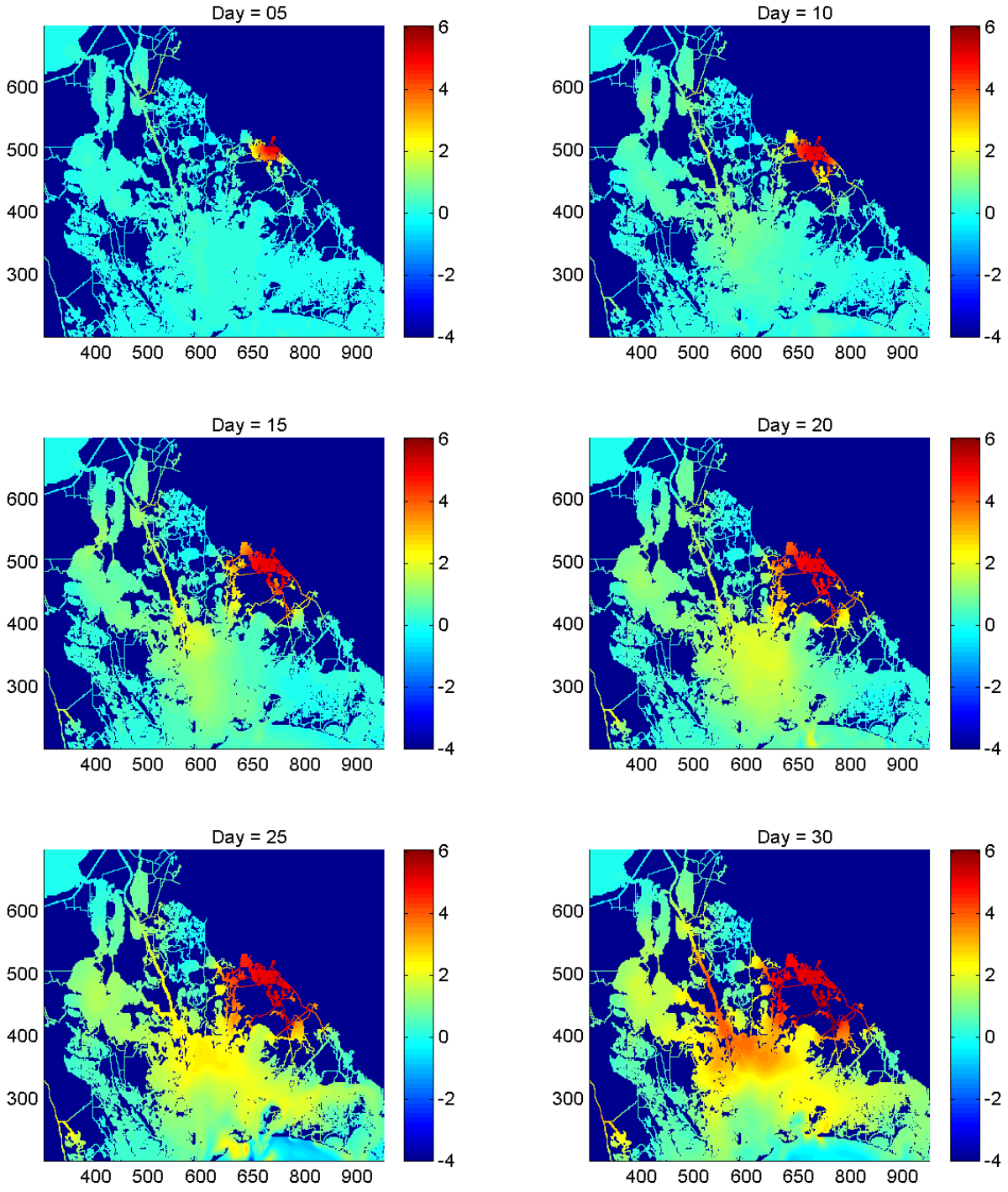

Figure 35. Salinity difference (*ppt*) snapshots for the 5-day interval.

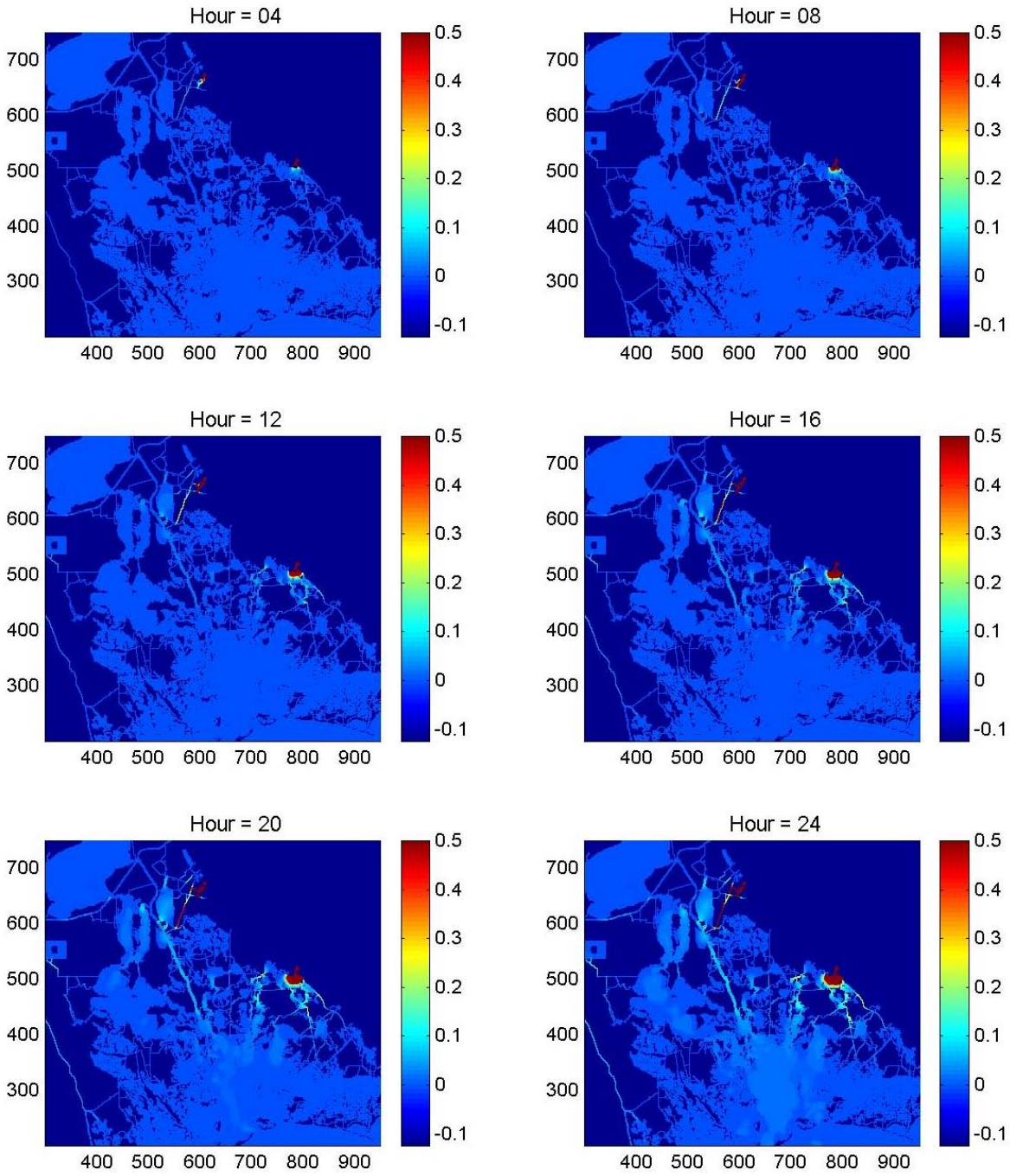

Figure 36. Salinity difference (*ppt*) snapshots 4-hour intervals the first day.

The dark red represents regions where the difference was equal to or bigger than 0.5 *ppt*. At hour 4, the signal is only concentrated near the diversion sites. At hour 8, the signal is detectable through the narrow canal near Naomi. In reality, this may be over-estimated since the Naomi site is surrounded by marshes and narrow canals, which cannot be resolved due to the model grid size used. Because of the narrow connections and relatively bigger local receiving volume near West Pointe à la Hache, the signal from West Pointe à la Hache propagates much slower than that from Naomi. Near West Pointe à la Hache, the large difference is easily detectable. At hour 12, it is easily seen that the signal is spreading from West Pointe à la Hache. At hour 16, though the signal is weak, it is detectable in Barataria Waterway. By hour 20, the signal from Naomi extended into the northern part of Barataria Bay. Although the values are small and difficult to detect, the signal reached the middle of Barataria Bay, and some parts propagated to Little Lake. The latter signal seems to be contributed by the Naomi diversion. Once the signal from Naomi reaches the Barataria Waterway, it propagates quickly due to the relatively deep and narrow waterway. Clearly, the signal from Naomi reached Bayou Rigolettes through Barataria Waterway. The snapshot from hour 24 is similar to that from hour 20. Figure 37 shows the current differences between two different simulation results. Due to the water level difference between simulations with and without diversion, current speed differences are found in the downstream region. In particular, current differences in Barataria Waterway are noticeably large due to the influence of the Naomi diversion. At four stations, the mean flow differences are toward the southeast, seaward.

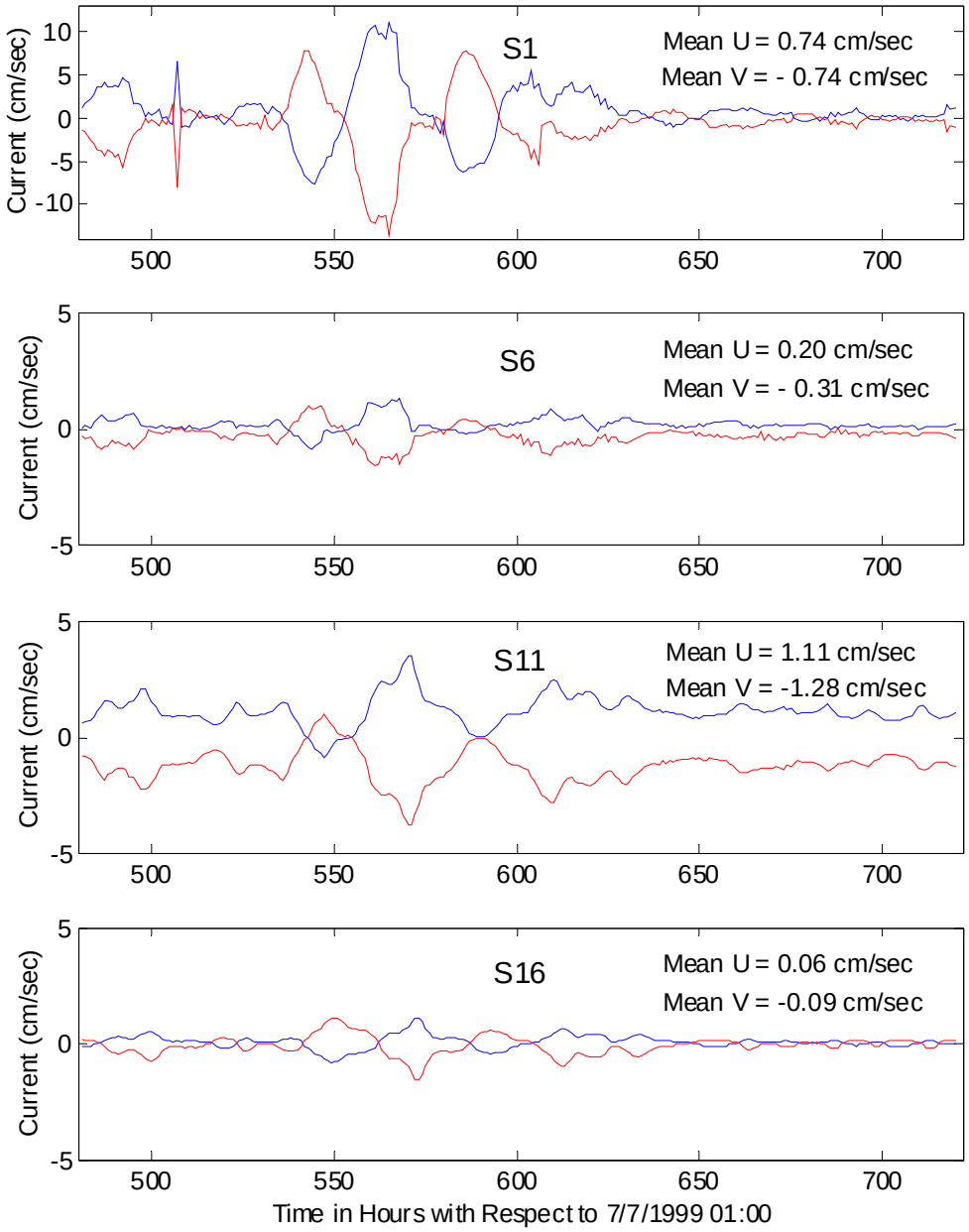

Figure 37. Current speed differences from the results between with and without diversions along the line AC on figure 28 (blue: latitudinal speed; red: longitudinal speed).

Due to the salinity signal propagating slowly, it may be good to see daily interval snapshots for several days (Figure 38). The maximum difference to be plotted was set at 1 *ppt*. The signal, both from Naomi and West Pointe à la Hache, reached Barataria Bay and extended to Little Lake. On day 3, the signal in Barataria Bay and Little Lake was clearly visible and some part reached Lake Salvador. On day 4, most of the area of Barataria Bay was covered by salinity bigger than 0.2 *ppt*, and some signal reached the Gulf of Mexico. Strong salinity differences entered upstream within Barataria Waterway. On day 5, differences bigger than 0.8 *ppt* occurred in Barataria Waterway.

Figure 39 shows 5-day interval snapshots colored with the maximum difference set at 2 *ppt*. On day 10, Barataria Waterway contained a nearly 1.5 *ppt* difference. When freshwater from West Pointe à la Hache reached Barataria Bay, the impact seemed to accelerate. It is clearly visible that high salinity difference values concentrate in the northern region of Barataria Bay. It is roughly estimated that the impact of freshwater diversion reaches the Gulf of Mexico in around 10 to 15 days after freshwater release. After about 15 days, the freshwater diversions seemed to impact most of the downstream region of the Barataria Basin except the eastern part of Barataria Bay and Caminada Bay. In the middle of Barataria Bay, the difference reached near 2 *ppt*. By day 25, most of the downstream basin was measurably impacted by freshwater diversion. Even after day 30, though, some isolated areas still remained without noticeable influence of the diversion. It is apparent that near the mouth and inside the bay, freshwater impact was reduced due to the strong tidal movement.

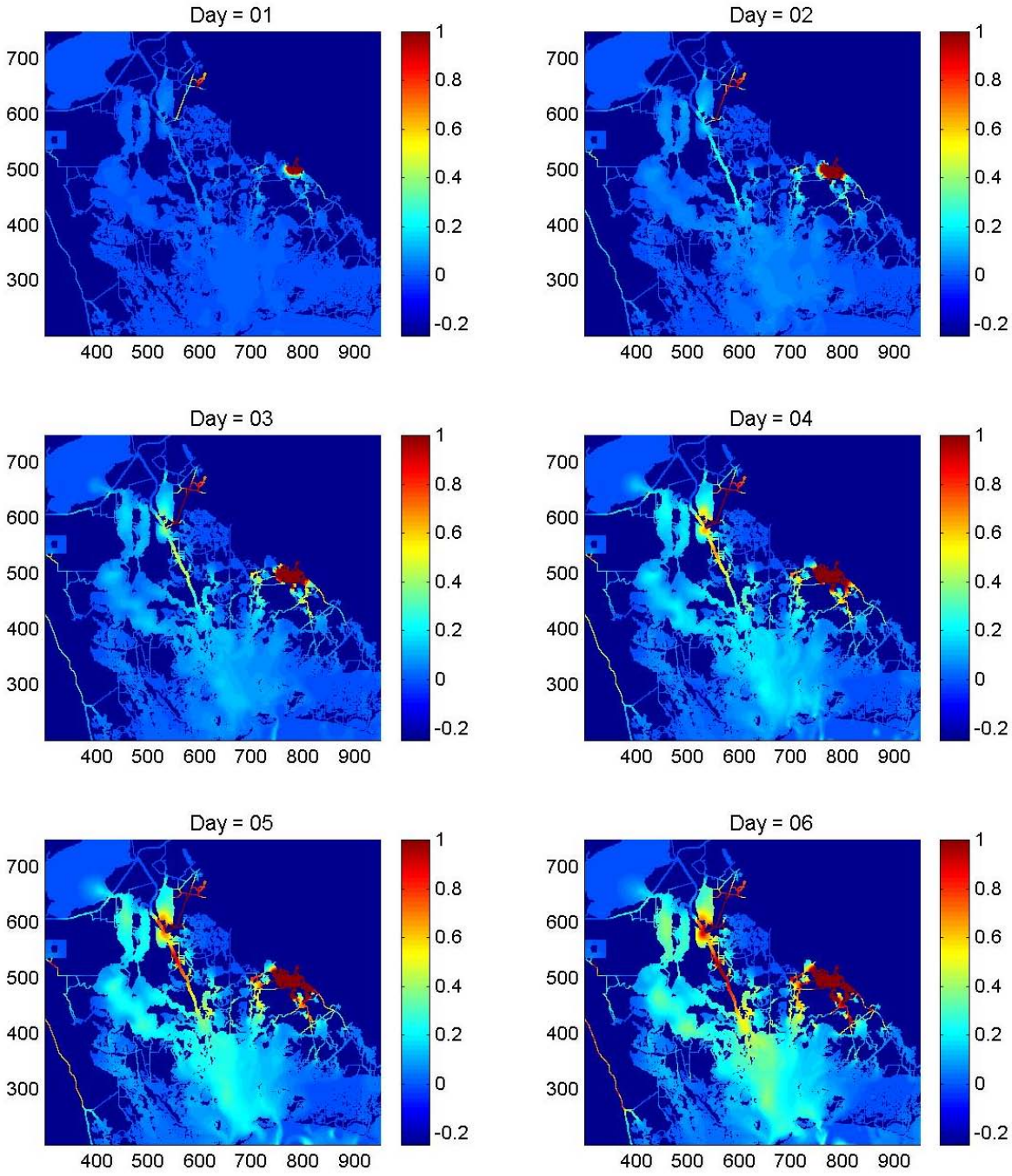

Figure 38. Salinity difference (*ppt*) snapshots daily intervals for the first six days.

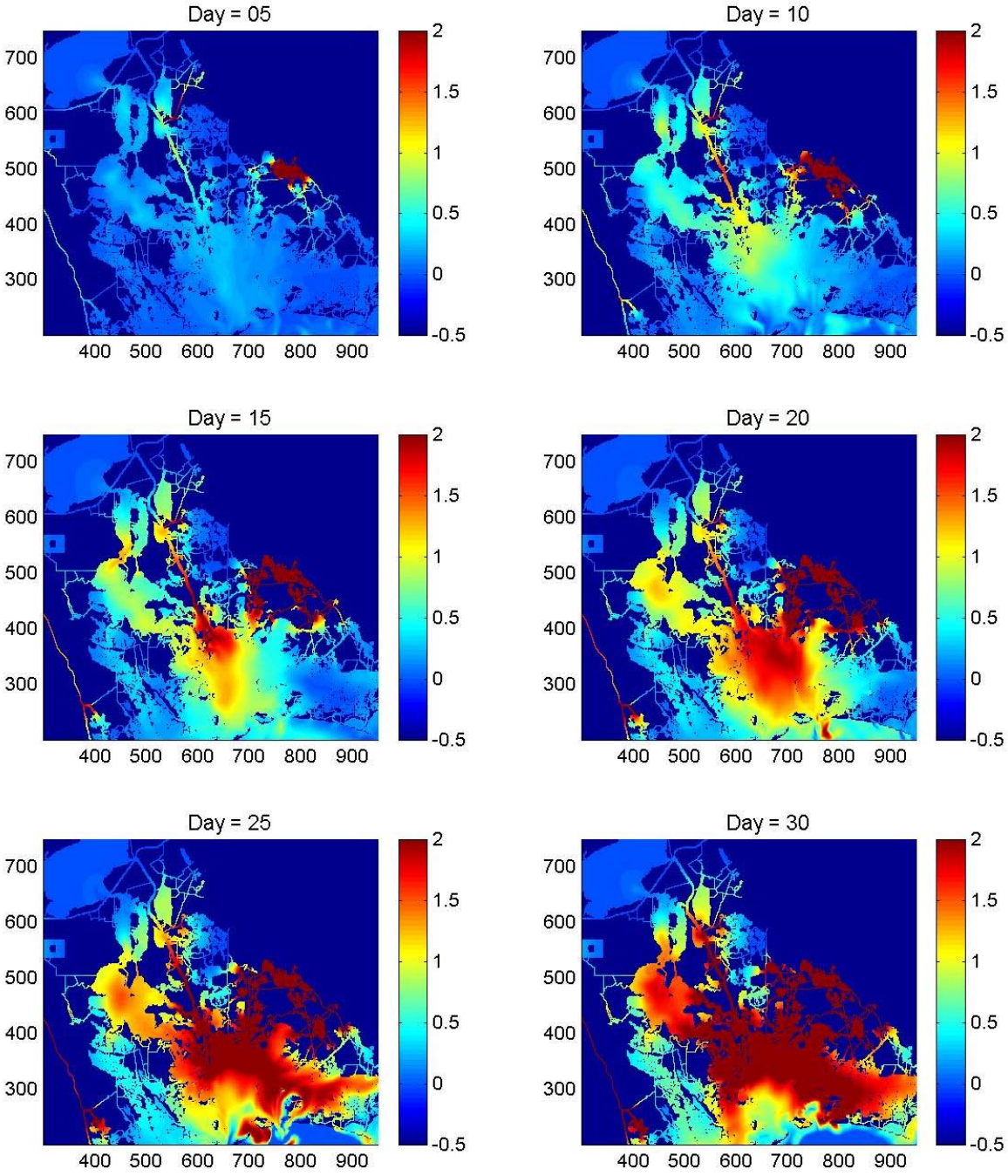

Figure 39. Salinity difference (*ppt*) snapshots at five-day intervals.

7. CONCLUSIONS

In order to understand the physical processes in the Barataria estuary, a previously developed two-dimensional, depth-integrated hydrodynamic model was applied to simulate estuarine processes. This study was focused on examining the impact of freshwater dispersion by controlling the freshwater sources. Thus, a hydrologic model was developed to estimate runoff. Furthermore, grid size was reduced, a new advective code added, and baroclinic effects were included. The model was run with and without freshwater diversions from the Mississippi River.

During several initial model runs, the model was calibrated by adjusting the Manning's coefficient until the model reproduced, as closely as possible, the observed water elevation. The phase of modeled water level was delayed two hours with respect to observations, moving from lower Barataria Bay to sites further upstream. When compared to observations, the correlation coefficients (r^2) of model water levels are larger than 0.9 at all but one station. For the hydrologic calibration, a big flood event was tested. Agreement between observed and model results with runoff was surprisingly good. The observed agreement provides a justification for adopting 100 % coupling between the hydrologic model and hydrodynamic model, at least for this flood event.

In terms of water level within the basin, a number of points were noted:

- The freshwater diversions seem to affect most of the Barataria Basin system water level within three days. These effects, though, were small except near the diversion sites and Gulf Intercoastal Waterway connection.
- The basin is made of four different sub-regions separated by sudden tidal amplitude changes. Within Barataria Bay the tidal amplitude was 40-45 *cm*. The

tidal amplitude decreased with increasing distance upstream from the mouth of the bay. Finally, the tidal amplitude at Lac des Allemands attained values less than 3-4 *cm*.

- Using a Hovmüller diagram, tidal phase speed was estimated for the basin. It was found that the phase takes 16 hours to travel from the mouth of Barataria Bay to the top of the basin, Lac des Allemands.

Using two different scenarios of diversion pumping rates, zero and their maximum rate ($60\,m^3\,s^{-1}$), salinity variability was studied. Even though the model did not reach spin-up for salinity, the results give realistic relative salinity distributions in space and time.

Tidal mixing and flushing of the basin is clearly observable in the results:

- A plume 3 *km* in diameter formed at the mouth of the Barataria Bay. This is the biggest plume at the passes of Barataria Basin. The second biggest plume, a well-developed plume, occurred at the Quatre Bayou Pass. A relatively small plume formed outside Pass Abel due to the shallowness of the pass.
- The dominant inflow plume traveled nearly 11 *km* into the Barataria Bay.

To observe the impact of the freshwater diversions from the Mississippi River in terms of salinity, the results with diversion and without diversion, were compared by subtracting one from the other. It was found that:

- The impact of freshwater diversion reached Barataria Bay within 5 and 10 days from Naomi and West Pointe à la Hache, respectively.
- The impact of freshwater diversion reached the Gulf of Mexico 15 to 20 days after freshwater release.

- By the 20th day after freshwater release, most of the downstream region was impacted.
- Maximum impact appeared to be concentrated in the upper portions of Barataria Bay and lower Little Lake and Barataria Waterway, as well as in the marshes immediately surrounding the outfall regions.

Remaining issues exist with the model:

- Three dimensional effects may need to be modeled or parameterized in the deeper regions, such as Barataria Pass and Barataria Waterway.
- Improvement of open boundary salinities and water levels.

When a fully verified model is developed, it should be of significant impact in forcasting the effects of different diversion operation scenarios. It will also characterize the transport of suspended sediment and nutrients. Finally, it will be of use in defining the recruitment of larvae and spat to different regions of the basin.

REFERENCES

Banas, P. J., 1978. An investigation of the circulation dynamics of a Louisiana bar-built estuary. M.S thesis, Louisiana State University, Baton Rouge, La.

Barrett, B. B., 1971. Cooperative Gulf of Mexico estuarine inventory and study. Louisiana Phase II, Hydrology; Phase III, Sedimentology. LWFC, New Orleans, La.

Beven, K. J., 2000. Rainfall-runoff modelling. Wiley, 360 pp.

Blaha, J., and W. Sturges, 1981. Evidence for wind-forced circulation in the Gulf of Mexico. J. Mar. Res., 39(4), 711-734.

Boshart, William M., 1998. Naomi freshwater diversion. Louisiana Department of Natural Resources, Coastal Restoration Divesion. Three-year comprehensive monitoring report, Monitoring series No. BA-03-MSTY-1098-1, 22 pp.

Bowman, P. E., W. S. Perret, and J. E. Roussel, 1995. Freshwater introduction and implication for fisheries production in Louisiana. Baton Rouge, LA: Department of Wild and Fisheries.

Butler, P. A., 1949. Gametogenesis in the oyster under conditions of depressed salinity. Biol. Bull., 96(3), 263-269.

Butler, T. J., 1975. Aquatic metabolism and nutrient flux in a south Louisiana swamp and lake system. Masters Thesis. Department of Marine Sciences, Louisiana State University, 58 pp.

Byrne, P., M. Borengasser, G. Drew, R. A. Muller, B. L. Smith Jr. and C. Wax, 1976. Barataria Basin : Hydrologic and climatologic processes. Louisiana State University Center for Wetland Resources. Sea Grant Publ. No. LSU-T-76-010.

Camerlengo, A. L., and J. J. O'Brien, 1980. Open boundary conditions in rotating fluids, J. Comput. Phys., 35, 12-35. Cloern, J. E.,1984. Temporal dynamics and ecological significance of salinity stratification in an estuary (South San Francisco Bay, USA). Oceanologia Acta 7, 137-141.

Chabreck, R. H., 1970. Marsh zones and vegetation types in the Louisiana coastal marshes. Ph. D. dissertation, Louisiana State University, Baton Rouge, La.

_____, R. H., 1972. Vegetation, water, and soil characteristics of the Louisiana coastal region. Louisiana State University Exp. Sta. Bull., 664 pp.

Chuang W. S., Wm. W. Schroeder, and Wm. J. Wiseman, Jr., 1982. Summer current observations off the Alabama coast. Marine Science, 25, 121-131.

_____ W. S., and Wm. J. Wiseman, Jr., 1983. Coastal sea level response to frontal passages on the Louisiana-Texas Shelf. J. Geophys. Res., 88(C4), 2615-2620.

Colon, J. A., 1963. Seasonal variations in heat flux from the sea surface to the atmosphere over the Caribbean Sea. J. Geophys. Res., 68, 1421-1430.

Denes, T. A. and Caffrey, J. M., 1988. Changes in seasonal water transport in a Louisiana Estuary, Fourleague Bay, Louisiana. Estuaries 11, 184-191.

Dinnel, S. P. and Wm. J. Wiseman, Jr., 1985. Fresh water on the Louisiana and Texas shelf. Continental Shelf Res., 6(10), 765-784.

Drinkwater, K. F., 1986. On the role freshwater outflow on coastal marine ecosystems: a workshop summary. NATO ASI Series, V. G7, Springer-Verlag, Heidelberg, 429-438. Dyer, K. R., 1973: Estuaries: A Physical Introduction. Great Britain at The University Press, Aberdeen, 140 pp.

Fisher, H. B., E. J. List, R. C. Y. Koh, J. Imberger and N. H. Brooks, 1979. Mixing in inland and coastal waters. Academic Press, New York, 483 pp. Louisiana Coastal Wetlands Conservation and Restoration Task, 1993a. Louisiana Coastal Wetlands Conservation Plan. Barataria Basin. Appendix D, 149 pp.

Gagliano, S. M., P. Culley, D. W. Earle, P. King, C. Latiolais, P. Light, A. Rowland, R. Shlemon, and J. L. van Beek, 1973. Hydrologic and geologic studies of coastal Louisiana-environmental atlas and multiuse management plan for South-Central Louisiana. Report No. 18, V. I, 132 pp.

_____, S. M., H. J. Kwon, and J. L. van Beek, 1970. Salinity regimes in Louisana Estuaries. LSU Center for Wetland Resources, Hydrologic and geologic studies of coastal Louisiana. Baton Rouge, La. , Rept. 2.

_____, S. M., S. M., P. Light, R. Muller, M. Al-Awady, 1973. Water balance in Louisiana estuaries. Hydrologic and Geologic Studies of Coastal Louisiana, Report No. 3., Coastal Resources Unit, Center for Wetland Resources, Louisiana State University, 177 pp.

Galtsoff, P. S., 1964. The American oyster, Crasostrea virginica (Gmelin). U. S. Dept. of the Interior, Fish and Wildl. Serv., Fish. Bull., 64.

Gerdes, R., C. Koberle, and J. Willebrand, 1991. The influence of numerical advection schemes on the results of ocean general circulation models. Climate Dynamics, 5, 211-226.

Gosselink, J. G., Wm. H. Patrick Jr., R. T. Parrando, G. S. Hopkinson, and K. Kneller, 1975. Productivity and stress physiology of marsh plants in Louisiana wetlands. U. S. Army Corps of Engineers, Washington, D. C.

Gutierrez de Velasco G., and C. D. Winant, 1996. Seasonal patterns of wind stress and wind stress curl over the Gulf of Mexico. J. Geophys. Res., 101(C8), 18127-18140.

Hacker, S., 1973. Transport phenomena in Estuaries. Ph.D. dissertation, Louisiana State University, Baton Rouge, La.

Hansen, D. V., and M. Rattray Jr., 1965. Gravitational circulation in straits and estuaries. J. Mar. Res., 23(2), 104-122.

Hasumi, H. and N. Suginohara, 1999. Sensitivity of a global circulation model to tracer advection schemees. J. Phys. Oceanogr., 29, 2730-2740.

Hearn, C. J., J. R. Hunter, and M. L. Heron, 1987. The effect of deep channel on the wind-induced flushing of a shallow bay or harbor. J. Geophys. Res., 92, 3913-3924.

Henderson, F. M., 1966. Open Channel Flow. Macmillan, New York, 544 pp.

Henry, W. K., 1979. Some aspects of the cold fronts in the Gulf of Mexico. Mon. Weather. Rev. 101, 1078-1082.

Ho, C. L. and B, B, Barrett, 1975. Distribution of nutrients in Louisiana's coastal waters influenced by the Mississippi River. Louisiana Wildlife and Fisheries Comm., Div. Oysters, Water, Bottom, and Seafoods, Tech. Bull., 17, 39 pp.

Howard, P. C., 1982. Quatre Bayou Pass, Louisiana: Analysis of currents, sediment and history. Masters Thesis, Department of Geology, Louisiana University, Baton Rouge, Louisiana 111 pp.

Hsu, S. A., 1988. Coastal meteorology. Academic Press, San Diego, CA. 260 pp.

___, S. A., 1997. Effects of cold air outbreaks on evaporation and heat loss from three regions in the Gulf of Mexico. Gulf of Mexico Science, 2, 71-76.

___, S. A., 1994. Determining the power-law wind-profile exponent under near-neutral stability conditions at sea. J. of Applied Meteorology, 33(6), 757-765.

___, Y. and A. Arakawa, 1990. Numerical modeling of the atmosphere with an isentropic vertical coordinate. Mon. Wea. Rev., 118, 1933-1959.

Huh, O. K., Rouse, L. J., Jr., and Walker, N. D., 1984. Cold air outbreaks over the northwest Florida continental shelf: heat flux processes and hydrographic changes. J. Geophys. Res. 89, 717-726.

Inoue, M., Wm. J. Wiseman, Jr. and D. Park, 1998. Coastal marine Environmental Modeling. OCS Study MMS 98-0052. U.S. Dept. of the Interiors, Minerals management Service, Gulf of Mexico OCS Region, New Orleans, La., 133pp.

____, M. and Wm. J. Wiseman, Jr., 2000. Transport, stirring and mixing process in a Louisiana estuary: A model study. Estuarine. Coastal and Shelf Science, 50, 449-466.

____, M., Wm. J. Wiseman, Jr., D. Park, D. Justic, and G. Stone, 2001. Dispersion in Broad, Shallow Estuaries: A Model Study. OCS Study MMS 2001-054. U.S. Dept. of the Interior, Minerals Management Service, Gulf of Mexico OCS Region, New Orleans, La. 54 pp.

Keck, R., D. Maurer, and L. Walting, 1973. Tidal stream development and its effect on the distribution of the American oyster. Hydrobiologia, 42(4), 369-379.

Kjerfve, B., 1971. A field study of Airplane Lake, Lake Palourde and Lake Laurier area of coastal Louisiana. Unpublished manuscript, Coastal Studies Institute, Louisiana State University, Baton Rouge, Louisiana, 31 pp.

Kjerfve, B., 1973. Dynamics of the water surface in a bar-built estuary. Ph.D. dissertation, Louisiana State University, Baton Rouge, La.

Koutitonsky, V. G., Wilson R. E., and El-Sabh, M. I., 1990. On the seasonal response of the Lower St. Lawrence Estuary to buoyancy forcing by regulated river runoff. Estuarine, Coastal and Shelf Science 31, 359-379.

Leendertse, J. J., 1967. Aspects of a computational model for long period water wave propagation. 165 pp., RM-5294-PR, Rand Corporation, Santa Monica, CA.

Light P., R. J. Shelemon, P.T. Culley, and N. A. Roques, 1973. Hydrologic models for the Barataria-Terrebonne area, south-central Louisiana. Hydrologic and geologic studies of coastal Louisiana. No.16, 43 pp.

Linacre, E. T., 1994. Estimating U.S. Class-A pan evaporation from few climate data. Water International 19, 5 - 14.

Mackin, J. G. and S. H. Hopkins, 1961. Studies on oyster mortality in relation to natural environment and to oil fields in Louisiana. Pub. Inst. Mar. Science. University of Texas. 7, 1-131.

Maier-Reimer, E., U. Mikolajewicz, and K. Hasselmann, 1993. Mean circulation of the Hamburg LSG OGCM and its sensitivity to the themohaline surface forcing. J. Phys. Oceanogr., 23, 731-757.

Marmer, H. A., 1947. The tide in Barataria Bay. Texas A&M Research Foundation, Project 9.

_____, H. A., 1948. The currents in Barataria Bay. Texas A&M Research Foundation, Project 9.

_____, H. A., 1954. Tides and sea level in Gulf of Mexico. U.S. Fish and Wildlife. Service, Fish. Bull., 89, 101-118.

Muller, R. A., 1975. Freshwater potensial in the Louisiana coastal marshes and estuaries. Geoscience and Man 12:1-7. Department of Geography and Anthropology, Louisiana State University. Baton Rouge, LA 70803.

Panofsky, H. A., and J. A. Dutton, 1984. Atmospheric Turbulence. Wiley, 397 pp.

Park, D. H., 1998. A modeling of the Barataria Basin. M. S. thesis, Louisiana State University, Baton Rouge, Louisiana.

Penman, H. L., 1948. Natural evaporation from open water, bare soil and grass. Proc. Roy. Soc., A. 193, 120-145.

Perkins, E. B., 1952. Some observations on migrations and setting of oyster larvae. A part of Proc. Nat'l Shellfisheries Assoc, 99-104.

Philomena, A. L., 1983. The distribution of macrobenthos in Barataria Basin, Louisiana. M. S. thesis, Louisiana State University, La.

Pickard, G. L., and K. Rogers, 1959. Current measurements in Knight Inlet, British Columbia. J. Fish. Res. Board Can., 16, 635-678.

Pritchard, D. W., 1952a. Estuarine hydrography. Advan. Geophys., 1, 243-280.

_____, D. W., 1967. What is an Estuary: Physical Viewpoint. Estuaries, G. H. Lauff, ed., American Association for the Advancement of Science, 3-5.

Raudkivi, A. J., 1979. Hydrology: An advanced introduction to hydrological processes and modelling. Pergamon Press, 479 pp.

Roberts, D. W., J. L. van Beck, S. Fournet, and S. J. Williams, 1992. Abatement of wetland loss in Louisiana through diversions of Mississippi River water using siphons, U. S. Geological Survey Open- File Repost 92-274, Reston, VA.

Roll, H. U., 1965. Physics of the marine atmosphere. Academic Press, New York.

Signell, R. P., R. C. Beardsley, H. C. Graber, and A. Capotondi, 1990. Effect of wave-current interaction on wind-driven circulation in narrow, shallow embayments. J. Geophys. Res., 95(6) 9671-9678.

Sittel, M., 1994. Differences in the Means of ENSO extremes for temperature and precipitation in the United States. COAPS Technical Report 94-2.

Sklar, F. H., 1983. Water budget, benthological characterization, and simulation of aquatic material flows in a Louisiana freshwater swamps. Doctor Dissertation, Louisiana State University, 280 pp.

Smith N. P., 1978. Long-period, estuarine-shelf exchange in response to meteorological forcing. Hydronamics of estuaries and Fjord, J. C. J. Nihoul, ed., Elsevier, Amsterdam, 147-159.

Smith, S. D., 1980. Wind stress and heat flux over the ocean in gale force winds. J. Phys. Oceanogr., 10, 709-726.

Smolarkiewcz, P. K., 1984. A fully multidimensional positive definite advection transport algorithm with small implicit diffusion. J. Computational Physics., 54, 325-362.

Stanhill, G., 1976. The CIMO International Evaporimeter Comparisons. WMO Publ 449 (World Meteor. Organ.), 38 pp.

Swarzenski, Christoper M., A. N. Traver, and C. K. Labbe, 1999. The Gulf Intercoastal Waterway as a conduit of freshwater and sediments to coastal Louisiana wetlands, 1999. Poster Presentation.

Swenson, E. M., and R. E. Turner, 1998. Past, present and probable future salinity variations in the Barataria Basin System. Prepared for Coastal Restoration and Management, Louisiana Department of Natural Resources, 112 pp.

Takacs, L. L., 1985. A two-step scheme for the advection equation with minimized dissipation and dispersion errors. Mon. Wea. Rev., 113, 1050-1065.

Tuner, R. E., 1990. Landscape Development and Coastal Wetland Losses in the Northern Gulf of Mexico. American Zoologist 30:89-105.

Van Sickle, V. R., B. B. Barrett, and T. B. Ford, 1976: Barataria Basin: Salinity changes and oyster distribution. Louisiana State University Center for Wetland Resources. Sea Grant Publ. No. LSU-T-76-002.

Viessman, Warren, Jr., G. L. Lewis, and J. W. Knapp, 1989. Introduction to hydrology. Harper & Row, Publishers, 780 pp.

von Arx, W. S., 1950. The Barataria Bay model. Unpublished report to the Freeport Sulphur Company.

Walesh, Stuart G., 1989. Urban surface water management. A Willy-Interscience Publication. 518 pp.

Wang, D. P., 1979. Wind-driven circulation in the Chesapeake Bay: winter 1975. J. Phys. Oceanogr., 9(3), 964-972.

Wax, C. L., M. J. Borengasser, and R. A. Muller, 1978. Barataria Basin: synoptic weather types and environmental response. Center for Wetland Resources, Louisiana State University, Baton Rouge, LA 70803. Sea Grant Publication Number LSU-T-78-001.

Weisberg, R. H., and W. Sturges, 1976: Velocity Observations in the West Passage of Narragansett Bay: A partially mixed estuary. J. Phys. Oceanogr., 6(3), 345-354.

Wiseman, Wm. J., Jr., 1986: Estuarine-shelf interactions. Baroclinic Processes on Continental Shelves, C. N. K. Mooers, ed. American Geophysics Union, Washington D. C., 109-115.

_____, Wm. J., Jr., and E. M. Swenson, 1989. Modelling the effects of produced water discharges on estuarine salinity. Part of " Environmental impact of produced water discharges in coastal Louisiana," ed. Donald F. Boesch and N. N. Rabalais., 287.

_____, Wm. J., Jr., E. M. Swenson and J. Power, 1990. Salinity trends in Louisiana estuaries. Estuaries, 13(3), 265-271.

_____, Wm. J., Jr., and M. Inoue, 1993: Salinity variations in two Louisiana Estuaries. Proceedings Coastal Zone ’93, 8th Symposium on Coastal and Ocean Management, New Orleans, La, July 19-23 (O. T. Magoon, W. S. Wilson, H. Converse and L. T. Tobin, eds.), 1, 1,230-1,242.

_____, Wm. J. Jr., and M. Inoue, 1994. Salinity variability and transport processes. pp. 3.1-3.31. In H. H. Roberts. Critical physical processes of wetland loss. Final Report to U. S. Geological Survey. Coastal Studies Institute, Louisiana State University, Baton Rouge, LA.

_____, Wm. J., Jr., S. P. Murray, J. M. Bane, and M. W. Tubman, 1975: Offshore physical oceanography. Vol.2: Technical appendices, app. 2, in Environment Assessment of Louisiana Offshore Oil Port and Appertinent Storage and Pipeline Facilities. Louisiana Offshore Oil Port, Inc., New Orleans, La.

Wolanski, E. and P. B. Ridd, 1986. Tidal mixing and trapping in mangrove swamps. Estuarine, Coastal and Shelf Science, 23, 759-771.

Wood. T., 1979: A modification of existing simple segmented tidal prism models of mixing in estuaries. Estuarine and Marine Science, 8, 339-347.

VITA

Dongho Park was born on March 10, 1957,in Pusan, Korea. He entered National Fisheries University of Pusan, Korea, in 1982 after serving three years of his duty in the army. In 1986, he was accepted into the graduate school of National Fisheries University of Pusan, Korea, to continue his studies after obtaining a Bachelor of Science degree in oeanography. Two years later, he obtained the Master of Science degree. In 1994, he entered the Department of Oceanography and Coastal Sciences, Louisiana State University. He obtained his Master of Science degree in 1998.

He has continued his studies at the same school and is presently a candidate for the degree of Philosophy in the Department of Oceanography and Coastal Sciences.